VYSOKÉ UČENÍ TECHNICKÉ V BRNĚ
BRNO UNIVERSITY OF TECHNOLOGY

FAKULTA STROJNÍHO INŽENÝRSTVÍ
FACULTY OF MECHANICAL ENGINEERING

ÚSTAV MECHANIKY TĚLES, MECHATRONIKY A BIOMECHANIKY
INSTITUTE OF SOLID MECHANICS, MECHATRONICS AND BIOMECHANICS

VLIV MECHANICKÝCH VLASTNOSTÍ INTRALUMINÁLNÍHO TROMBU NA NAPJATOST V ANEURYSMATECH ABDOMINÁLNÍ AORTY
EFFECT OF THE MECHANICAL PROPERTIES OF INTRALUMINAL THROMBUS ON WALL STRESS OF ABDOMINAL AORTIC ANEURYSMS

DIPLOMOVÁ PRÁCE
MASTER'S THESIS

AUTOR PRÁCE　　　　　Bc. Michal Hřičiště
AUTHOR

VEDOUCÍ PRÁCE　　　　Ing. Stanislav Polzer, Ph.D.
SUPERVISOR

BRNO 2017

Zadání diplomové práce

Ústav:	Ústav mechaniky těles, mechatroniky a biomechaniky
Student:	**Bc. Michal Hřičiště**
Studijní program:	Aplikované vědy v inženýrství
Studijní obor:	Inženýrská mechanika a biomechanika
Vedoucí práce:	**Ing. Stanislav Polzer, Ph.D.**
Akademický rok:	2016/17

Ředitel ústavu Vám v souladu se zákonem č.111/1998 o vysokých školách a se Studijním a zkušebním řádem VUT v Brně určuje následující téma diplomové práce:

Vliv mechanických vlastností intraluminálního trombu na napjatost v aneurysmatech abdominální aorty

Stručná charakteristika problematiky úkolu:

Intraluminální trombus je častou součástí aneurysmat abdominální aorty a jeho přítomnost ovlivňuje napětí ve stěně aneurysmatu, které je klíčové pro posuzování rizika ruptury. Mechanické vlastnosti intraluminálního trombu však mají velký rozptyl a je třeba znát nejistoty v konečnoprvkových výpočtech napětí ve stěně, způsobené neznalostí mechanických vlastností konkrétního pacienta.

Cíle diplomové práce:

1) Provést rešerši literatury a zjistit publikované hodnoty tuhosti intraluminálního trombu.
2) Provést mechanické zkoušky intraluminálního trombu konkrétních pacientů.
3) Srovnat napětí získané konečnoprvkovým výpočtem při použití buď patient-specific hodnot tuhosti intraluminálního trombu nebo průměrných tuhostí z literatury.

Seznam literatury:

Wang D.H., Makaroun M.S., Webster M.W. and Vorp D.A., 2002. Effect of intraluminal thrombus on wall stress in patient-specific models of abdominal aortic aneurysm. J Vasc Surg, 36, 598-604.

Vande Geest J.P., Sacks M.S. & Vorp D.A., 2006. A planar biaxial constitutive relation for the luminal layer of intra-luminal thrombus in abdominal aortic aneurysms. J Biomech 39:2347-54

Vorp D.A., 2007. Biomechanics of abdominal aortic aneurysm. J Biomech, 40, 1887-902

Di Martino E., Mantero S., Inzoli F., Melissano G., Astore D., Chiesa R., et al. 1998. Biomechanics of abdominal aortic aneurysm in the presence of endoluminal thrombus: experimental characterisation and structural static computational analysis. Eur J Vasc Endovasc Surg, 15, 290-9

Fillinger M.F., Marra S.P., Raghavan M.L. and Kennedy F.E., 2003. Prediction of rupture risk in abdominal aortic aneurysm during observation: Wall stress versus diameter. J Vasc Surg 37:724-732.

Gasser T.C., Gorgulu G., Folkesson M. and Swedenborg J., 2008. Failure properties of intraluminal thrombus in abdominal aortic aneurysm under static and pulsating mechanical loads. J Vasc Surg, 48, 179-88
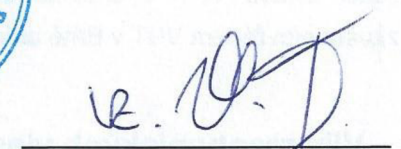
Termín odevzdání diplomové práce je stanoven časovým plánem akademického roku 2016/17.

V Brně, dne 4. 11. 2016
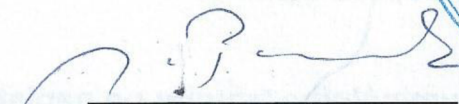
_____
prof. Ing. Jindřich Petruška, CSc.
ředitel ústavu

_____
doc. Ing. Jaroslav Katolický, Ph.D.
děkan fakulty

Abstract

The aim of this thesis is the problematic of abdominal aortic aneurysm wall stress in relation to a different material behavior of intraluminal thrombus, which is in most cases present in the aneurysmal volume. In this thesis, the influence of neglecting the patient-specific material properties of the intraluminal thrombus, on the aneurysmal wall stress, obtained from finite element stress-strain analysis, is investigated. In terms of solution method selection, a system approach was applied so that the solution method was selected in order to respect a system of essential variables as much as possible.

The first part of this thesis is focused on a description of the problematic and the human cardiovascular system with important aspects contributing to development and growth of the abdominal aortic aneurysm. Next, this part of the thesis includes a description of the characteristics, risk factors and mechanical properties of abdominal aortic aneurysm. Additionally, following chapters are devoted to the intraluminal thrombus in terms of its basic characteristics (anatomy, physiology, pathology), structure and its influence on processes within the abdominal aneurysm.

The second part of this work is devoted to the accomplishment of the first and second goal of this thesis, which is analyzing the available literature to obtain mean population stiffness values of the intraluminal thrombus and conducting biaxial experimental tests of provided samples of intraluminal thrombus. The experimental testing was conducted in order to obtain the patient-specific mechanical properties, which are used as the inputs in the finite element analysis. The experimental testing confirmed the stiffness negligibility of the intraluminal thrombus's outer layer, which is mentioned is several studies, however, the influence of this layer on resulting aneurysmal wall stress has been to this date not tested.

The dominant part of this thesis is focused on the third goal of this work, which is a comparison of aneurysmal wall stress obtained from the finite element computation that included mechanical properties of intraluminal thrombus obtained either from the literature analysis of experimental testing. This part includes discerption of idealized geometry model development, which was used to analyze the sensibility of computed stresses on a number of ILT layers representing different material properties. In order to obtain this analysis, a macro was created prescribing each element of the intraluminal thrombus finite element mesh with material properties derived from its distance from the lumen. Next, this chapter contains description of patient-specific geometry models development, material models, and boundary conditions selection. In the end of this part, results of the finite element computations are presented together with their statistical analysis.

Within the last part of this thesis, discussion of results and conclusions of this thesis is included. Also, an overview of important aspects entering computational modeling of abdominal aortic aneurysms is presented.

Abstrakt

Tato práce se zabývá problematikou napětí ve stěně aneurysmatu abdominální aorty ve vztahu k různému materiálovému chování intraluminálního trombu. Přítomnost intraluminálního trombu v objemu abdominálního aneurysmatu je velmi častá. Byl zkoumán vliv zanedbání patient-specific mechanických vlastností intraluminálního trombu pacienta na napětí ve stěně aneurysmatu, získaných jako výstup z konečnoprvkové deformačně-napěťové analýzy tohoto aneurysmatu, realizované variační metodou-MKP. Pří výběru metody bylo respektováno systémové pojetí v tom smyslu, že metoda řešení byla vybírána tak, aby co nejvíce respektovala systém podstatných veličin.

První část této práce je zaměřena na popis řešené problematiky. Dále se tato část věnuje deskripci kardiovaskulární soustavy člověka se zaměřením na podstatné jevy spojené s aneurysmatem abdominální aorty, popisu jeho charakteristik, mechanických vlastností a rizik spojených s jeho vznikem. Dále se tato práce zabývá základními charakteristikami intraluminálního trombu (anatomie, fyziologie, patologie), jeho strukturou a vlivem na procesy probíhající v abdominálním aneurysmatu.

Druhá část je věnována řešení prvního a druhého cíle této práce, kterým jsou provedení rešeršní studie literatury s ohledem na publikované a běžně používané hodnoty mechanických vlastností intraluminálního trombu a provedení dvouosých experimentálních zkoušek vzorků intraluminálních trombů. Experimentální zkoušky byly provedeny za účelem získání pacient-specific mechanický vlastností, které jsou dále použity jako vstupy do konečnoprvkové analýzy. Provedené experimentální testování potvrdilo zanedbatelnost tuhosti vnější části intraluminálního trombu, která již byla popsána v některých studiích, ale jejíž vliv na napětí ve štěně aneurysmatu dosud nebyl zkoumán.

Dominantní část této práce je zaměřena na řešení třetího stanoveného cíle, kterým je srovnání napětí ve stěně aneurysmatu, získaných konečnoprvkovým výpočtem, při použití tuhostí intraluminálního trombu získaných z literatury nebo patient-specific hodnot z provedeného experimentálního testování. V této časti je popsána tvorba idealizovaného modelu geometrie, na němž byla provedena analýza vlivu počtu materiálově odlišných vrstev intraluminálního trombu na napětí ve stěně aneurysmatu. Za účelem vytvoření geometrie bylo vytvořeno makro, přiřazující každému elementu konečnoprvkové sítě trombu materiálové vlastnosti, podmíněné vzdáleností od krevního řečiště. Dále je uveden popis tvorby pacient-specific modelu geometrie, konečnoprvkových sítí obou modelů geometrie, modelů materiálů a volby okrajových podmínek. Závěr této části je věnován prezentaci výsledků a jejich statistické analýze.

Poslední částí práce je diskuze výsledků a podstatných veličin vstupujících do výpočtového modelování abdominálních aneurysmat a závěr.

Bibliographic citation

HŘIČIŠTĚ, M. *Vliv mechanických vlastností intraluminálního trombu na napjatost v aneurysmatech abdominální aorty*. Brno: Vysoké učení technické v Brně, Fakulta strojního inženýrství, 2017. XY s. Vedoucí diplomové práce Ing. Stanislav Polzer, Ph.D..

Declaration

I declare that I have written this master's thesis *Effect of the mechanical properties of intraluminal thrombus on wall stress of the abdominal aortic aneurysms* on my own according to the instructions of my master's thesis supervisor Ing. Stanislav Polzer, Ph.D., and using the sources listed in references.

May 22, 2017

....

Michal Hřičiště

Acknowledgements

CONTENT

1 Introduction

Among men over the age of 60, abdominal aortic aneurysm (AAA) rupture is an increasingly frequent cause of death, being the 10th most common cause of demise [3,21]. A diagnosed AAA (figure 1) can be repaired by conventional or endovascular procedures to avoid its rupture. However, surgery is not always possible since the majority of patients suffering from this disease are people above 60 years of age and repair process can be associated with mortality rates of 4.0 and 2.9 %, respectively [38]. Therefore, to avoid unnecessary surgery but also the death by AAA rupture, a reliable criterion indicating a need for a surgical repair of patient's AAA is needed [2]. In current practice, a diameter of 5.0 cm in women and 5.5 in men, or an aneurysm grow rate exceeding 0.5 - 1 cm per year, is used as an indicator of necessity for intervention, despite the observation that many AAAs less than 5.5 cm in diameter rupture while others exceeding the critical geometry values do not [21]. Therefore, a more advanced criterion is clearly necessary to predict the risk of AAA rupture [21]. In terms of biomechanics, the AAA rupture is an event when the stress of the degenerated and weakened aortic wall exceeds a local strength of the tissue resulting in a final stage failure of the material. According to this fact, the knowledge of the wall stress distribution is critical in connection with AAA rupture prediction [22].
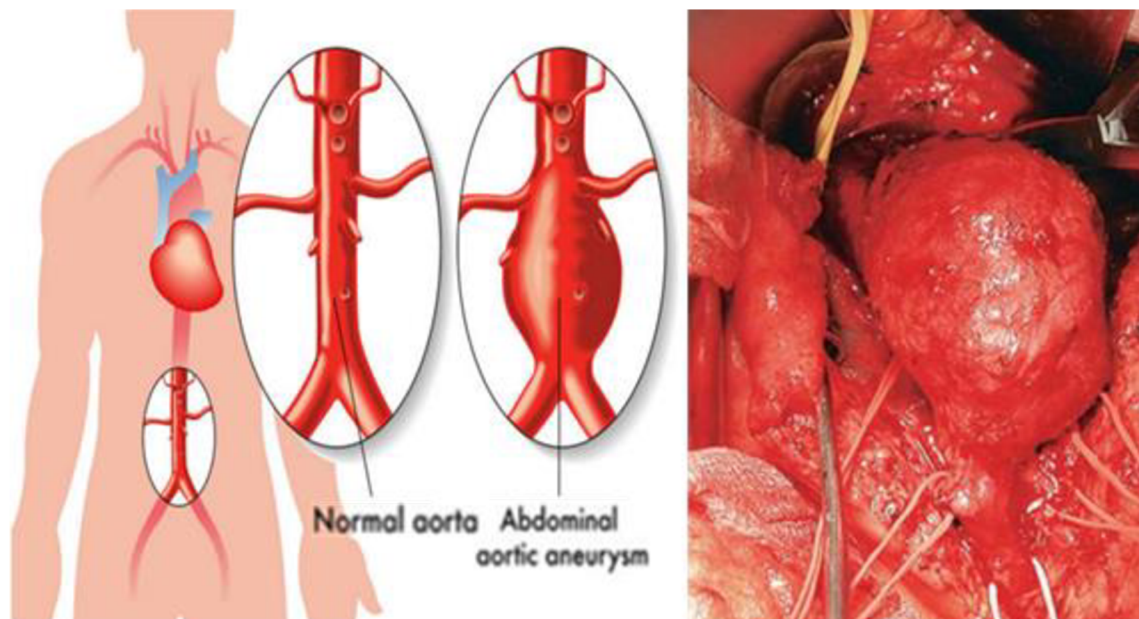
Figure 1 Schematic view of abdominal aortic aneurysm (left) [28], AAA during surgery (right) [80].

Additionally, it has been found that intraluminal thrombus (ILT) (see chapter 4), which is present in most AAAs of a clinically relevant size, may cause hypoxia in the underlying vessel wall that leads to increased neovascularization and degradation of extracellular matrix contributing to the vessel wall weakening. Moreover, the part of the AAA wall that overlays ILT is also thinner, contains a greater number of inflammatory

cells and undergoes increased smooth muscle cells (SMC) apoptosis which have a great impact on the changes of mechanical stress in the aneurysm wall [2]. Consequently, the thickness of the ILT is proportional to the amount of the wall weakening above the ILT, resulting in increased risk of AAA rupture [3,46]. On the other hand, few studies have shown that ILT can be viewed as an elastic material protecting the thin vessel wall from high stress and acting as a buffer, hence decreasing the AAA rupture risk [2,40]. In addition, the average thickness of an intraluminal thrombus (ILT) in ruptured AAAs is lower than in non-ruptured [25]. In both cases, ILT itself plays a significant role in the biomechanics of AAAs, however, due to a great complexity of its structure, the overall role of the ILT in AAA growth and rupture is not completely discovered [3,25]. Based on the ILT properties, gender or luminal diameter, the presence of ILT alters both magnitude and distribution of the stress in AAA wall [2].

Evaluation of the risk of AAA rupture based on wall stress has been suggested to provide more reliable results [49], however computational models based on an understanding of all the aspect of AAA structure, including patient-specific geometries, must be developed in order to improve the dependability of this method [21,59]. By revealing the uncertainties of finite element method (FEM) analysis without comprising patient-specific values of ILT properties, this thesis may help in future AAA rupture risk analysis.

1.1 Description of Problem Situation

As being mentioned, the AAA rupture occurs if the mechanical stress is greater than a local wall strength. Therefore, in addition to the maximum allowed diameter criterion another assessing criterion in terms of AAA wall stress data analysis, is needed to predict the rupture since the maximum diameter assessment provides flawless results [1,2]. In order to determine the AAA wall stress, some studies neglected the influence of ILT and did not include ILT in their calculations [47,48]. However, in almost all AAAs, an ILT is found with dimensions great enough to possibly increase a risk of AAA rupture. The ILT interacts with the underlying vessel wall and has multiple effects on its mechanical behavior and properties. By spacing the vessel wall out of the bloodstream, ILT may cause local hypoxia which could possibly lead to increased neovascularization and other remodeling effects [36], all contributing to the regional weakening of the vessel wall and change of its structural composition. Since the ILT has a significant impact on the wall biomechanics, the ILT signally influences the magnitude and distribution of the resulting stress inside the aortic wall [3]. Also, as being conducted by evaluation of AAA wall rupture from a CT data sets, most of the ruptures occur in the parts influenced by ITL [3]. Therefore, not only the mechanical properties of AAA wall but also properties of the ILT may play a significant role in AAA rupture risk assessment [3]. In a current practice, mean mechanical properties of ILT, obtained from in vitro measurements on specimens without a precise description of their position within the ILT body, available in the literature [3,27,40] are used in AAA wall stress analysis, even though the dispersion of patient-specific ILT properties compared to the mean data is unknown. Therefore, the motivation for this thesis was to determine the uncertainties in finite element method (FEM) AAA wall stress analysis caused by the lack of information about the ILT properties of a specific patient and thereby contribute to developing a computational model to assess AAA rupture risk.

1.2   Problem Formulation

Intraluminal thrombus is a very common part of abdominal aortic aneurysms and it is a very important aspect in terms of AAA wall stress assessment to be used as a decisive criterion for rupture [2, 3, 22, 25, 26, 27, 36, 37, 38, 40,41, 42, 44, 45, 50, 54, 55,73,77]. Thus, it is necessary to know the uncertainty in wall stress caused by using mean mechanical properties and not patient-specific properties, which is the aim of this thesis.

1.3   Goals of this thesis

Based on the problem formulation mentioned above, the goals of this thesis were formulated by the thesis supervisor as follows:

1) Analyze the available literature and obtain mean population stiffness of the intraluminal thrombus.

2) Perform experimental tests of provided samples of intraluminal thrombus.

3) Compute and compare wall stresses obtained from FE analysis using either patient-specific or mean stiffness of intraluminal thrombus.

1.4   Modeling

Importantly, when modeling real objects, numerous assumptions need to be introduced causing the FE models to represent the biomechanics of the real AAA to some level of precision. Thus, modeling of any kind is always a certain extent of simplification of the reality (figure 2). In this thesis, both, an idealized model of geometry together with 5 patient-specific models of geometry, were considered (7.3.1 and 7.4.1).
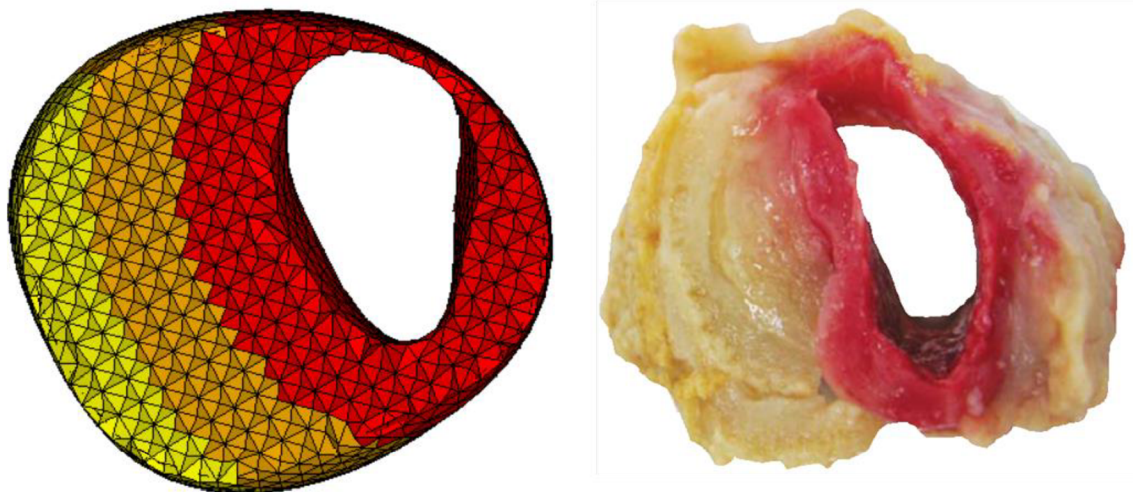

Figure 2 Comparison of a real part of the ILT (right) [83] with an FE mesh model (left). Note that these ILT examples does not correspond to each other and were only randomly chosen for illustrative reasons.

.

1.4.1 Modeling of structural properties

As described in 2.3 and 4.3, AAA wall and ILT are composed of complex biological material structures. Importantly, in this thesis, materials of the AAA wall and ILT were considered as hyperplastic (non-linear), isotropic, incompressible and homogeneous (see 6.3, 7.3.2 and 7.4.2). Consequently, large deformations were considered.

1.4.1.1 Large deformations

In order to describe the behavior of soft tissues, it is necessary to consider a finite deformation instead of the regular assumption of small deformation that is used for steel structures. In the mechanics of continuum, to describe the finite deformations, two approaches are used. A Lagrange approach uses as a reference geometry the unreformed state while the Euler approach uses the deformed geometry state [82]. The stress and deformation tensors used mentioned in this thesis are defined below.

Green-Lagrange strain tensor

This tensor respects the Lagrange approach, therefore the finite strains are referenced to the undeformed geometry with the element rotation being respected, as well [82].

$$E_{ij}^{L} = \frac{1}{2}\left[\frac{\partial u_i}{\partial X_j} + \frac{\partial u_j}{\partial X_i} + \frac{\partial u_k}{\partial X_j}\frac{\partial u_k}{\partial X_i}\right] = \frac{1}{2}\left(\lambda_i^2 - 1\right)$$

(1)

Cauchy-Green tensor of deformation

Instead of strain, this definition works with the stretch ratios λ, with the principal coordinates of this tensor being the squares of the stretch ratios in the principal directions.

$$C = \begin{bmatrix} \lambda_1^2 & 0 & 0 \\ 0 & \lambda_2^2 & 0 \\ 0 & 0 & \lambda_3^2 \end{bmatrix}$$

(2)

2. Piola-Kirchhoff stress tensor

The second Piola-Kirchhoff stress tensor uses a modified element force referenced to the undeformed geometry.

$$S_i = \frac{dF_{0i}}{dX_j \cdot dX_k}$$

(3)

Despite, the fact that this tensor does not have a physical interpretation, it is widely used due to its ability to remain symmetrical even for large deformations. Also, it forms an energetically conjugate pair with the Green- Lagrange strain tensor.

1.4.1.2 Hyperelasticity

Generally, soft biological tissues belong among materials that exhibit large finite reversible deformations. As shown in figure 11, the stress-strain dependence of these materials is non-linear. These attributes are typical for hyperelastic materials among which arterial walls belong [52].

Definition of hyperelastic material

A material is called hyperelastic if there is an elastic potential function W which is a scalar function of strain tensor. The function's derivative with respect to any strain components gives a corresponding component of stress. In the equation 4, S_{ij} represents a component of the 2. Piola-Kirchhoff stress tensor and E_{ij} is a component of the Green-Lagrange strain tensor [52].

$$S_{ij} = \frac{\partial W}{\partial E_{ij}}$$

(4)

The advantage of modeling a soft tissue as hyperelastic is the possibility of the constative models to prescribe material as totally incompressible.

2 Basic information on human cardiovascular system

To fully understand the problematic of abdominal aortic aneurysm and the risk of its rupture, introduction to a human cardiovascular system, with a focus on important aspects in relation to AAA, is necessary.

The human cardiovascular system works mainly as a transportation system distributing substances to and from cells. The cardiovascular system's essential components are the heart, blood and blood vessels. The heart, that can be described as two serially functioning pumps, is a drive unit pumping the blood, carrying medium of the substances, through the blood vessel forming two circulation loops. In pulmonary circulation, the blood is driven through lungs whereas systemic circulation brings the blood to the rest of the body [4].

More detailed description of the above-mentioned components with a focus on their relations and contributions to AAA formation and rupture risk evaluation will be the subject of the following chapters.

2.1 Blood

Since blood is the medium that causes the pressure load on arterial walls as well as thrombosis, that is associated with ILT formation, the knowledge of its physiology and behavior is valuable when dealing with aortic wall stresses and ILTs. As mentioned above, blood is a liquid that serves as a medium for substances transport in the cardio-vascular system. The blood consists of blood cells (erythrocytes, leukocytes, blood platelets) suspended in blood plasma. The total volume of a blood in the human body is about 8% of body weight from which 55% corresponds to the blood plasma [4].

2.1.1 Hemorheology

From the physical point of view, blood is a non-Newton fluid which means that its physical behavior can't be described by a single coefficient of viscosity (given by ratio

of shear stress and shear rate) at a certain temperature and that its rheological properties are derived from shear rate (figure 3), size and geometry of the surrounding vessel [5]. Rheologically, blood can be characterized as a two-phase liquid consisting of the liquid phase (plasma) and solid phase (cellular elements) [6]. Therefore, the viscosity of blood is determined by plasma viscosity (approximately 1.8 times more viscous than water), hematocrit (volume percentage of red blood cells in blood), mechanical properties of red blood cells (RBCs) and temperature, giving the blood 3 or 4 times higher viscosity than water [6,11]. The red blood cells (RBCs) are highly deformable and more importantly have the ability to undergo reversible aggregation. The instantaneous size of RBCs strongly influences the apparent blood viscosity and is inversely proportional to the magnitude of shear forces as the particles stick together under low-flow or static conditions and are being separated when the shear forces grow. Therefore, the value of blood viscosity depends on existing shear forces which corresponds to the definition of non-Newton fluids [6].
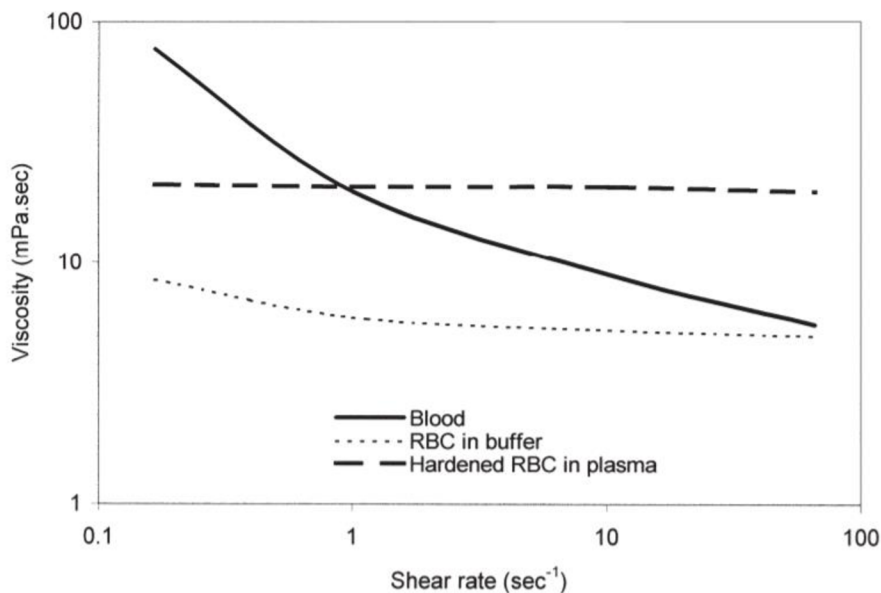
Figure 3 Dependence of viscosity on shear rate of a normal blood. As shown in the diagram, hardened RBCs that are present in the plasma does not contribute to the non-Newton behavior while RBCs suspended in buffer, a medium that prevents RBCs from aggregation, show response close to Newton fluids, demonstrating the effects of RBC behavior on blood fluid mechanics [6].

Moreover, the particular nature of blood causes that the apparent viscosity is not the only function of RBC concentration (hematocrit) but also depends on vessel diameter. Studies conducted that the apparent viscosity of blood decreases as the diameter of the vessel becomes smaller. This behavior applies till the diameter reaches values of 5–7 μm [7]. If the diameter drops below this boundary value, the apparent viscosity raises greatly since the size of the blood cells becomes greater than the tube and in order to maintain the flow of the blood inside the vessel, blood cells must be deformed. This phenomenon is called Fahraeus-Lindqvist effect [6].

Also, similarly to the Fahraeus-Lindqvist effect, Fahraeus effect (or plasma skimming) is another phenomenon describing the of blood flow characteristics. As the diameter of vessel decreases the average concentration of red blood cell also decreases lowering the apparent viscosity. To do so, RBCs are not evenly distributed throughout the cross-section of the vessel. More likely the RBCs will gather in the middle of the cross section creating low-concentration zones around the vessel wall (figure 4). Consequently, the RBCs at the central region have a higher velocity due to low shear forces at the center of the vessel, while RBC poor zones around the vessel wall experience lower velocities. Thus, hematocrit of blood flow in smaller conduits leading off a vessel with existing hematocrit radial gradient (figure 4) is lower which corresponds to lower apparent viscosity [6,7].
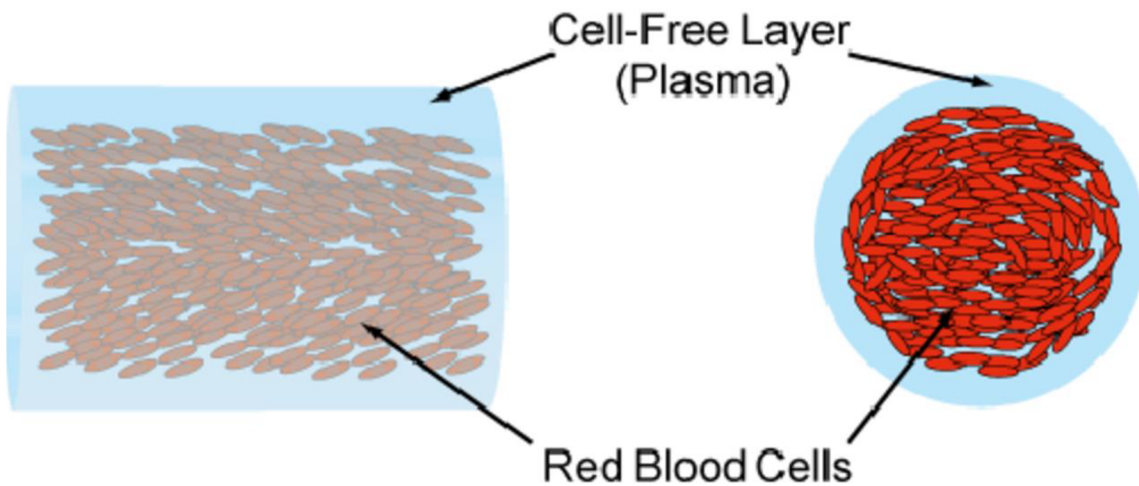
Figure 4 Blood entering the side branches comes from the RBCs poor zones of the blood stream caused by the accumulation of red blood cell in the central zone of large vessels [7].

2.1.2 Hemodynamics

In terms of hemodynamics, it is necessary to distinguish between blood velocity expressed by the distance over a unit of time (usually cm/s) and blood flow given by a volume over a unit of time (cm^3/s). According to the following formula:

$$\mathbf{V} = \frac{Q}{A}$$

(5)

the velocity of blood (V) is directly proportional to the blood flow (Q) and indirectly proportional to the tube cross-section (A). The average velocity in any position of a parallel system of tubes is indirectly proportional to the total cross-section of the tubes. Therefore, the average blood velocity in the aorta is higher than the velocity in capillaries with the total cross-section 1000 times greater than the cross-section of the aorta (Figure 5) [4].
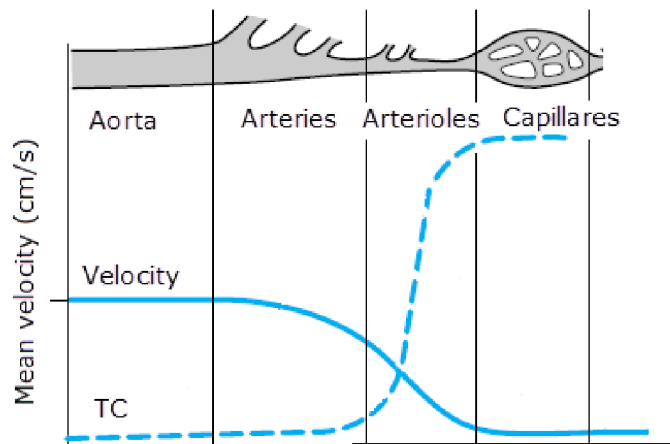
Figure 5 Dependence of mean blood velocity on the total cross section (TC) of the vessels [4].

The mean blood velocity in the aorta is 40 cm/s, however, the blood velocity is dependent on the cardiac cycle phase and ranges from 120cm/s during systole to negative values during the closing of the aortic valves [4].

In a normal state, blood flow in the vessel is laminar with the central region having the highest velocity while an infinitely thin layer of blood in contact with the vessel wall does not move at all. On the other hand, a turbulent flow occurs when the flow velocity exceeds a critical value or when the laminar flow is interrupted by unusual conditions of vascular geometry [4]. Another type of flow that can occur under certain conditions is the vortex flow. While in turbulent flow region the particles are moving randomly, vortex flow regions consist of slowly moving streamlines that separated from the laminar current within a vessel and are often moving in a countercurrent direction (figure 6) [12].
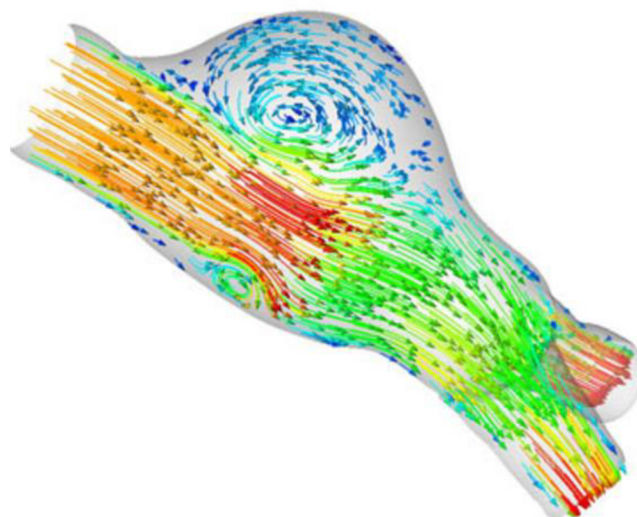
Figure 6 Nature of a blood flow in abdominal aorta aneurysm. The presence of intraluminal thrombus was not considered therefore this figure is only schematic, suggesting the presence of vortex flow in aortic dilatations contributing to ILT formation [13].

The intrusion of aortic geometry by the formation of AAA disrupts the otherwise laminar nature of blood flow causing the blood to travel in non-laminar stream lowering the average blood flow velocity inside the aneurysmatic bulge. Possibly, platelets, blood cells responsible for clot formation, are transported towards the distal aneurysm region. The combination of high residence times and high shear stresses may contribute to activation of the thrombus formation mechanism [9].

2.2 Heart

In order to fully understand the nature of loads acting on the arterial walls, breath knowledge of their sources is necessary. The heart is the drive unit of the human cardiovascular system that works as a suction and pressure pump that by its rhythmical function provides a blood circulation and pressure [10]. For the purposes of this thesis, only basic description of the heart anatomy and physiology is sufficient.

When the blood is passing through the heart it flows through four chambers: right atrium, left atrium, right ventricle and left ventricle. The atria are the receiving chambers while ventricles are discharging. Between each atrium and ventricle and at the exit of each ventricle a valve preventing the blood from reverse motion is located [10].

The heart activity is cyclic. Each cardiac cycle consists of relaxation (diastole) and contraction of the heart (systole). During diastole, the chambers are gradually filling with blood so that when the heart contracts during systolic phase, the blood can by squeezed out of the heart [10]. This process repeats with frequencies ranging from 65/min to 230/min, theoretically even around 400/min. The systolic phase for a frequency of 65/min lasts 0.3 s while the diastolic phase can last up to 0.6 s. Moreover, the cardiac muscle possesses a unique ability to shorten the systolic and diastolic phases at higher working frequencies, when the shortening of the phases is predominantly at the expense of ejection process [4]. As mentioned above, the heart secures two circulation loops. The systemic circulation starts at left ventricle leading oxygenated blood through the body and back to the right atrium from with the blood is entering the pulmonary circulation starting from the right ventricle, passing through the lungs and terminating the circulation in the left atrium (figure 7) [10].
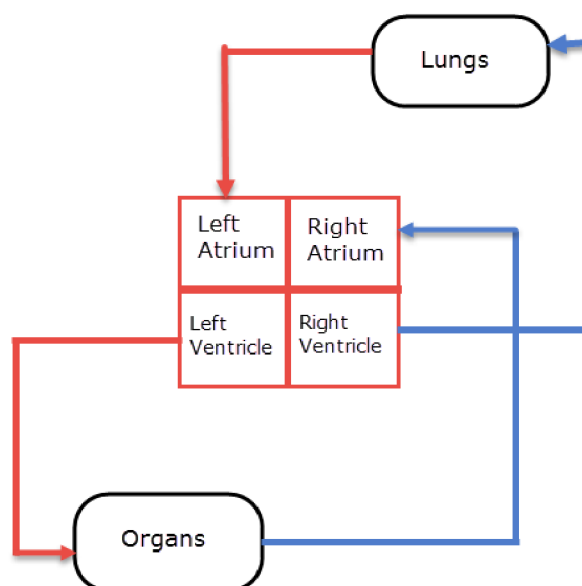

Figure 7 Diagram showing systemic and pulmonary circulation.

2.2.1 Blood Pressure

Together with the cardiac cycle phases, blood pressure is changing over time as well with normal values around 16 kPa for systolic pressure and around 9 kPa for diastolic pressure [4]. Among patients of age over 60 years, thus those in increased risk of AAA development (3.1), the mean systolic pressure has been recorded 16.5 kPa (SD 2.5 kPa) [11]. The sudden increase of arterial pressure can by caused by exercise or any kind of stress [4]. Also, in a normal state, blood pressure in systemic circulation is approximately 6 times higher than in pulmonary circulation [20]. Permanently increased arterial pressure is called hypertension. Moreover, values of arterial pressure depend on gravitation forces as well. The influence of gravitation on a referential pressure at the heart level is given by the product of blood density, gravitational acceleration and the vertical distance between the heart and the certain point on the vessel. When standing, the difference of pressure is rising by 0.11 kPa per 1cm of vertical distance for vessels below the heart level assuming normal blood density. For example, the arterial pressure in the aorta at the iliac bifurcation region with referential pressure (at the heart level) 16.0 kPa and vertical distance of being around 35 cm is 19.85 kPa under the assumption of normal blood density [4,39]. However, values of arterial pressure or vertical distances among certain point are subjected to strong patient diversity [11,39].

During the systolic phase of the arterial cycle, the expelled blood not only drives the blood flow but also creates a pressure wave which propagates in the vessel wall. For a young adult person, the wave velocity in the aorta is about 4 m/s while in small arteries it reaches 16 m/s. The velocity of the wave does not correspond to the blood velocity and increases with aging as the vessel wall becomes stiffer [4]. For example, in the abdominal aorta, it has been documented a 1.6-fold increase in pressure wave velocity from 21 to 72 years of age corresponding to velocities of 5.1 and 8.0 m/s respectively [14].The aortic pressure wave can be decomposed into two parts, the forward traveling wave generated by the left ventricle contraction and the reflected wave traveling in opposite direction generated mainly by vascular bifurcations with the iliac bifurcation being assumed as a dominant reflection source [16,18]. The summation of these two waves is a result of pressure augmentation and gives the overall pressure load profile on the vessel through which they propagate [17]. The shape of the pressure waveform depends on the velocities of the respective waves and their mutual position. Therefore, as mentioned above, since the arterial stiffening increases the pressure waves velocities, an earlier reflection of the backward wave occurs causing a change in the waves mutual position. Consequently, due to the alignment of the waves peaks, the overall systolic peak increases while diastolic pressure decreases (figure 8) [17].
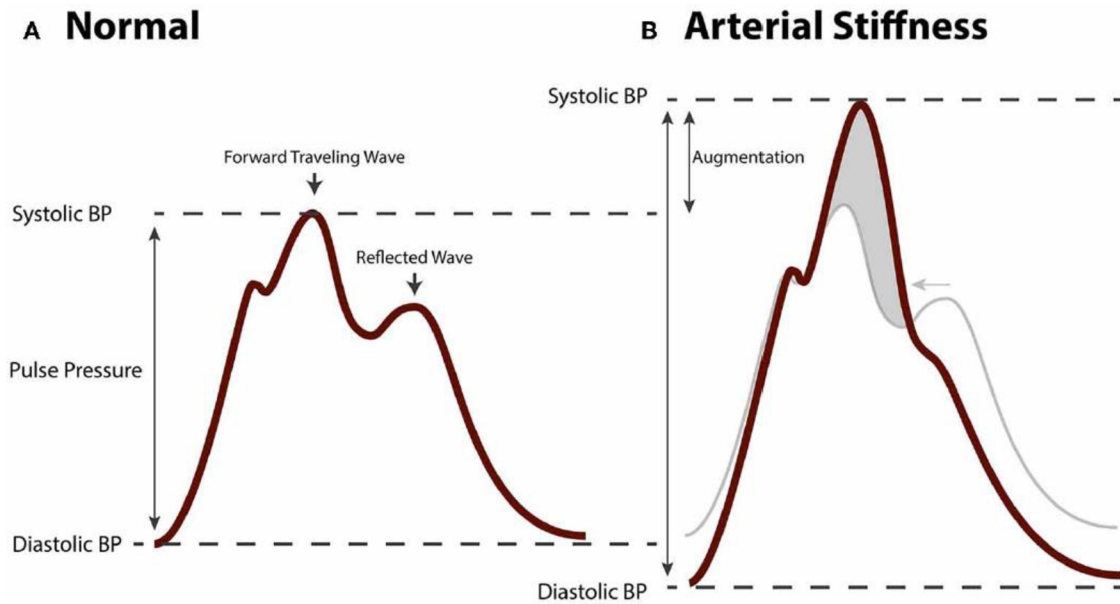
Figure 8 The pressure waveform changes due to arterial stiffening. The increase in pressure wave velocities causes a difference in forward and reflected wave alignment resulting in the waveform peaks growth [17].

Also, the increased blood pressure pulsatile behavior creates greater stresses acting on the vessel walls. Thus, with each cardiac cycle, the vessel wall undergoes increased contractions and expansions leading to a higher stretch of elastin and collagen fibers inside the vessel wall. This may lead to increased risk of material fatigue, degradation or other damage as well to AAA development [17,35].

2.3 Blood vessels

Blood vessels form a closed system of elastic tubes of different cross sections that are responsible for the transport of blood through the body. The vessels can be divided into five categories: arteries, arterioles, capillaries, venules and veins each having a unique structure and properties to serve a unique function [10,20]. For the purposes of this thesis, only a description of abdominal aorta anatomy is relevant.

2.3.1 Abdominal aorta

Transporting the oxygenated blood towards all abdominal and pelvic organs, abdominal aorta is a direct unpaired continuation of the thoracic aorta. Abdominal aorta travels through the abdomen on its posterior wall, inferior to the vertebral column beginning at the level of the last thoracic vertebrae and ending at the iliac bifurcation. The abdominal aorta has several branches that can be divided into parietal branches (most often located at the anterior side, supplying surrounding walls) and visceral branches (supplying organs) that are either paired or unpaired (figure 9) [19].
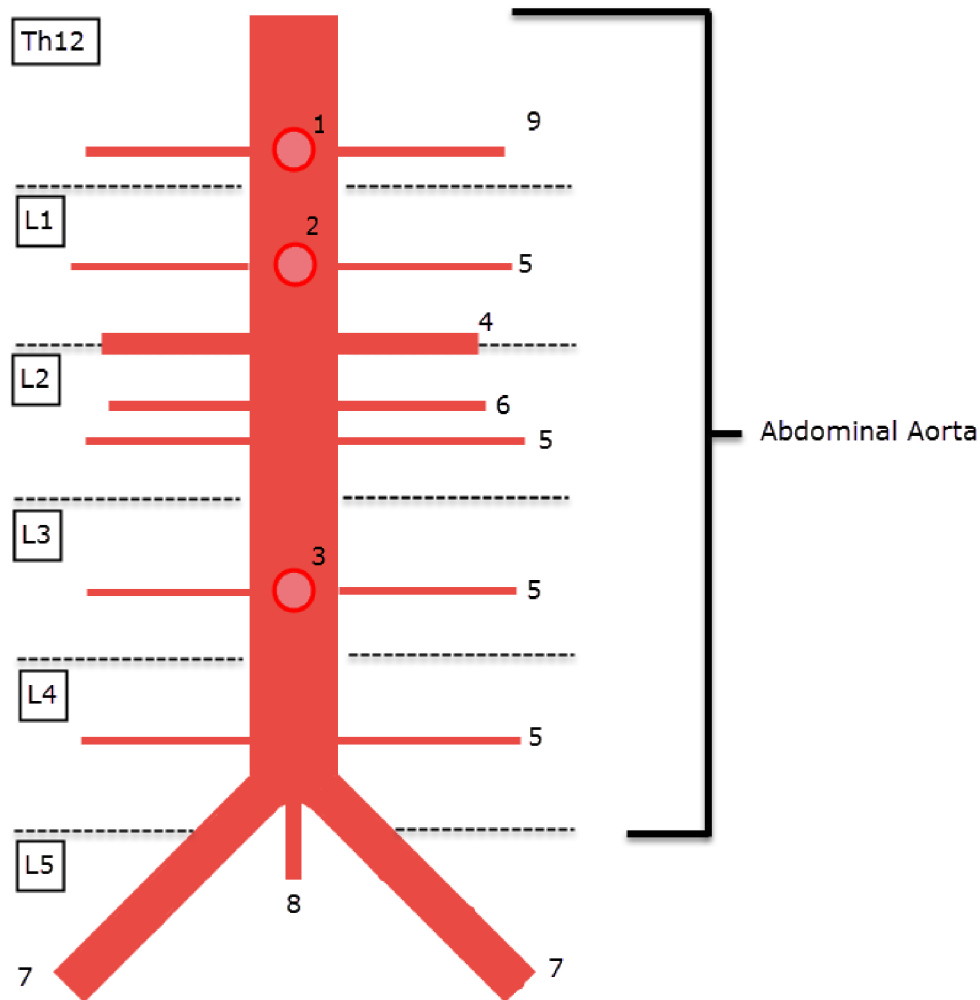
Figure 9 Diagram of the abdominal aorta with its parietal (5,8), unpaired visceral (1,2,3), and paired visceral (4,6,9) branches. 1- Coeliac axis, 2- Superior mesenteric artery, 3-Inferior mesenteric artery, 4- Renal arteries, 5- Lumbar arteries, 6- Testicular arteries, 7- Common iliac arteries, 8- Medial sacral artery, 9- Middle suprarenal arteries.

2.3.2 Arterial wall structure

Certain cardiovascular vessel walls are made to withstand their functional demands. Aorta is an elastic artery adapted for pulsatile loading generated by the heart. It is made of nerves, smooth muscle, extracellular matrix and another different type of cells each fulfilling a specific purpose, creating three distinguished layers: tunica externa, tunica media, and tunica intima. Moreover, due to the great thickness of the artery wall, local system of blood vessels is necessary to nourish the layers spaced out of the blood stream and can not be reached by the diffusion of nutrients through the wall [10,19]. The artery wall with the distinguished layers is shown in figure 10.
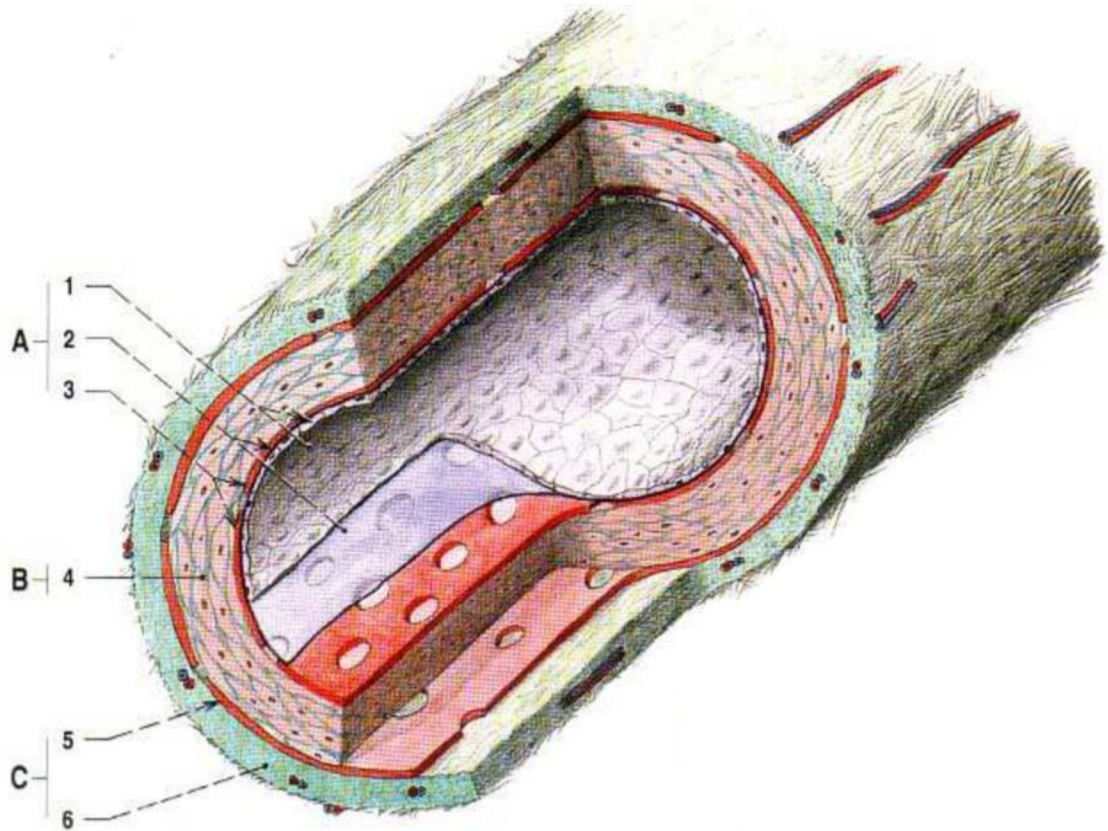
Figure 10 Arterial wall structure [19].

A Tunica intima

   1 endothel

   2 lamina basalis (serves as attachment for cells)

   3 membrana elastic interna

B Tunica media

   4 smooth muscle cells

C Tunica externa containing blood vessels (vasa vasorum)

   5 membrana elastic externa

   6 connective tissue containing small branches

2.3.2.1   Tunica externa

Tunica externa, or Adventitia, is the outer layer of the arterial wall containing sparse elastin fibers, nerves but mainly fibroblasts producing irregularly oriented type I collagen [20]. Fibers on the outer surface overlay each other creating a network that interacts with the connective tissues in the near surroundings forming a flexible attachment of the artery in space while on the inner side, an elastic layer (membrana elastica externa) separates the adventitia from the muscle cells of the media layer [19]. Also, the collagen fibers remain most of the time corrugated as they straighten only in cases when over-distention of the media layer (smooth muscle cells) occurs protecting the vessel from tearing apart

27

[20]. Additionally, in large arteries, small branches, own or from a neighbor artery, are present providing oxygen and nutrients [20].

2.3.2.2 Tunica media

Tunica media is the most robust out of the three layers. It comprises primarily of smooth muscle cells (SMCs), that are circumferentially (potentially in low spiral threads) oriented, embedded inside a spatial network of elastin, collagen (types I, III, V) fibers, and proteoglycans. Elastin fibers create elastic lamellas separating the media into layers [19, 20]. Even though the primary purpose of the SMC is synthesizing proteins that are during maturing forming the elastic network, it also provides the ability of the artery to remodel its geometry to enhance blood flow regulation [20]. Smooth muscle hypertrophy (increase in size), hyperplasia (increase in number), apoptosis (cell suicide), and migration each play essential roles in diseases such as aneurysms [19]. Elastin, on the other hand, is responsible for absorbing the load created by the pulsatile blood flow properties allowing the artery to dilate and contract which help to the blood movement [20]. Thus, a number of elastin fibers and SMCs vary based on the size and location of the artery with the content of elastin increasing with the artery bulk while decreasing with the distance from the heart [19,20].

2.3.2.3 Tunica intima

The inner layer of the arterial wall, tunica intima, is made of a monolayer of endothelial cells attached to the adhesive basal layer which is made of mesh-like type IV collagen and molecules of fibronectin and laminin having primarily adhesive function [19,20]. Similarly, to the adventitia-media interface, tunica intima is separated from the media by a thin elastic layer called membrana elastic interna [19]. The endothelium creates a smooth non-thrombogenic contact between the blood and the arterial wall. Moreover, the endothelium serves as a sensitive sensor that based on mechanical and chemical stimuli affect remodeling, cell replication, protein synthesis or the clotting process. [20].

2.3.3 Biomechanical properties of aorta

The knowledge of the biomechanical properties of either healthy or diseased arterial wall is a key feature for proper modeling. In abdominal aorta, arterial pressure is projected into mechanical wall stress. Thus, from the mechanical point of view, the aorta can be treated as an inflated tube, since it maintains its volume under deformation [24]. Physiologically, the diameter of a certain part of aorta corresponds to the magnitude of the arterial pressure that it needs to withstand. The higher the pressure is the thicker is the aorta as well as the aortic wall. The increased size in the arterial wall is given by a number of the medial lamellar units (MLU), resulting in a constant overall average load of a single MLU of 2 ± 0.4 N/m [24]. Also, since the aorta becomes stiffer under strain, the same part of the aorta will be stiffer when loaded with hypertensive pressure than in a normal state [24].

Due to a high content of water, this composite-like material is nearly incompressible as well as manifests nonlinear stress-strain behavior (figure 11) as the, in normal state corrugated, collagen fibers straighten during increasing deformation stiffening the whole structure. Also, the arterial wall, a soft tissue material, exhibits viscoelastic behavior as

hysteresis, creep and stress relaxation phenomena can be observed under cyclic loading [31]. However, in the majority of physiologic and pathophysiologic states, the assumption of hyperelasticity (for definition see 2.3.3.1) is relevant [20]. In a normal state, arterial walls are pre-strained in the axial direction and pre-stressed in the circumferential direction. This is caused by smooth muscle cells maintaining ideal stress-strain conditions [31,67]. Therefore, samples subducted from the body shorten in the axial direction and open up when cut in the axial direction as a consequence of the residual stresses [31].
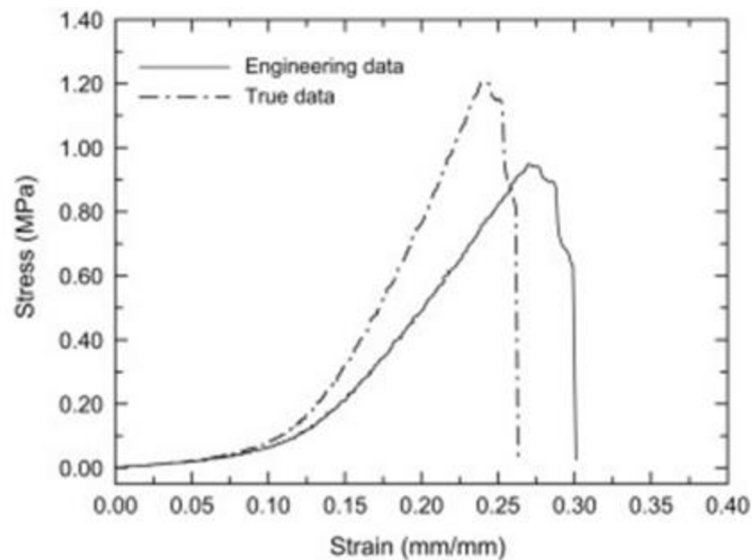
Figure 11 Human aorta stress-strain curves determined by engineering and true stress definitions, showing stiffening of the material at higher strains due to collagen fibers activation [32].

2.3.4 Arterial wall remodeling and aging

As a consequence of an injury or disease, changes in arterial wall structure and function occur. To some level, remodeling of the arterial wall is a part of natural aging of the organism, however, early changes of the wall properties may cause disruption of natural hemodynamics and respective cardiovascular complications. Among the most common mechanism damaging the arterial wall properties are fibrosis, changes in vascular collagen and elastin or calcification [17]. In cases of AAA, calcification is usually present in the external regions of the media layer, inhibiting the aneurysmal expansion [71]. Very often in the aneurysmal wall, there is a lack of elastin fibers compared to a healthy wall [20]. It has been found that the number of elastin fibers in medial lamellas during AAA development decreases to 20% of the normal values resulting in a destruction of the lamellar structure of the medial layer. As a substitution collagen fibers are synthesized or recreated from other degraded tissue reacting on the increases stress stimuli as the wall becomes thinner. The disappearing elastin has a negative impact on the wall mechanical properties as it is very important for a wall stability and stiffness especially in lower strains [17,32]. However, the ability of the vascular SMCs to synthesize extracellular matrix containing elastin fibers is decreasing as well which has a major impact on arterial wall mechanics [33], since also the collagen

fibers are perishable. Even though there are associations speeding up collagen degradation process, it is also just a natural consequence of aging that is nothing more than a material fatigue caused by cyclic loading of the fibers during each cardiac cycle. Since higher loads, shorten the elastin fibers lifespan, hypertension can significantly influence the stretches of the fibers and speed up their degradation, consequently raising the chances of cardiovascular disease development of any type [17].

3   AAA

Pathological remodeling process of the connective arterial tissues that can not be reversed lead to a disease called aneurysm [23]. This asymmetrical dilatation most often develops from aged vessels under the influence of co-morbidities affecting the mechanical properties of the vessel wall [21]. The remodeling process includes substituting elastin for collagen and increased collagen cross-linking altering the stiffness of the vessel wall [23].

Typically, AAA occurs in the infrarenal aorta, located between the renal arteries and aortoiliac bifurcation (figure 12), which is smaller in diameter (around 2 cm) and has a thinner wall (around 0.2 cm) than the suprarenal aorta. These geometrical differences are caused by the fact that 19% of the blood volume is drained out by the renal arteries decreasing the volumetric blood flow in infrarenal aorta [21]. The aneurysm wall is in majority of cases dilatating into the anterior or anterior-lateral side due to a support from the spine on the posterior side [34]. Moreover, the direction of the bulk's growth is important due to the formation of contacts with the surroundings when the deformation of a posteriorly oriented bulk may be significantly restricted by the stiff vertebral column. Also, according to hemodynamics studies, infrarenal aorta experiences oscillatory shear stresses due to a momentary reversed blood flow which also makes this region more sensitive to AAA development [21], as well as the fact that the iliac bifurcation is assumed to be a dominant reflection source of the pressure wave causing summation of the forward and backward traveling wave and thus increasing the overall pressure load of the vessel [16,18].
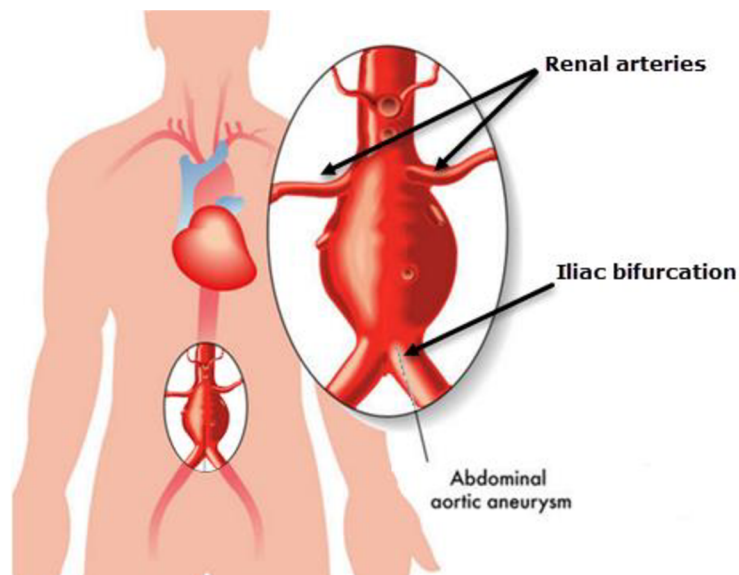

Figure 11 General location of Abdominal aortic aneurysm between renal arteries and iliac bifurcation [28].

3.1 AAA risks

Preventive ultrasound screening can reveal aneurysms in dangerous of rupture and reduce mortality, however, the screening is available only for a limited group of the population that is associated with increased AAA rupture risks, raising the importance for the determination of the risk factors [35]. There are several risk factors increasing the chances of AAA development. The main risk factors are male gender, age, cigarette smoking and hypertension, however, atherosclerosis, prior surgery, spinal cord injury or genetics can contribute to the AAA development as well [21]. While it is observed that spinal cord injury or prior surgery can disrupt the infrarenal aortic hemodynamics, the reason of gender importance is unknown, even though men are 6x more likely to develop AAA than women and women with existing AAA are 3-4 x more likely to experience AAA rupture [21]. Nevertheless, due to a study containing cohort of more than 3 million patients, providing a distribution of occurrence of wide range of variables among population with and without AAA (table 1), despite these risk factors, AAA affect large fraction of non-smokers (19.8%) and women (20.7%) as well [35].

| | Screened population | |
	Without AAA	With AAA
Variables	(N =3,033,009)	(N =23,446)
Gender		
Females	65.07%	20.66%
Males	34.93%	79.34%
Age groups		
<55	20.24%	1.83%
55-59	15.99%	4.87%
60-64	19.19%	13.26%
65-69	16.97%	20.14%
70-74	13.24%	23.48%
Other		
Smokers	42.47%	80.22%
Current smokers	10.68%	28.09%
Past smokers	31.79%	52.14%
High blood pressure	65.02%	81.51%
Controlled	19.49%	22.86%
Uncontrolled	27.09%	38.61%
High cholesterol	53.89%	68.06%
Coronary artery disease	6.72%	26.69%
Family history		
AAA	2.48%	7.95%
Overweight	66.73%	73.30%

Table1 Occurrence of variables among people with and without developed AAA giving a summary of certain aspects importance. The data obtained from [35].

3.2 Mechanical properties of the AAA wall

As being mentioned above, the structure of the aneurysm wall is very different from the one in a normal state. Therefore, substantial changes in biomechanical properties are the consequence of the wall remodeling. The material properties report a significant dependence on the location of the tested specimen. As shown in figure 13, the material response is different for lateral, posterior, and interior regions as well as for longitudinal and circumferential direction [34].
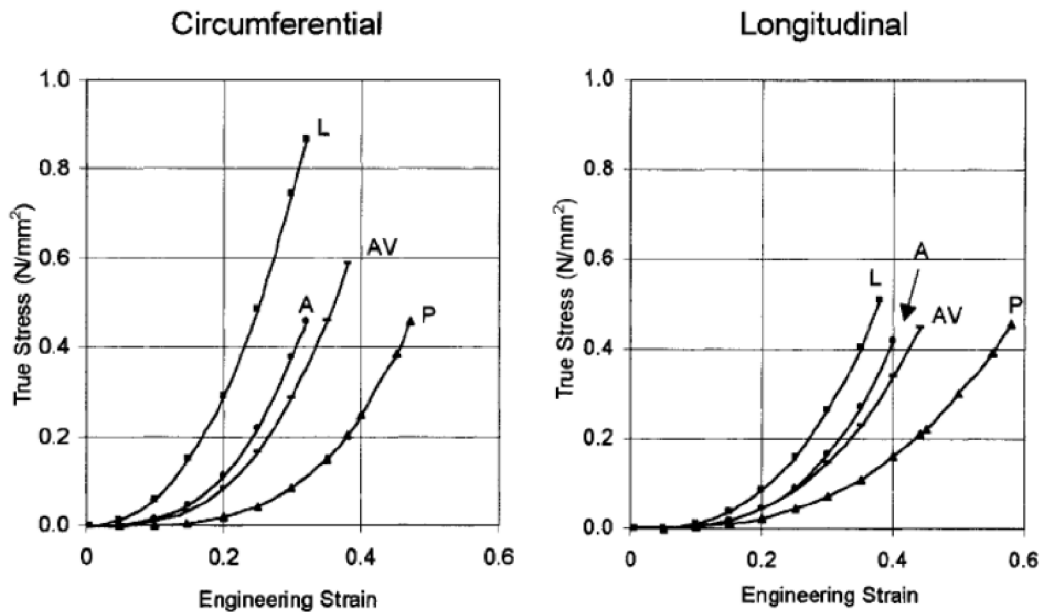
Figure 13 Stress-strain curves for lateral (L), anterior (A), posterior (P) region of AAA are showing that the stiffness of aneurysm wall decreases from lateral to anterior to posterior zones. The AV curve represents the average of all samples [34].

To compare the results obtained for the aneurysmal wall with a normal aortic wall, the changes of internal wall structure causes that the aneurysmal wall manifests overall stiffer behavior (figure 14) [34]. This is the consequence of straightening collagen fibers which in a normal state are slack and remain unloaded. Due to the elastin degradation, the elastin to collagen ratio for the aneurysm wall is smaller than the one of normal wall, being the cause of the changes in stress-strain material response when the small strains zone characterized by the load being carried by elastin fibers, while the collagen fibers are slack, is reduced [33,45]. As a consequence of the wall remodeling, especially a difference in collagen orientation and crosslinking causes anisotropy of the aortic wall, which circumferential and longitudinal stiffness at normal state differs, disappear [24].
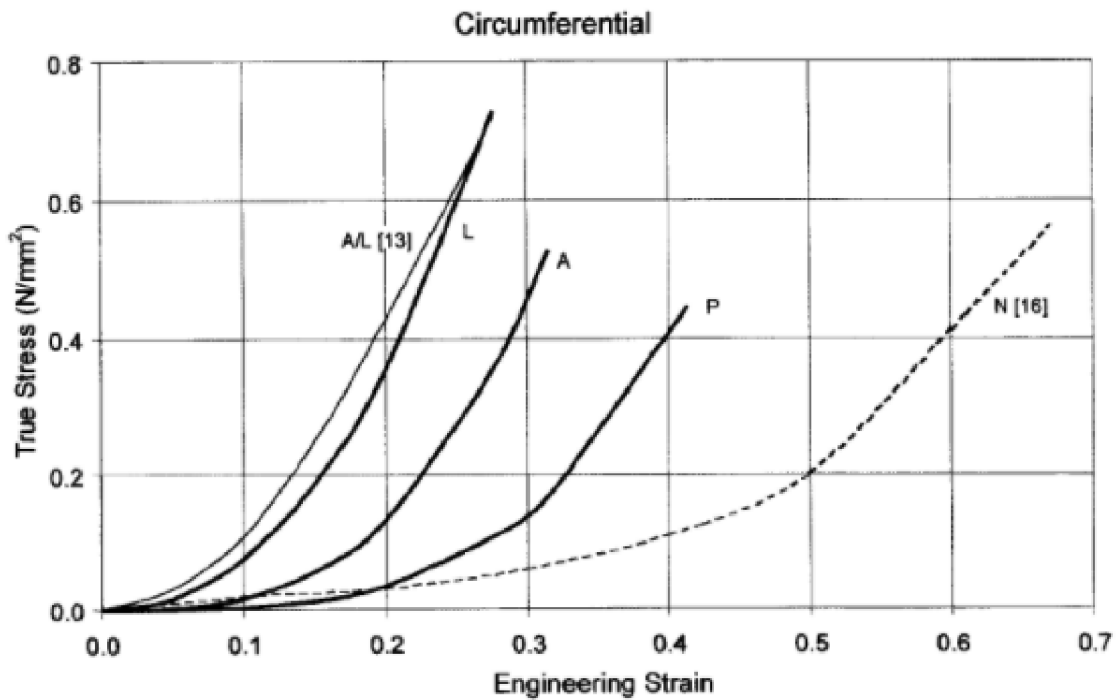
Figure 14 Comparison of the AAA wall and normal aortic wall stress-strain curves in circumferential direction where L, A, and P are lateral, anterior and posterior samples of the AAA wall respectively while N corresponds to a normal wall response. The A/L curve is present for comparison with a different study [34].

4 ILT

The variability of AAAs clinical outcomes has been attributed to the presence of ILT, which can be found in the most of the AAAs (figure 15). The size of ILT can be anywhere in the range from few millimeters to several centimeters [25]. ILT consists of activated platelets creating an interconnected fibrin mesh, with various amounts of red and white entrapped blood cells. The ILT is a complex structure with histology dependency on time and location within the AAA body [3,25].
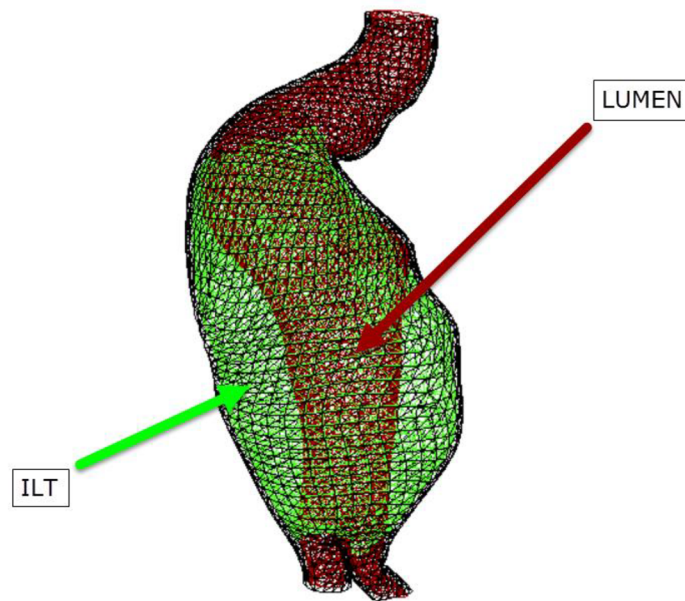
Figure 15 Example of an ILT presence in AAA.

4.1 Development of ILT

Following text is based on findings in [25]. Disturbed blood flow in the AAA region is responsible for a development of vortical structures that most likely play a key role in creating an environment that allows processes necessary for ILT formation and grow. The presence of vortices (2.1.2) creates zones of high fluid shear stresses that cause activation of blood platelets. On the other hand, it has been recorded that the shear stresses measured close to the aneurysm wall are lower than stresses experienced by healthy endothelium. This allows for increased adhesive conditions at the aneurysm wall and gathering of the activated platelets. In the early stages of ILF development, the gathered activated platelets start to break down fibrinogen into fibrin. Followingly, polymerized fibrin creates a mesh that contains a small amount of entrapped erythrocytes and leukocyte. As new platelets are captured from the blood stream and old blood cells captured in the mesh lyse, the fibrin density of the porous structure increases and becomes unsuitable for new cells entrapment.

4.2 Types of ILT

Based on the ILT structure and mechanical properties, there are two distinguishable types. For the first type of ILT gradual transmural changes of structure and strong connectivity in the radial direction are typical, when on the other hand the second (discrete) type exhibits layered structure with sharply defined boundaries and weak mutual connectivity. Consequently, properties of these, typically three, layers are generally different. It was observed that the structure type of the ILT corresponds to the process of its formation when a gradual build up results in ILT with a continuous

transition of structure and properties while discrete and temporary deposition is characteristic for the creation of heterogeneous layers (figure 16) [25].
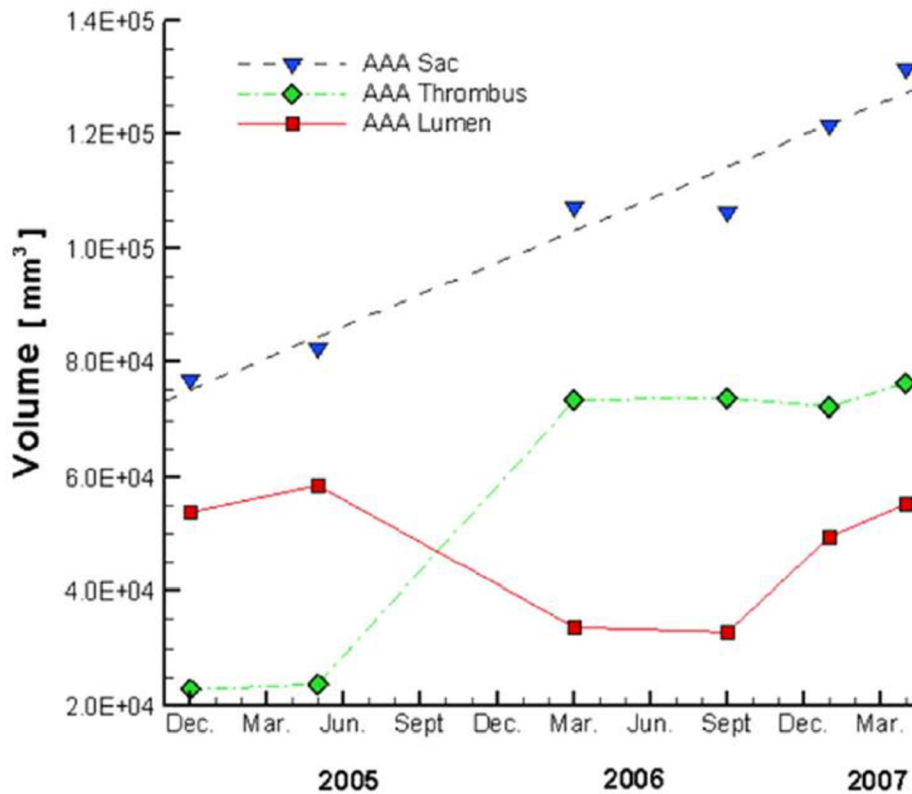
Figure 16 History of patient's AAA volume (AAA Sac) development with distinct temporary ILT (AAA Thrombus) deposition between Jun. 2005 and Mar. 2006. It can be observed that the increase in AAA volume is compensated by the increase of either thrombus of lumen (AAA Lumen) volume with one being indirectly proportional to the other [25].

All ILT tested in this thesis had distinguishable layers, therefore only the layered type of ILT will be discussed in the following chapters.

4.3 Layered ILT

As mention above, layered ILT usually consist of three layers: luminal, medial and abluminal as it refers to their position relative to the aneurysm lumen (figure 17), however, this characterization does not correspond to the ILT tissue biochemical or biomechanical properties and not all thrombi consist of all three layers. It was suggested that there is a need for further classification of ILT since the mechanical and histological aspects of all three layers evolve with aging as degradation of all layers was recorded with increasing age. On the other hand, it has been found that unlike most thrombi in the human body that resolve over time, ILT experience replacement of the fibrin network with collagen and other processes that may be signs of healing [25].
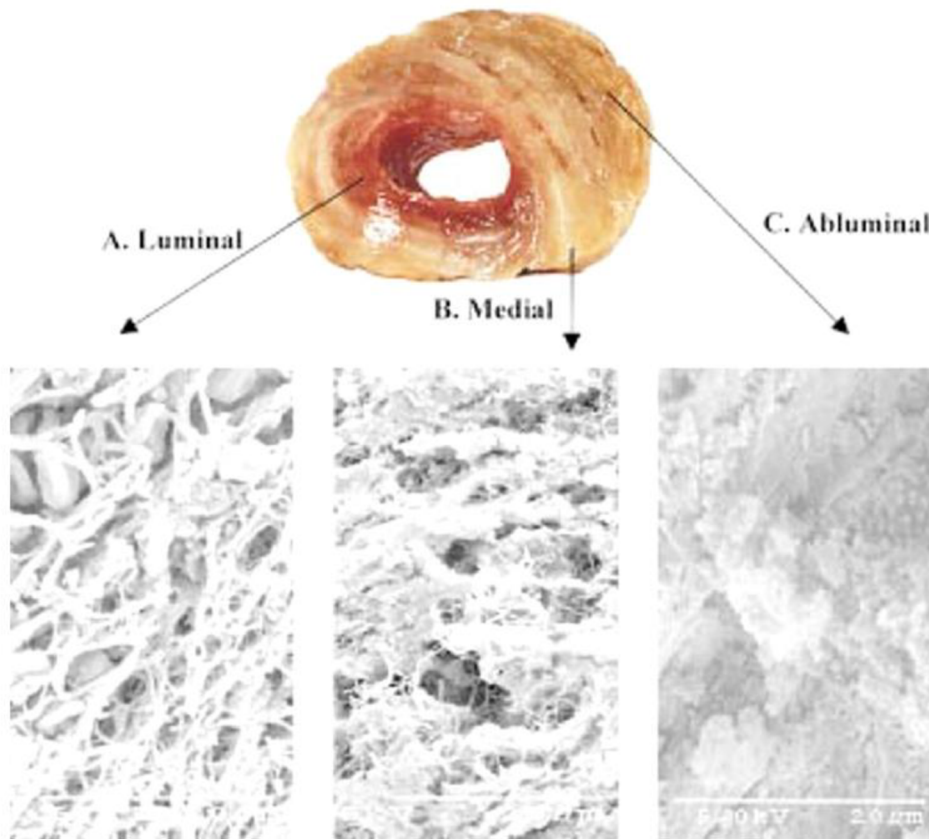
Figure 17 Overall and structural images of an ILT consisting of luminal, medial and abluminal layers. There are entrapped blood cells distinctly visible in the structure of the luminal layer while the older medial layer is porous. Degraded abluminal layer with no fibrin mesh organization is shown in the bottom right layer [25].

The nearest layer to the lumen, the luminal layer, is also the youngest and has a red color due to a high content of entrapped red blood cells which lyse over time making the adjacent medial layer to be yellow or white. Despite a dense fibrin network, the medial layer lacks the presence of leukocytes and intact erythrocytes. As the ILT becomes older its distance from the lumen increases due to new thrombi deposition at the ILT-blood stream interface. Thus, the ILT changes its structure and properties because of lysis of erythrocytes, leukocyte apoptosis, and fibrinolysis. In some cases, the most distant from the blood stream, abluminal, layer appears brown. The abluminal layer may also by separated from the arterial wall by a thin film of liquid that may be a consequence of full ILT degradation. Also, as shown in the bottom images of figure 17, aging of ILT is associated with the fibrin mesh degradation. In the young, luminal layer, the fibrin mesh is formed by thick primary, and thin secondary fibers of fibrin, creating a well-organized and finely interconnected mesh. As the ILT becomes older, the secondary fibers disappear contributing to the mesh degradation as seen in the medial structure. In abluminal layer, almost no fibrin mesh organization is found. The structural decomposition of ILT layers is adequate to the different mechanical properties [25].

According to mechanical tests, increased stiffness and strength for the luminal layer was found compared to the medial and abluminal layers, as the stiffness of the layers from the lumen to the wall decreases. Also, comparison of axial and circumferential values indicates material isotropy and nonlinear hyperelastic behavior [25].

4.4 Effects of ILT on AAA

Thorough AAA wall rupture data analysis revealed that the majority of ruptures is located in the region covered by the ILT or in its near surroundings [44]. On the other hand, despite the fact that in comparison with a wall covered with thin thrombus, AAA wall covered with a thick thrombus has fewer elastin fibers, a higher amount of inflammation and lower tensile strength, higher average thrombus thickness is reported for non-ruptured AAAs compared to ruptured AAAs [25]. Therefore, most of the wall degenerative processes may occur in the wall in contact with the luminal layer while further deposition and ILT enlargement may have a protectivity role, shielding the wall from stresses as well as spacing the wall from the biologically active luminal layer [2,25]. Thus, if thin thrombus cause degradation of the AAA wall by excess proteases, the subsequent wall expansion creates disturbed hemodynamics inducing a new thrombus deposition making the growth rate of ILT better rupture prediction parameter than maximum size of the ILT as the growth rate may correspond to amount of the damage induced in the wall [25].
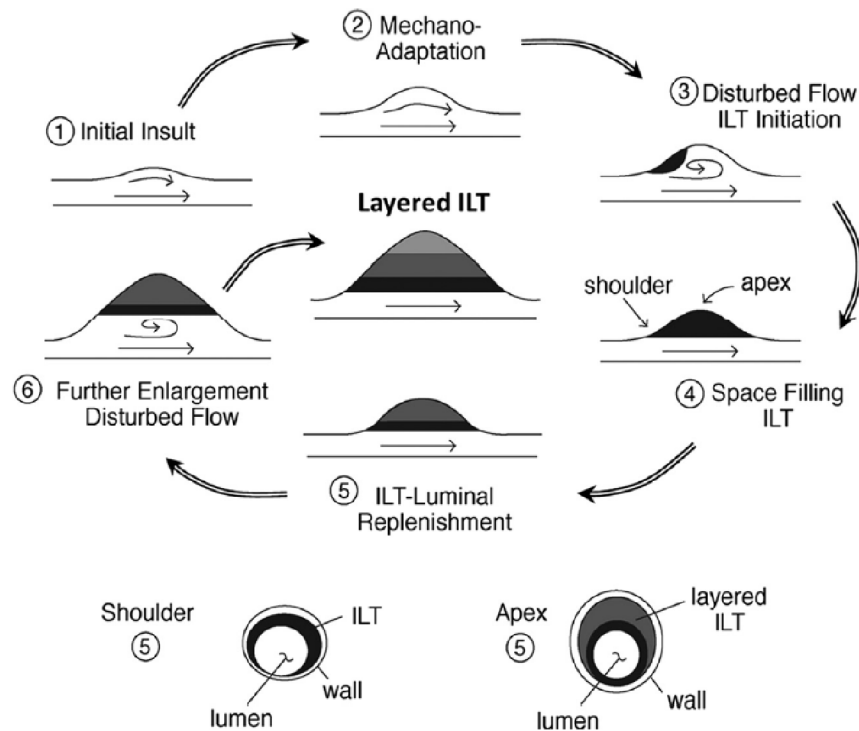
Figure 18 Formation of layered ILT by stepwise bulk enlargement and thrombus filling due to disruption of the blood flow. The initiation of thrombus formation in 3 is schematic. Pictures 5 - Shoulder and 6 - Apex represent two cross-sectional views at the AAA shoulder and apex respectively. Notice the luminal layer being in contact with the wall in AAA shoulder but shield from the wall by the older layer at the apex region [25].

However, even a thick thrombus with the apex spaced out from the luminal layer by medial and abluminal layers causes damage to the wall by the biologically active luminal layers at the aneurysm shoulder regions. The shoulder regions are proximal and distal zones between the dilated and intact aorta (figure 18). Thus, in these zones, the developing aneurysm wall remains in direct contact with the fresh luminal layer

experiencing more thrombus-derived proteases. These shoulder regions may play an important role in predicting the aneurysm axial expansion into proximal and distal non-dilated surroundings (neck regions) [25]. On the other hand, since the thrombus tissue tends to stymie oxygen transport from the bloodstream to the underlying aneurysm wall, the more ILT tissue occurs between the lumen and the wall the stronger hypoxia of the wall supervene. As a response of the wall tissue, increased vascularization and inflammation takes place further contributing to the wall weakening by decreasing the synthesis of collagen and elastin as well as activating other mechanisms that contribute to the material degradation [36]. The appearance graphical representation of the above-mentioned consequences of increased ILT thickness is shown in figure 19.
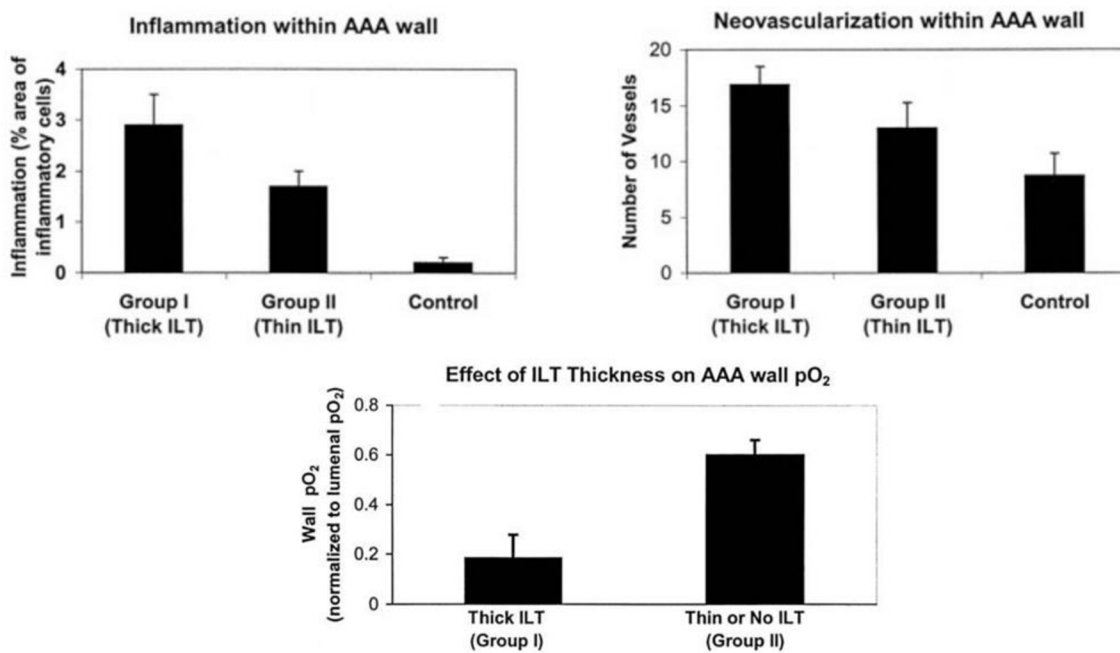
*Figure 19 Representation of inflammation, neovascularization, and oxygen saturation dependence on ILT thickness. The oxygen saturation is described by PO₂ (*100%). PO₂ corresponds to partial oxygen pressure. A cohort of 11 patients with AAA was divided into group I that corresponds to patients with ILT thickness of 4 mm or greater while group II represents patients with ILT thickness of 4 mm or less or no ILT at all. A control sample was obtained from a non-aneurysmal wall [36].*

Even though, some papers conclude that the ILT does not significantly reduce the pressure near the aneurysm wall and therefore does not a reduce the rupture risk [8,37], as being mentioned previously, many computational studies [25,40,72] on the other hand support, that ILT presence in AAA provides mechanical protection of the dilatated wall. However, this protection by pressure shielding strongly depends on the form of attachment of the outside ILT layer to the aneurysm wall and the variable mechanical properties of the ILT itself, especially the level of porosity. Since the external layer of the ILT may be a liquid phase, strongly degraded abluminal layer or in cases of small ILTs

an active luminal layer, the adhesive interphase between ILT and AAA wall may acquire a wide range of forms. For instance, it has been suggested that only partial attachment of the border ILT layer to the AAA wall may create stress concentration and increased wall stress. Therefore, further testing is needed in order to solve this question [25].

Due to the ILT structure complexity and variability, the overall role in influencing the AAA rupture with all its aspects remains unsolved and may be a subject for further investigation. However, since the ILT alters both, the strength of the weakened vessel wall and the mechanical stress that the wall needs to withstand, understanding the ILT role in AAA mechanics may contribute to better rupture risk predictability, especially in cases where the ILT failure occurs prior the AAA wall failure and may be the cause of the rupture [2,3,25]. The fact that maximal and minimal circumferential stresses at a pressurized thick-walled tube occur at the inside and outside of the tube wall, respectively, support this possible scenario [3].

5 Existing data of ILT Mechanical Properties

According to studies determining that the in vivo inner circumferential strains of AAAs during systole can reach 15% [38], it is obvious and has been conducted that ILT undergoes large deformation in vivo [26]. As being conducted by noninvasive ultrasound investigations, ILT is incompressible and the majority of computational works to date consider incompressibility when modeling ILT [3,25,26]. Due to mechanical testing, isotropy and linear response of ILT material can be considered when modeling [22,25,27] which is also supported by the results of mechanical testing in 6.3.

Among studies performing mechanical tests of ILT specimens vande Geest et al. [30] provided data obtained from the uniaxial test of luminal layers when Gasser et al. [3] performed biaxial tests for all three layers. A comparison of models describing biaxial tension behavior from both sources is shown in figure 20.
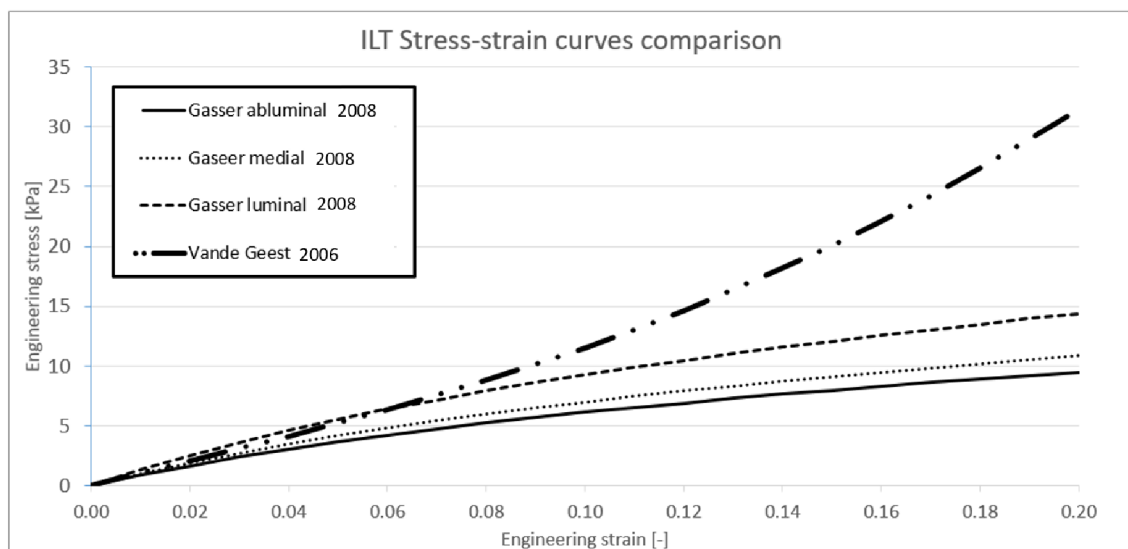

Figure 20 Comparison of models describing the stress-strain response of an ILT tissue. Vande Geest in [30] tested luminal layer and based his model on uniaxial tensile test while Gasser [3] used biaxial test for all three tested layers of the ILT.

Assessing the values of the ILT mechanical properties available in the literature, a big range of experimental results can be observed, increasing the importance of patient-specific values in a relevant modeling of AAA including the ILT. More importantly, in most studies [3,22,25,27,38,42], the ILT is defined of having three distinguished layers (luminal, medial and abluminal). Thus, the tested specimens are referenced to these layers without any information about their distance from the lumen or aneurysm wall, which would give more precise information when considering these data as an input for computational modeling. As being mentioned earlier, the mechanical properties are gradually decreasing with the distance from the luminal wall and the gradient of properties across the thickness of the ILT body is also different for each thrombus. It has been suggested that the magnitude of differences in mechanical properties across one thrombus is of the same order as the variations among different patients [38]. Thus, it is difficult to answer the question if the differences in obtained mechanical properties from available studies are caused by the morphology of tested ILTs or by the fact that these compared results, in fact, correspond to ILT parts with different distances from the lumen, therefore having different structure [25,38,42]. Importantly, since till this date there are no studies that would describe their tested specimens of ILT by the precise distance from the lumen or AAA wall, the goal of this thesis is to induce data from such samples, described by precise position within the ILT body, in computational modeling revealing the uncertainties of FEM AAA wall stress analysis without using patient-specific values of ILT mechanical properties.

It has been suggested that the AAA wall stresses can by overestimated by 67% [60] when using material models based on uniaxial tensile test, therefore, ILT stiffness value introduced by Gasser et al [3], who based his model on biaxial tensile test protocols, were used in this thesis as a mean population values in AAA wall stresses computations.

6 Mechanical tests of ILT

Samples of ILT from 5 patients were obtained from AAAs surgical repairs (figure 21 shows the orientation of the sample) and stored frozen for several months. A negative influence of freezing the ILT samples on its mechanical properties has not been found. [3,38]. Before preparation of the test specimens, the ILT was thawed at room temperature. Each ILT bulk was sliced into layers of thickness roughly around 3 mm, as illustrated in figure 22, in order to obtain sheets of ILT tissue with different distances from the lumen and thus with different structure and mechanical properties [38].
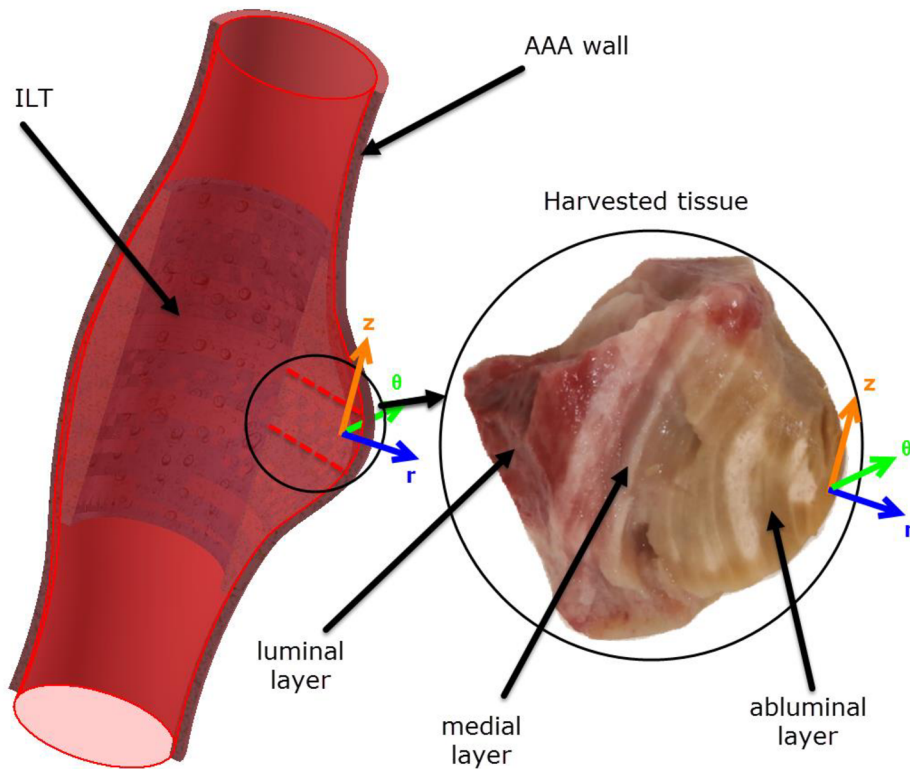
Figure 21 Schematic view of the harvested samples position with determination of the sample orientation

According to the condition of each ILT sample, as many sheets were obtained throughout the ILT thickness as possible. From each sheet, one biaxial sample was obtained. In some cases, the tissue closest to the lumen was not large enough for a biaxial specimen to be obtained. More importantly, in all cases, the tissue closest to the AAA wall (abluminal layer) was unsuitable for testing due to its poor mechanical state. The summary of the in total 8 biaxial specimens described by their position with respect to the lumen is shown in table 2. Sample B3 from patient 1 fell apart during the initial stage of testing due to its poor condition caused by previous surgical and preparation procedures and therefore, was excluded from the further experimental testing.

				Distance			Thickness		
Patient #	Age	AAA ø	ILT Thickness	B1	B2	B3	B1	B2	B3
1	71	76	28.00	9.63	12.71	16.15	3.08	3.44	3.98
2	68	49	9.50	0.00	2.80	-	2.80	3.51	
3	76	55	21.00	0.00	-	-	3.59		
4	80	58	25.00	4.50	-	-	3.46		
5	66	-	7.00	0.00	-	-	3.20		

Table 2 Overview of the patient's age, AAA diameter [mm] (data not available for patient 5), ILT thickness [mm] (refers to the thickness of the harvested sample) and the biaxial tested specimens (B1-B3). The values indicate the distance [mm] of the specimen from the lumen. Samples with one side being part of the lumen have values 0 mm.

41

6.1 Biaxial testing rig

Testing of specimens was performed by using a biaxial testing rig (figure 22) consisting of a base desk and four arms enabling movement in two perpendicular directions. Mounted on two orthogonal ball screws, the arms are made by force gauges, servo motors and four carriages connected by sets of levers to clamps submerged in a testing pool allowing for testing samples in physiological saline of specific temperature (37 ± 0.5°C) preserving the samples in close to in vivo environment to avert biological degradation. It has been suggested that such an environment has negligible effects on the ILT elastic properties [3]. The clamps are equipped with sprigs of reduced stiffness. Above the pool, CCD programmable camera is located measuring displacements of contrasting points on the tested specimen by a contactless method. To control the measuring process, computer software is used to set inputs and collect results.

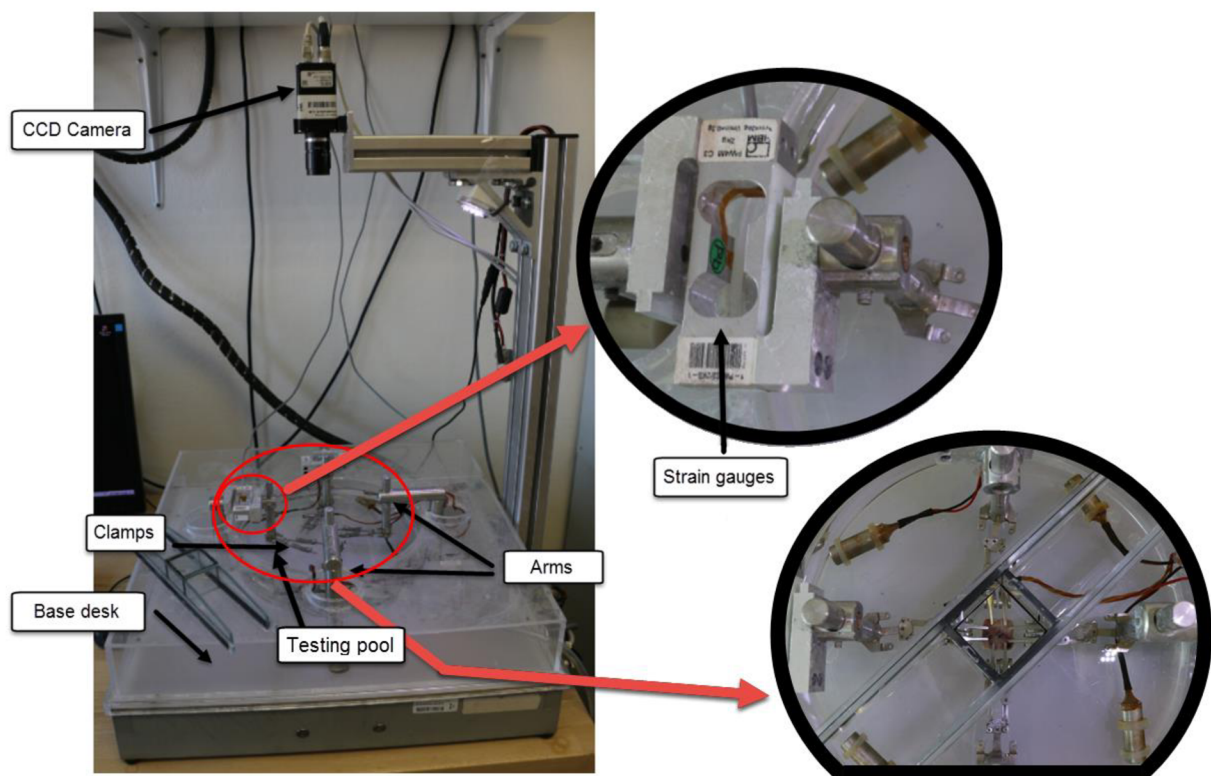*Figure 22 Biaxial testing rig*

6.2 Experimental procedure

During the experimental procedure following task were completed:

1. Preparation of the samples from ILT bulk
    a. Slicing the ILT into layers and measuring their thickness
    b. Punching out of specimens of defined dimensions
    c. Creating contrast marks for displacement software processing
2. Test set up
    a. Mounting the specimens

       b. Preloading the specimens

       c. Applying defined loads

3. Recording of measured load with corresponding displacements and evaluation of stress-strain curves

6.2.1 Preparation of the samples from ILT bulk

AS being pointed out in the review section, mechanical properties of the ILT depend on their distance from the bloodstream [25]. Therefore, in order to obtain the gradient of ILT stiffness from the luminal to the abluminal part, tested ILT bodies were sliced along their thickness into approximately 3 mm thin slices. Followingly square specimens (dimensions in 6.2.1.1) for the biaxial tests, were cut out from the slices so that the circumferential and longitudinal directions remained parallel to their edges and uniquely labeled. Special pattern blade with derived dimensions was used (figure 23). For the CCD camera contactless evaluation of displacements, contrast marks, approximately forming a 5 mm x 5 mm square, were drawn on the center of the samples top surface by alcohol-based ink. Due to the fact that the samples contained a high amount of liquid (by their nature) and were wet from the physiological saline, the adhesive properties of the ink were very poor and creating sufficient marks, in order not to decrease the detective abilities of the camera, was a difficult task. This part of the preparation process has a room for improvement. In other to preserve the tissue structure, samples were kept in physiological saline of $37 \pm 0.5°C$ temperature. This step has been reported as a crucial in order to obtain reliable results [3]. Before mounting the specimen in the testing machine its average thickness, derived from three measurements, was obtained by a drift meter. When mounting the specimens in the testing machine, special attention was given to the sample clamping process by clamps with reduced stiffness in order to avoid damaging the sample and any kind of failure. Importantly, all specimens were kept hydrated in a physiological saline (0.9% NaCl) of 37°C temperature during the preparation process. The prepared specimen is shown in figure 24.
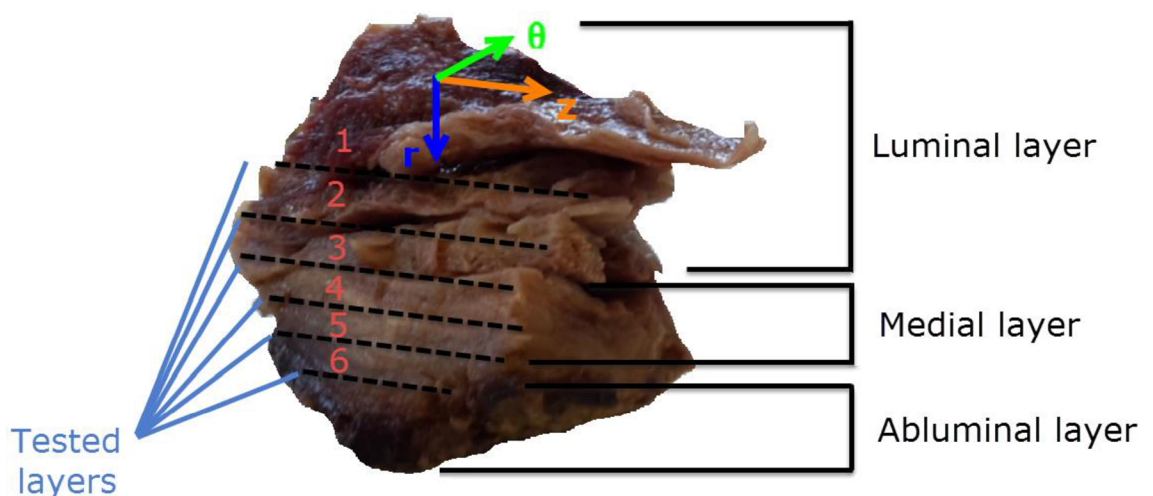
Figure 23 Schematic view of ILT bulk slicing into gradual layers with defined orientation according to their position within the AAA (figure 21).

6.2.1.1   Specimens

One type of test specimen was used during the experimental procedure with dimensions derived from the shape of pattern cutting device shown in figure 24. The thickness of the specimens was derived from the thickness of the ILT layers which were roughly around 3mm. Due to an absence of a device which would cut the layers with precise thickness, maintaining the same thickness across the entire specimen area was difficult.

Figure 24 Dimensions [mm] of tested biaxial specimen

6.2.2   The test set up

The tested specimens were held in the correct position by 4 sets of thoroughly placed clamps ensuring uniform distribution of the load (figure 25). It was ensured that the clamps stretch the sample without causing damage due to stress concentrations induced in the material around its edges. After mounting, the specimen was loaded by a small force of 0.1 N in order to straighten the sample and then loaded by a constant displacement rate. Due to the expected linear response of the ILT tissue, the initial small force was not expected to cause any significant strains. This would not be the case if testing healthy arterial walls with observed small initial stiffness [32].
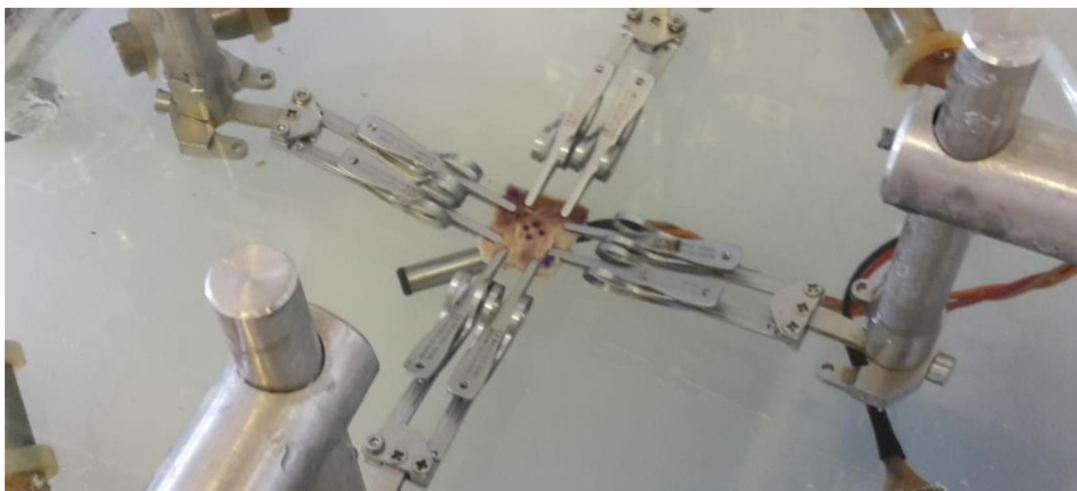
Figure 25 Mounting of the ILT biaxial specimen

6.2.3 Performed tests

Accounting for a general incompressibility of biological tissues due to their high water content, biaxial tensile testing is the most suitable method for testing soft tissues allowing for a two-dimensional stress state being the best method to describe their mechanical properties [29,30]. Summary of performed displacement controlled test protocols:

1. Equibiaxial tension test (strain in x and y-direction are equal)
2. Proportional tension tests (the amount of strains in x and y directions are proportional: 1:2; 2:1; 1:5; 5:1)

The tested specimens were elongated at constant displacement rates according to table 3, small enough so that the test can be described as quasi-static, and the test was stopped when the deformation reached 15% of the ideal specimen dimension.

Test type	equibiax	prop 2:1	prop 1:2	prop 5:1	prop 1:5
Elongation rate	0.333 - 0.333	0.333 - 0.167	0.167 - 0.333	0.833 - 0.167	0.167 - 0.833
Camera frame rate	210 ms	120 ms	120 ms	60 ms	60 ms
Max. elongations x - y	2.7 - 2.7	3.42 - 1.71	1.71 - 3.42	3.75 - 0.75	0.75 - 3.75

Table 3 Summary of the performed tests settings including elongation rates (mm/s), camera frame rates and maximum elongations (mm) in both directions.

6.3 Results

The goal of the mechanical testing was to obtain a range of mechanical properties of the ILT body across its radial direction. As the test was running, the CCD camera recorded displacement of the reference points on the specimen. The displacements were linked to current load values and the obtained data were transferred into Tibixus, a unique authorized software for experimental testing data assessment, where the following computations were performed.
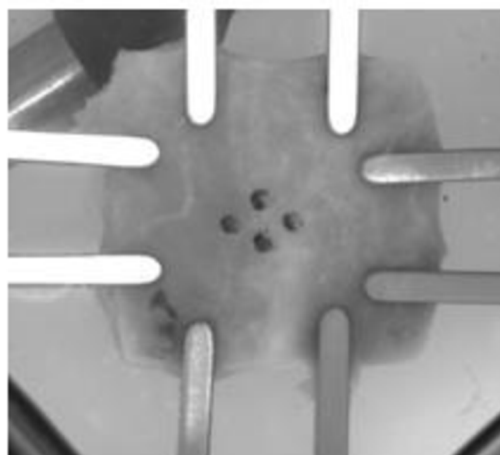
Figure 26 CCD camera images of biaxial sample

From the obtained data, stretch ratios (λ_1, λ_2) were calculated from the acquired values of initial (L) and elongated (l_i) distances between the marks $\lambda_i=l_i/L$; (i=1,2) in

desired directions. The undeformed cross-sectional area (A) of the tested specimen was determined and used to calculate engineering stresses (S_1, S_2) from the recorded force (F) as $S_i = F_i/A$; *(i=1,2)* by the first Piola-Kirchhoff stress definition. Followingly, stress-stretch curves (S_i-λ_i) were obtained for each specimen and test type (figure 27).
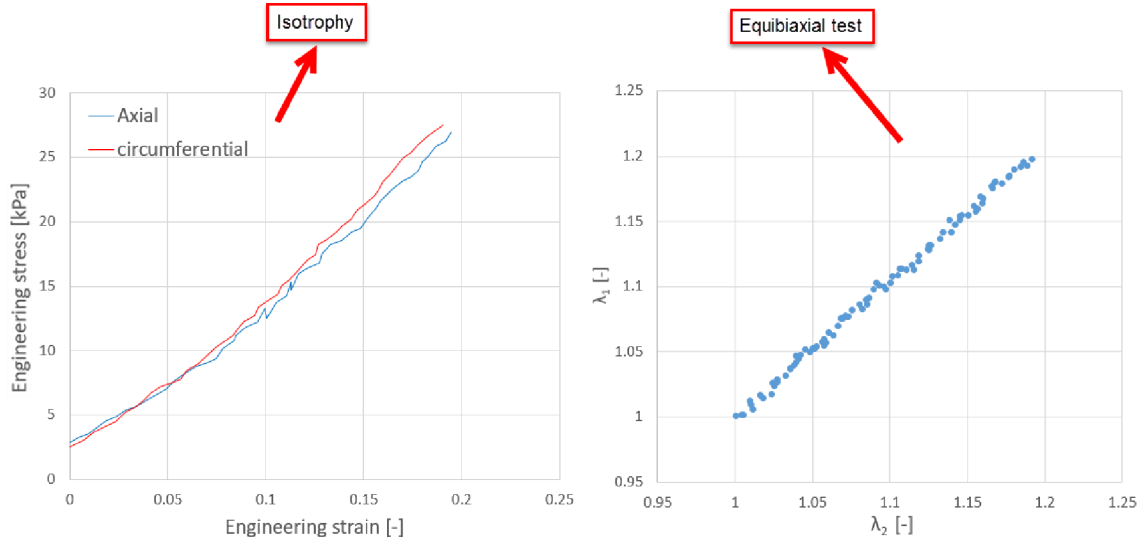
Figure 27 Engineering Stress – strain curves (left) of a biaxial specimen located at the distance of 16.51 mm from the lumen with corresponding λ_1, λ_2 dependence (right). The figure on the left (stress-strain curves) confirm the isotropic behavior of the ILT tissue while the figure on the right (λ_1, λ_2) proves that the stress-strain curves were obtained from a proper equiaxial test.

Unlike other biological tissues, a linear dependence of the stress on stretch ratio can be clearly observed as well as the material isotropy. The hyperelastic material behavior (see 2.3.3.1), obtained from the 5 biaxial tests, was modeled by 3rd order Ogden strain energy function under the assumption of incompressibility (equation 6).

$$W = \sum_{p=1}^{N} \frac{\mu_p}{\alpha_p} \left(\overline{\lambda}_1^{\alpha_p} + \overline{\lambda}_2^{\alpha_p} + \overline{\lambda}_3^{\alpha_p} - 3 \right)$$

(6)

Strain energy function *W* is given by material parameters μ_p, α_p and principal stretches $\lambda_{1\text{-}3}$. The principal stretches correspond to stretches in axial directions of a coordinate system describing the material shear-free deformation state. Followingly, stress-strain data fitting was carried out by software Hyperfit (license available at BUT, Czech Republic). A summary of the fitted material parameters is shown in table 4.

46

Patient #	Specimen	Material parametrs						R^2
		μ_1	α_1	μ_2	α_2	μ_3	α_3	
1	B1	4.926	8.079	18.815	1.000	1.033	1.000	0.96
	B2	6.052	6.349	23.771	1.000	1.189	1.000	0.82
2	B1	9.069	3.393	1.000	3.393	1.000	1.000	0.64
	B2	4.335	6.806	3.920	1.000	5.264	1.000	0.86
3	B1	5.047	5.914	2.560	1.092	1.021	1.000	0.90
4	B1	1.058	5.037	1.017	5.037	1.467	5.037	0.78
5	B1	4.236	4.882	1.000	1.000	3.906	4.882	0.61

Table 4 Summary of the fitted material parameters μ_p [kPa], α_p [-] carried out by Hyperfit software. The 3rd order Ogden model fitted the data well except two cases where the uncertainties were caused by the initial load introduced in order to straighten the tested specimen causing zero strains to correspond to small initial stresses.

Followingly, the obtained patient-specific models were compared to the available data in the literature (figure 28).
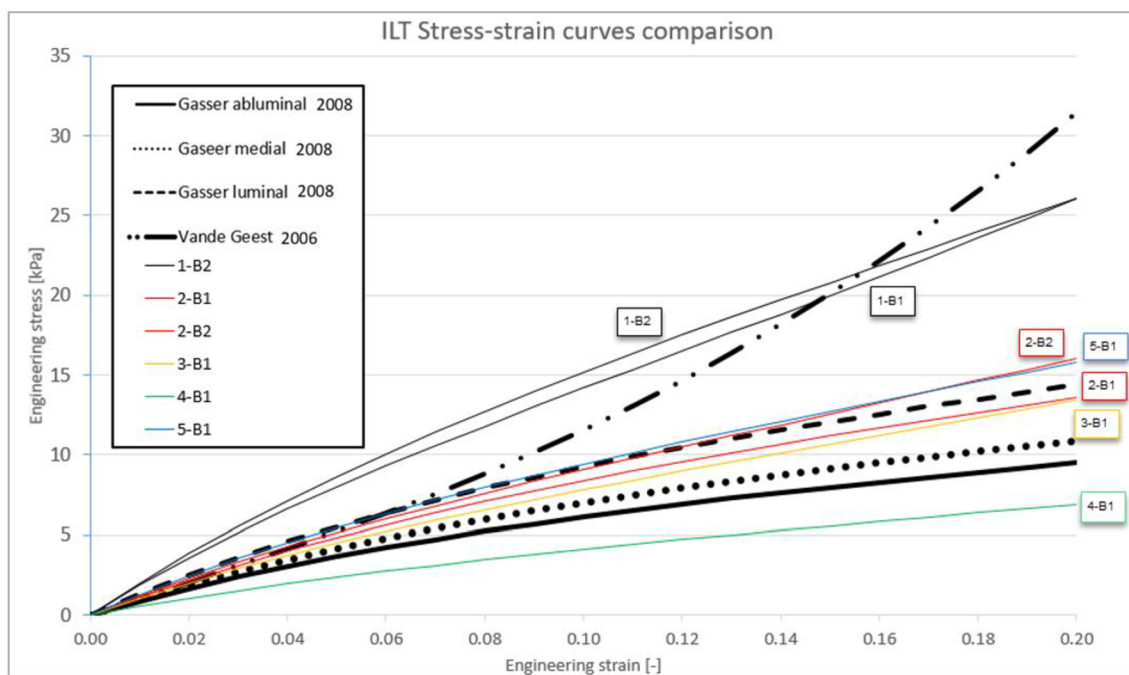
Figure 28 *Comparison of patient-specific and mean models describing equibiaxial stress-strain response of an ILT tissue. Vande Geest in [30] tested luminal layer and based his model on a uniaxial tensile test while Gasser [3] used biaxial test for all three tested layers of the ILT.*

Importantly, as seen in figure 28, the experimental testing gave **comparable results** to those presented by Gasser et al. [3] and Vande Geest et al. [30] which are the most frequently cited studies on this topic, since the partial differences are far within the

range of patient heterogeneity, presented by Gasser et al. [3], as it can be seen in figure 29.
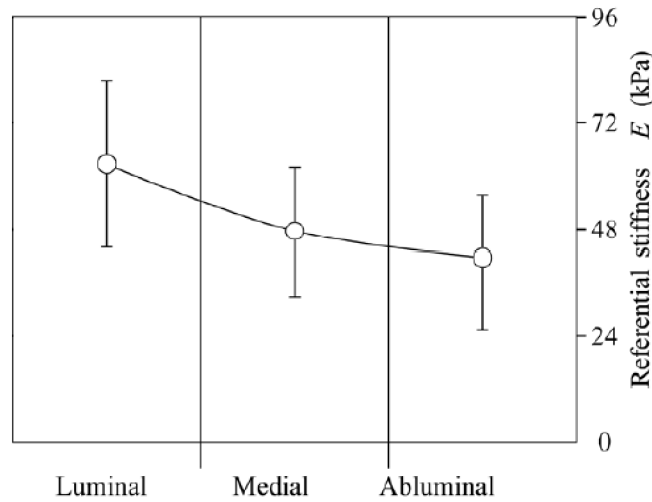
Figure 29 Variation of the ILT stiffness presented with error bars indicating standard deviations caused by the patient heterogeneity [3]

To summarize, in literature, there is a lack of relevant ILT values comparison since different definitions have been used [3]. Therefore, an overall comparison of available material models and patient-specific models obtained according to previous chapters was carried out (figure 28). As shown in figure 28 wide range of ILT mechanical properties can be observed with samples being more distant from the lumen behaving stiffer that the once closer. This indicates the necessity for patient-specific evaluation of the ILT properties when aiming for reliable ILT computational modeling. Also, in all cases, the most distant parts of the ILT bodies (abluminal part) were found unsuitable for testing due to its poor condition. **Therefore, it has ben found that stiffness close to zero value can be expected for this material.**

Among limitations of this mechanical testing belong the uncertainties of the specimen thickness measurements as it varies throughout the specimen cross-section due to lack of equipment that would ensure constant specimen thickness when slicing the ILT body into sheets. The resulting cross-sectional area directly influences the calculated stresses and thus contributing to the testing inaccuracies. Also, the more samples across the ILT thickness the more precise ILT material characterization across its radial direction increasing the following computational modeling reliability. However, in three cases only one specimen of the patients ILT was available due to either the ILT small size or poor mechanical state of its tissue.

7 Computational modeling

The motivation for computational modeling is defining of the uncertainties in AAA wall stress FEM (Finite Element Method) analysis caused by the lack of information about the ILT properties of a specific patient, based on a comparison of AAA wall stresses obtained from FEM analysis under the assumption of using input data from 6 and 7.3.

In terms of computational modeling and the most favorable method in biomechanics is FEM, current market offers several commercially available software that uses FEM as a solver method. In this thesis, ANSYS Mechanical APDL 17. was used (license available at BUT, Czech Republic).

7.1 Computational model

By analyzing available studies in literature (see table 5), based on studies performed by several researchers [2, 40, 41, 47, 53, 54, 55, 57, 59, 64, 65, 68, 73, 74, 75,77] it is obvious that a 3D model of geometry is necessary in order to obtain credible results. A limitation of a 3D patient specific model obtained by any of the available medical imaging methods is the inability to obtain patient-specific geometry in an unloaded state. Even though, there is a study attending to compute the unloaded AAA configuration from available loaded geometry by inverse modeling approach [56,57], in other cases [2, 40, 47, 53, 55, 59], including this thesis, the loaded geometry is treated as unloaded and loaded again by blood pressure. Despite the fact, that the resulting stress fields are unrealistic, for the purposes of this thesis are sufficient, since a comparison of stresses obtained from computational models, both affected by this simplification, will be evaluated. Another approach to this problematic is the use of idealized hypothetical AAA geometry model allowing for unloaded state simulations as presented in [55,58,59,76]. Two types of computational models were created in this thesis, a model based on the idealized hypothetical geometry of AAA including ILT and model based on patient-specific geometry. These computational models consisted of several partial models, each described in following chapters. Since the level of precision and accuracy of these partial models determines the reliability of the derived results, their detailed description is the purpose of following chapters:

1) Idealized AAA
    a) Model of geometry
        i. FEM mesh
    b) Material models
    c) Boundary conditions
2) Patient-specific AAA
    a) Model of geometry
        i. FEM mesh

Computations of all models considered large deformations [26,38].

Study	AAA wall material	Wall thickness	Homogeneity	Stress type	ILT	Geometry
Raghavan et al. (2000)	Isotropic Raghavan/Vorp	Constant 1.9 mm	Yes	Equivalent	none	PS
Wang et al. (2002)	Isotropic Raghavan/Vorp	Constant PS	Yes	Equivalent	Nonlinear Isotropic	PS
Fillinger et al. (2002)	Isotropic Raghavan/Vorp	Constant 1.9 mm	Yes	Maximum principal	none	PS
Venkatasubramaniam et al. (2004)	Isotropic Raghavan/Vorp	Constant 2.0mm	Yes	Equivalent	none	PS
Wolters et al. (2005)*	Isotropic Neo-Hooken	Constant 2.0mm	Yes	Maximum principal	none	PS
Speelman et al. (2007)	Isotropic Raghavan/Vorp	Constant 1.5mm	Yes	Maximum principal	Nonlinear Isotropic	PS
Lu et al. (2007)	Isotropic Raghavan/Vorp	Constant 1.9 mm	Yes	Equivalent	none	PS
Scotti et al. (2008)*	Isotropic Raghavan/Vorp	Variable	Yes	Equivalent	none	Idealized
Rodríguez et al. (2008)	Anisotropic Holzapfel	Constant 1.5mm	Yes	Maximum principal	none	Idealized
Speelman et al. (2008)	Isotropic Hyperelastic	Constant 2.0mm	Yes	Maximum principal	none	PS
Rissland et al. (2009)*	Anisotropic Holzapfel	Constant 2.0mm	Yes	Equivalent	Linear Isotropic	PS
Dorfmann et al. (2010)	Isotropic Demiray	Constant 2.0mm	Yes	Maximum principal	none	PS
Polzer et al. (2010)	Isotropic Raghavan/Vorp	Variable	Yes	Equivalent	Linear Isotropic	PS
Gasser et al. (2010)	Isotropic Raghavan/Vorp	Variable	Yes		Variable stiffnes	PS
Speelman et al. (2010)	Isotropic Raghavan/Vorp	Constant 2.0mm	Yes	Maximum principal	Linear Isotropic	Idealized

Table 5 Overview of several of studies performing nonlinear finite element analysis of AAA with their important aspects. Studies labeled by star include fluid-structure interaction analysis; PS stands for patient-specific; presented material models are according to Raghavan et al. [59], Holzapfel et al. [78] and Demiray [79].

7.2 Neglected parameters

Due to excessive complexity or negligible impact on the wall stress, several parameters were not included in the analysis:

- Variation in temperature of the human body
- Gravitational forces acting on the AAA structure
- Residual stresses

- Axial pretension of artery in vivo
- Calcification was not included
- Shear stress acting on a vessel wall caused by the blood stream
- Near surrounding of the AAA (organs, vertebral column, vessels) that may preclude free deformation on the AAA body.
- The AAA and ILT are modeled as single-phase solid bodies
- Permeability of the AAA wall and ITL
- The ILT was considered without fissures
- The layered composition of the aortic wall (intima, media, adventive) was neglected and the wall was modeled as a homogeneous material
- Distribution of elastic fibers directions causing anisotropy in the non-aneurysmal parts of the AAA wall
- Dynamic nature of this problem is neglected

A detailed discussion of the neglected parameters and their influence on AAA is provided in chapter 9.

7.3   Idealized AAA

In this thesis, an idealized geometry of AAA has been used for determination of FEM mesh convergence and results sensibility to different ILT material topologies, both explained in greater detail below.

7.3.1   Idealized model of geometry

For the purposes explained earlier, a hypothetical idealized geometrical model was created. First, a solid volume model was designed using 3D CAD modeling software Autodesk Inventor 2014 (student license) so that the model imitates the existing appearance of AAAs. As discussed in chapter 3, the AAA bulge usually appears at the anterior side due to the vertebral column limiting the posterior expansion, resulting in nonsymmetrical AAA shape [34,59]. The mid-section diameter was considered to be 5.5 cm, thus at the limit of the geometrical AAA rupture risk criterion. With the geometry, being 12 cm long in the axial direction, tapering, the diameter at both ends decreased to 2 cm [21,54]. The thickness of the wall was considered to be constant at 0.2cm and the cross section was kept circular throughout the length [21]. Followingly, idealized ILT geometry was created filling the AAA bulge so that the lumen remains cylindrical. Both models are shown in figure 30.
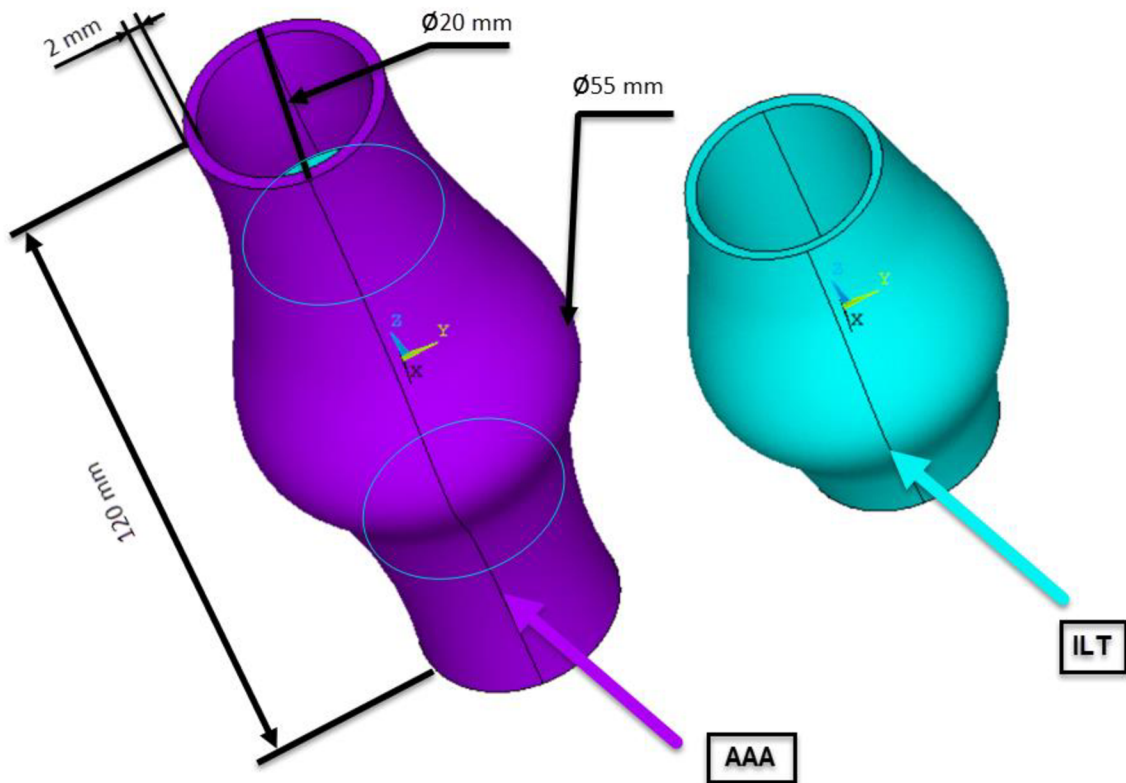
Figure 30 Hypothetical idealized geometry model of AAA including ILT.

7.3.1.1 Idealized geometry FEM mesh

The FEM mesh discretizing the ILT and AAA geometries was carried out separately. The AAA wall was meshed with linear structural solid element SOLID185 (3D 8-node) creating a pure hexahedral FE mesh. Hexahedral elements are suitable for modeling soft biological tissues and provide a great ratio of accuracy and computational efficiency [2]. On the other hand, due to an advanced geometry complexity of the patient-specific ILT structure, a quadratic tetrahedral element SOLID285 (3D 4-node) was used to create FE mesh of both, the idealized geometry model and patient-specific geometry model, so that the FE mesh attributes of the two geometry models match and the findings from idealized geometry analysis can be implemented in the patient-specific analysis. The idealized geometry FE mesh is shown in figure 31. In order to avoid a mistake in calculated stresses, caused by discretization, larger than 5%, which is a generally recognized mistake of the FEM, a mesh convergence study was carried out comparing maximal 1. principal stress value in the aneurysm wall and local peak stress on the inner side of the AAA wall apex region (figure 31). Consequently, FE mesh formed by two elements across the AAA wall thickness with a global size of 3 mm was selected to be used for the patient-specific AAA structure geometry model since lowering the global element size to 1.5 mm or introducing more elements across the wall resulted in maximal stress differences of 2.14% and significantly larger computational times.

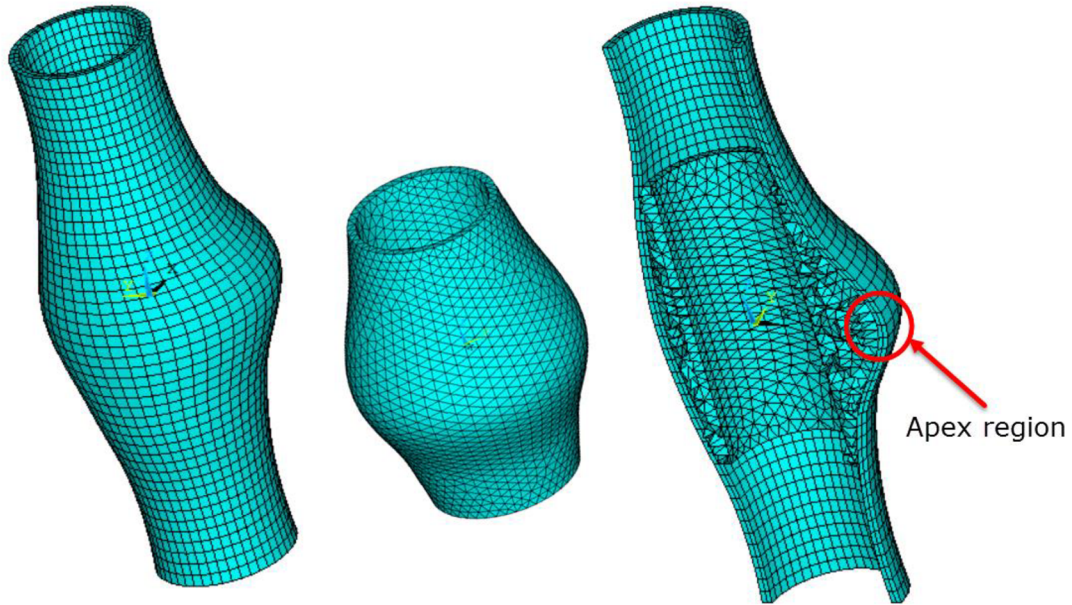*Figure 31 Finite element mesh of the idealized geometry model of AAA with ILT*

7.3.2 Material models

In order to evaluate stresses in the AAA wall, implementation of suitable finite strain constitutive models is necessary [59]. The purpose of introducing constitutive modeling is a prediction of a certain material mechanical response under a specified loading state. Therefore, to determine the necessary form and material constants, experimentations including all relevant deformations must by performed [29]. For the purposes of the idealized geometry, mean ILT properties values and material models were used (5). Material model of the AAA wall will be discussed in the following chapter.

7.3.2.1 AAA wall material model

According to the findings in 2.3.3 and 3, AAA wall was considered as a non-linear hyperplastic isotropic material that undergoes large deformations, therefore, a linear material model that has been used in some studies [47, 48] is not suitable for covering all material responses [59]. Also, according to chapter 2.3.4, it is obvious that AAA constitutive behavior is different from the one of the normal abdominal aorta, indicating the need for a constitutive model particularly suited for AAA [59]. In current practice, the most frequently used constitutive model for AAA wall was introduced by Raghavan et al. [59] who used Yeoh type material model (equation 8) to describe a material response derived from uniaxial tensile tests data of AAA wall tissue performed in vitro [2]. The Raghavan-Vorp constitutive model is then expressed by strain energy according to equation 7.

$$W = \sum_{i=1}^{n} c_{i0} \left(I_1 - 3\right)^i \tag{7}$$

$$W = c_{10}\left(\bar{I}_1 - 3\right) + c_{20}\left(\bar{I}_1 - 3\right)^2 \tag{8}$$

In equation 8, material constants $c_{10} = 174\text{kPa}$, $c_{20} = 1881\text{kPa}$ and I_1, I_2 are the first and second invariants of the Cauchy-Green tensor of deformation. As being described in (2.3.3.1) a certain stress component can be obtained as a derivative of the strain energy function W with respect to the corresponding strain component. A stress-strain curve representing the Raghavan-Vorp model is shown in figure 32. Despite fact that this model has only two parameters, describes mean population data reliably [59]. A limitation of this model is given by the fact that it has been developed on uniaxial tensile tests data, however, generally, the AAA wall undergoes biaxial stress state [2,29,30].
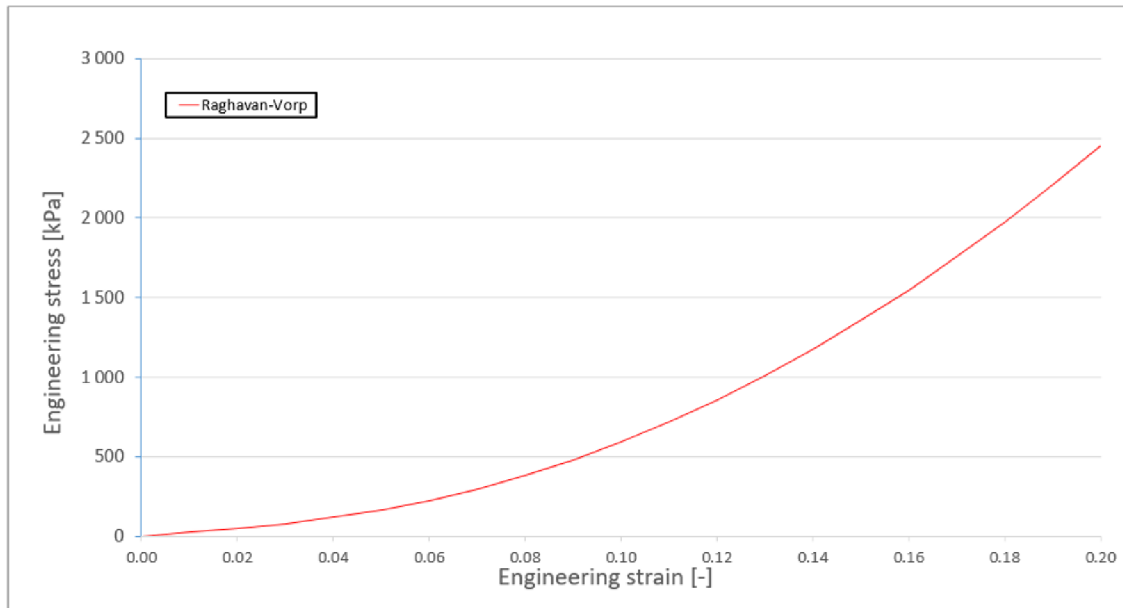
Figure 32 Equiaxial stress-strain curve given by Raghavan-Vorp material model

Raghavan-Vorp material model can be described as a 2$^{\text{nd}}$ order Yeah type material model which is implemented in Ansys Mechanical APDL 17, as well as Ogden material model that was used to fit the ILT experimental data by Gasser et al. [3] in chapter 5 or the experimental data in 6.3.

7.3.2.2   Material topology sensitivity study

After the mesh convergence study, the second purpose of developing an idealized hypothetical geometry model of AAA structure was to determine the sensitivity of resulting wall stress on ILT material topology. In other words, it was mentioned earlier (4.3) that the mechanical properties of the ILT are changing with the radial distance from the lumen [3,25]. In most studies [3,22,25,27,38,42] the ILT is considered to consist of three homogenous layers that are described by single values of stiffness or strength. However, considering that these values decrease as the ILT becomes older and more spaced out from the lumen, the change of mechanical properties may be in reality rather smooth and not stepwise as in the case of three homogeneous layers (luminal, medial, abluminal). Therefore, hypothetically, the more ILT layers, described by different

54

material properties, the smoother transition of the overall ILT material properties from the lumen to the AAA wall. Thus, the material topology sensitivity study carried out on the idealized geometry was performed, testing the influence of the described phenomena on resulting AAA wall stress.

In order to obtain the ILT layered structure, a macro file, containing cycle prescribing each element of the ILT FE mesh with material properties based on the element's distance from the lumen, was created. Followingly ILT described by 3, 6 and 9 layers of material, with each layer being defined by its minimal and maximal distance from the lumen, were created as shown in figure 33.
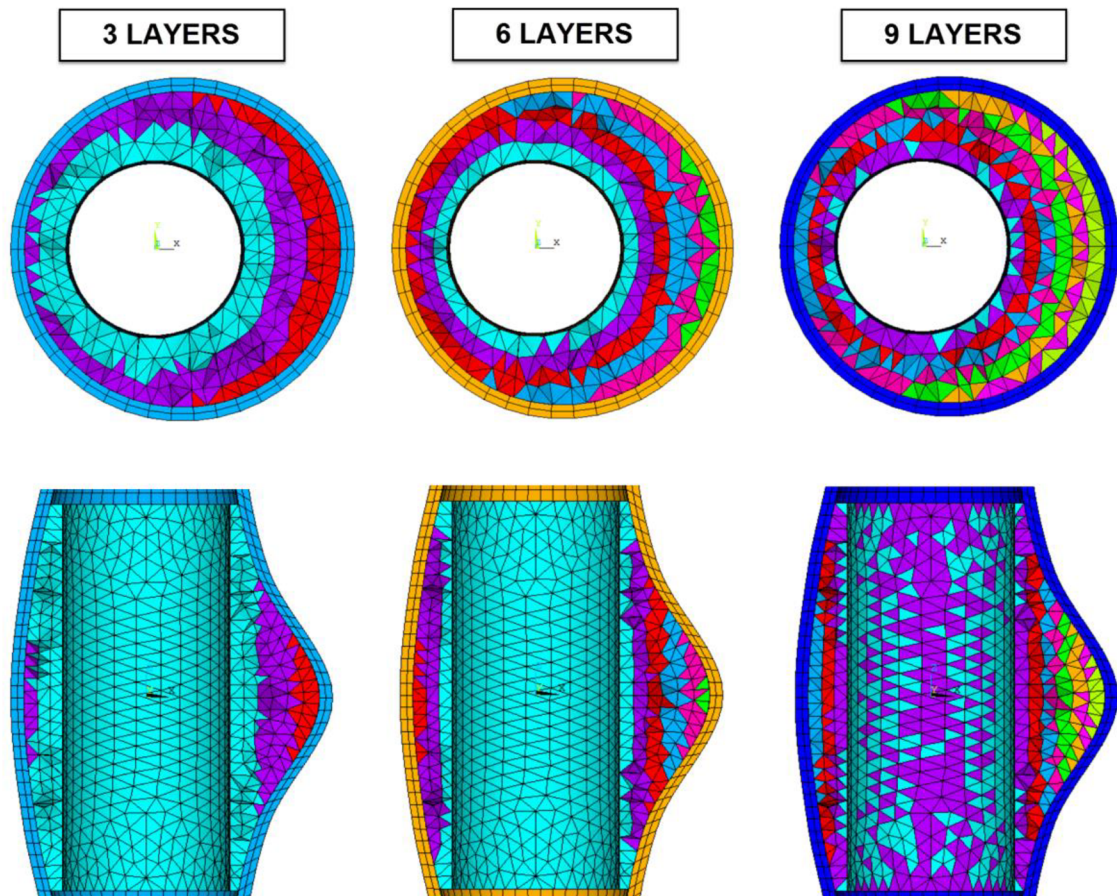
Figure 33 Overview of three different material topologies of the ILT geometry model. Each color represents different material properties.

Followingly, the distribution of material properties was assigned for each ILT layer according to figure 34. For the 3, 6 and 9 layers, mean stiffness values for luminal (62.88 kPa) and medial (47.52 kPa) layers from Gasser et al. [3] where used. As described in 6.3 the abluminal layer was found to have negligible stiffness. Therefore, from numerical reasons, the stiffness of the layer closest to the AAA wall was considered to be extremely low (1 kPa). Additionally, in the case of 6 and 9 layers, these three stiffness values were evenly distributed among the additional layers in order to better represent the hypothetical smooth curve (figure 34 – purple).
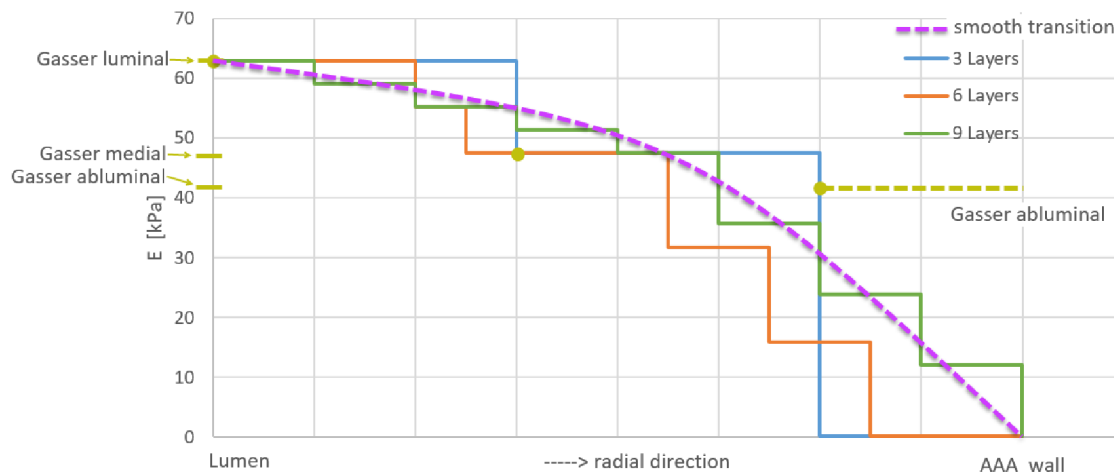
Figure 34 Distribution of material properties for 3, 6, 9 layers and values introduced by Gasser et al. [3] Purple dashed line represents the hypothetical smooth transition of the properties across the ILT thickness. Note that the smooth curve is only illustrative. To compare, the yellow dashed straight line represents mean abluminal stiffness according to Gasser et al. [3], which was not considered.

Similarly to the above-discussed mesh convergence, maximum 1. Principal stress in the AAA wall and local peak stress in the apex region was compared for each material topology. As it is listed in table 6, the percentage differences in resulting stresses are below 5% (mistake of the FEM), therefore the influence of refining the stepwise distribution of material characteristics across the ILT radial direction was found to be negligible. Consequently, this finding was implemented in the real patient-specific geometry stress-strain analysis (7.4).

| # of layers	Max. wall stress		Apex wall stress	
	Value [kPa]	Difference from previous	Value [kPa]	Difference from previous
3	252	-	136	-
6	255	1.21%	133	2.03%
9	255	0.22%	135	1.55%

Table 6 Summary of wall stresses sensitivity on different material topologies. The difference percentages were in all cases standardized to the sets of stresses corresponding to models of more layers.

7.3.3 Boundary conditions

In vivo, the AAA wall is loaded by the blood flow that is changing over time according to the heart activity making a determination of the blood flow loading effect a difficult task. Moreover, since the load is transmitted from liquid medium to a solid body, a fluid-structure interaction problem should be solved, as in [58,75,77], in order to determine the real blood flow loading effects on a certain AAA wall. On the other hand, others suggest that the influence of blood flow on in terms of loading the AAA structure is negligible and steady activation is fully acceptable [40,81], therefore, loading by a static

pressure was considered in this study. Anyway, this contradiction is a possible subject of further investigation. Also, an ideal model of boundary conditions would include loading by dynamic pressure, however, due to the problem complexity, the solution of the stress-strain analysis is considered to by quasi-static, which agrees with the assumptions of most studies [2,41,47,53,55,57,65,73,76]. To test the worst possible scenario for AAA rupture the computational model was loaded under the assumption of static load conditions by a systolic pressure of 20 kPa (2.2.1). The modeled ILT was considered not shielding the AAA wall from blood pressure [2,8,37]. Consequently, the loading pressure was applied in a normal direction to an inner surface of the AAA wall, simulating the above-mentioned assumptions (figure 35-B). Additionally, no loads were applied to the outer AAA surface since possible contacts with any of the abdominal organs or spine were not considered, as in [2, 40, 41, 47, 53, 54, 55, 57, 59, 60, 62, 63, 64, 65, 68, 73, 74, 75,77].

The model was fixed at both ends. In other words, all displacements were prescribed zero for all nodes of the proximal and distal cross-section of the AAA model (figure 35-B). This condition does not fully simulate the real conditions since the end regions are unable to expand in radial direction under the loaded state, however, at the end regions high stresses are not expected, therefore this zones can be excluded from the results analysis, which might be also the reason why this approach is common in the literature [2,40,41,47,55,57,59,60,62,63,64]. Due to the fact that the AAA wall and ILT geometrical models were created separately, their mutual interface had to by prescribed. This interface was modeled under the assumption of the ILT's perfect attachment to the AAA wall [8,40,55,62]. Therefore, the mutual movement between the ILT outer and AAA wall inner surface was prevented by applying a bonded contact (figure 35-A).
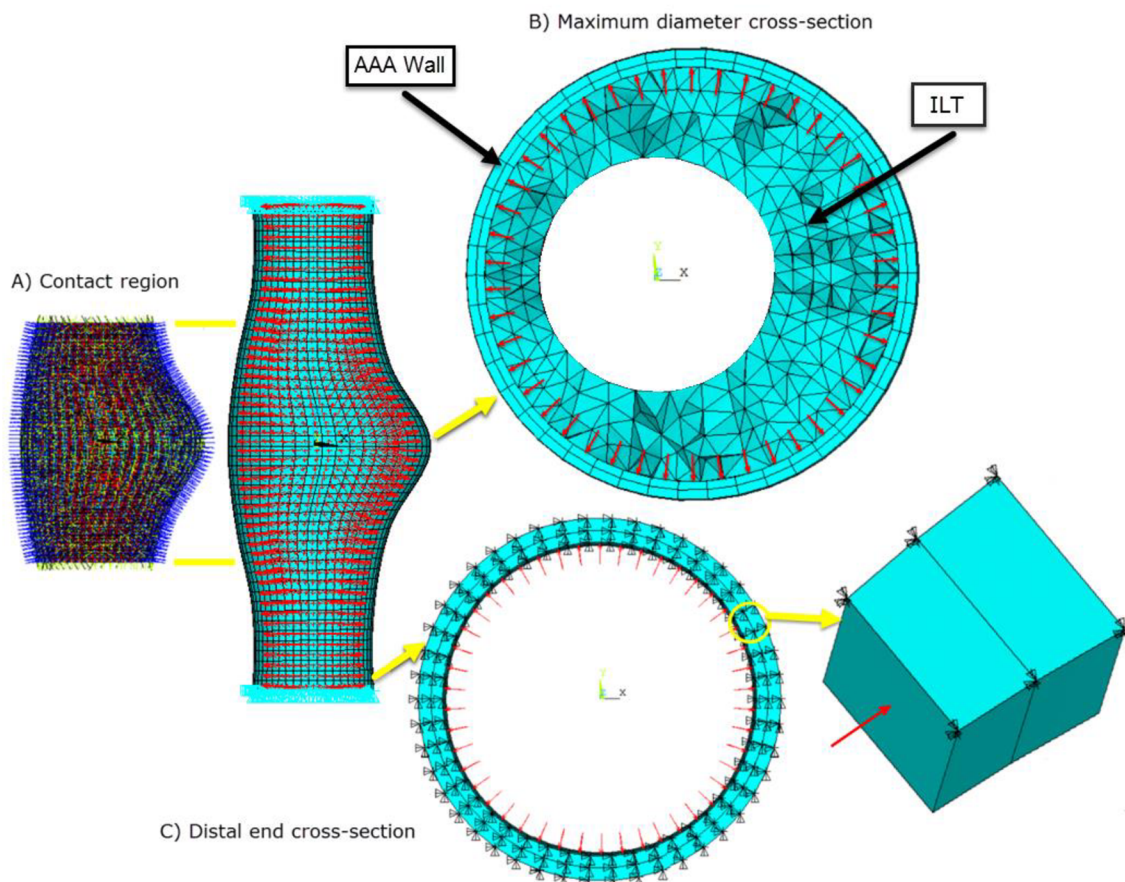

Figure 35 Schematic summary of the prescribed boundary conditions.

7.4 Patient-specific AAA

For reasons described in 7.1, 3D patient-specific computational models were used for FEM analysis to compute and compare wall stresses using either patient-specific or mean stiffness of intraluminal thrombus, as specified in 1.3. To do so, 5 geometry models created from CT datasets of 5 patients, obtained prior a surgical repair, were used. Mechanical tests of ILTs harvested from these 5 patients were conducted (chapter 6) to obtain patient-specific material properties. Consequently, 5 pairs of computational models based on the 5 patient-specific geometries were created. Each of the geometry pairs consisted of two identical computational models, prescribed with different material models based on either mean (5) or the patient-specific (6.3) material properties. Therefore, these pairs of computational models based on one geometry models and two different material models will be later referenced as a geometry couples. For all 10 computational models, constitutive representation of materials and model of boundary conditions was identical to those used for the idealized geometry studies (7.3.2; 7.3.4).

7.4.1 Patient-specific model of geometry

For the purposes of this thesis, 5 geometrical models of AAA including ILT were provided by the supervisor of this thesis Ing. Stanislav Polzer, Ph.D. in a form of 3D triangular mesh in STL format. The geometries were reconstructed from the 5 patient-specific CT data sets. These raw data needed to undergo image segmentation process where all materials that are not the subject of interest are excluded. The segmentation process is based on threshold value assessing material density. After the segmentation process is finished, an STL file is created and can be further processed in CAD or CAM software. Overview of the five geometry models is shown in the top row of figure 36.
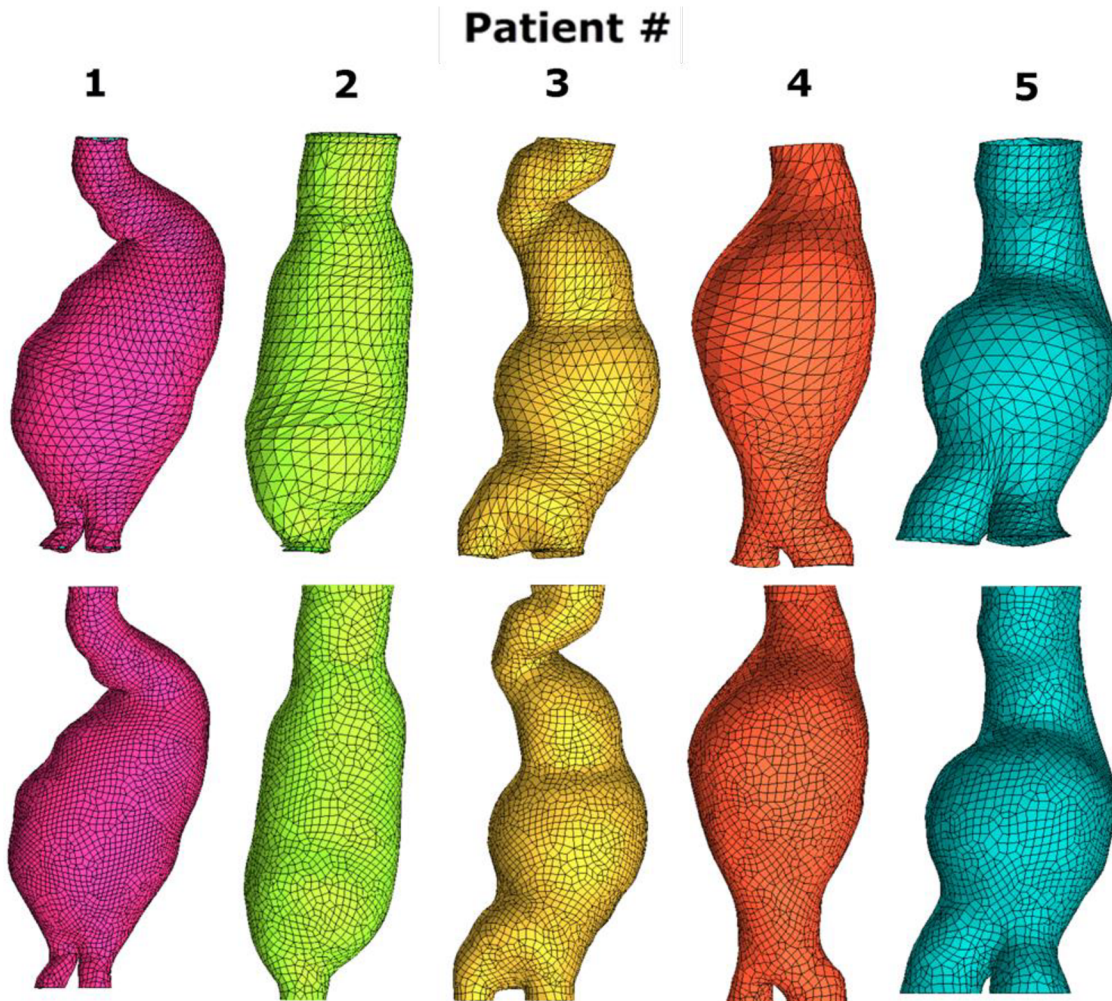
Figure 36 Comparison of the raw triangular meshes (top row) and final hexahedral dominant FE meshes (bottom row) for patients 1-5. The geometry 2 was obtained without an iliac bifurcation.

7.4.1.1 Patient-specific geometry FE mesh

FE mesh was created under the assumptions described in 7.3.1.1. However, in the case of patient-specific AAA wall geometry model, for obtaining a reasonable hexahedral FE mesh, a specialized software for FE mesh creation, ICEM CFD 17 (BUT, Czech Republic) was used.

The creation of the AAA wall FE mesh was a stepwise process (figure 37), where each step represents a potential threat of creating geometrical inaccuracies. First, a raw triangular mesh of the AAA outer surface was selected and smoothened by excluding all sharp corners or penetrating elements caused by reconstruction inaccuracies (figure 37-A). These sharp elements would cause stress concentrations and consequently unreliable conclusions. Secondly, the triangular mesh was transferred into a geometrical surface (figure 37-B) so that the surface can be meshed again by hexahedral shell elements (figure 37-C). Finally, the shell elements were extruded inside the AAA volume in the normal direction to the element surface creating 3D hexahedral dominated FE mesh comprising of two elements across the AAA wall thickness and global element size of 3 mm, as

determined in 7.3.1.1 (figure 37-D), creating AAA wall of constant thickness of 2 mm [21]. Final AAA wall FE meshes are shown in figure 36-bottom.
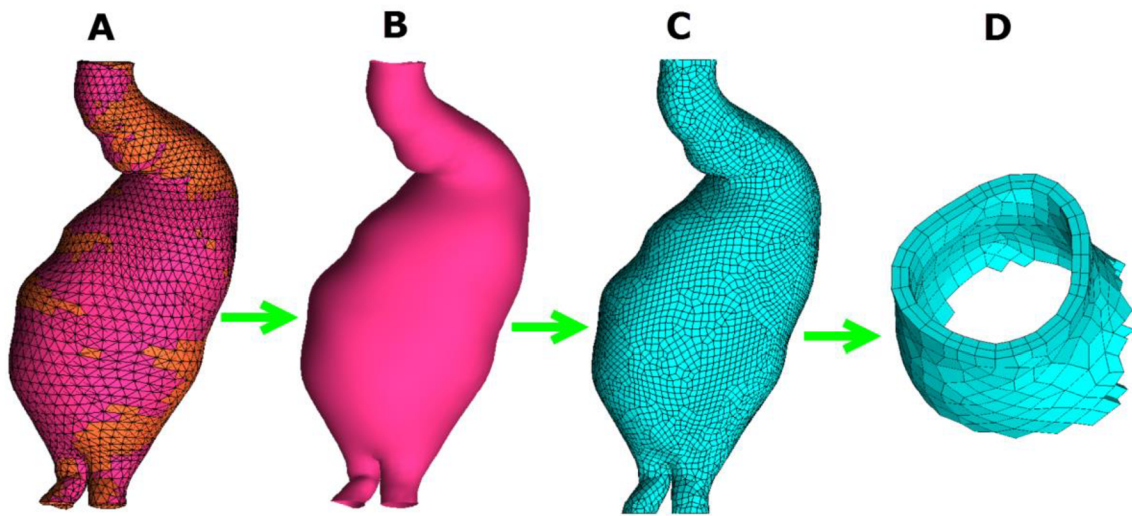
Figure 37 Overview of the AAA wall hexahedral dominated FE mesh stepwise creation process. Raw triangular mesh (A) was transferred to a surface (B), meshed with hexahedral shells (C) and extruded (D).

Next, as discussed in 7.3.1.1, the pure tetrahedral mesh was created for each ILT geometry. Similar process as in the case of AAA wall meshes was used, when the surfaces were meshed directly by the 3D tetrahedral elements. The ILF FE mesh for each patient-specific thrombus geometry is shown in figure 38.
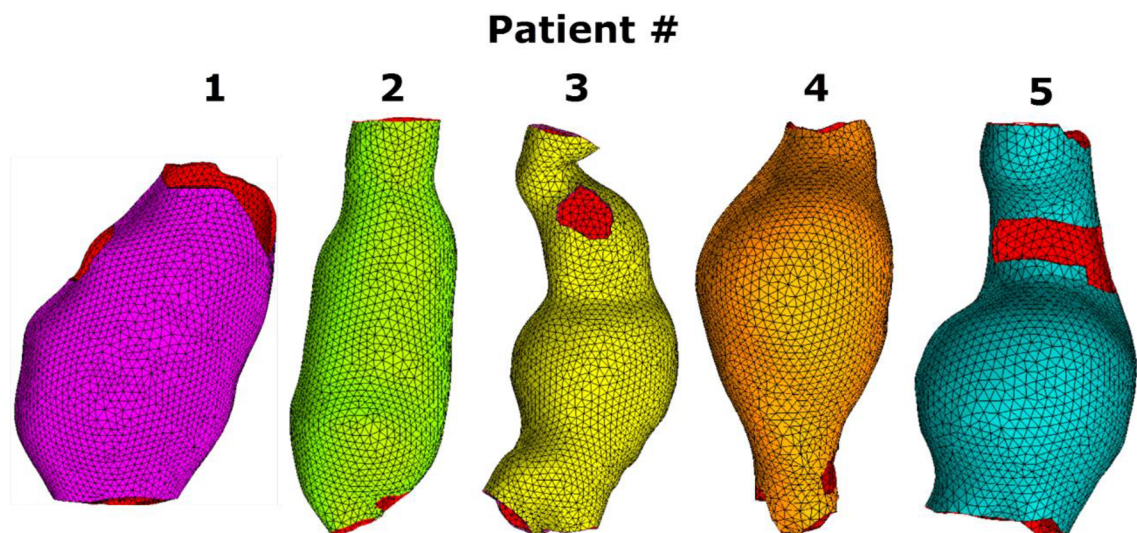
Figure 38 Tetrahedral FE meshes for patient-specific ILT geometries.

7.4.2 Material models

As a result of 7.3.3 for patient-specific ILTs topology described by three material types across its thickness was considered. In the case of mean ILT stiffness, values introduced by Gasser et al. [3] for luminal, media and abluminal were used. On the other hand, in the case of patient-specific approach, the layer in contact with AAA wall was considered to have a negligible stiffness (6.3) while the other two layers were given the material properties derived from the tested samples (table 2). However, for patients 3,4, and 5 only one sample was tested. Therefore, to ensure the gradually decreasing nature of the material properties across the ILT thickness, an additional material model, representing material properties between the negligible-stiffness outer layer and mechanically tested inner layer, need to be determined. To do so, from the Ogden type constitutive models used to describe the inner ILT layer (6.3) a shear modulus (G) was calculated according to equation 9.

$$G = \frac{1}{2} \sum_{p=1}^{N} \alpha_p \cdot \mu_p \tag{9}$$

In 6.3, to describe the measured ILT properties, 3rd order Ogden model was used, therefore $N = 3$ and α_p, μ_p are the model material parameters listed in table 4. Since the stiffness of the outer layer was negligible, to obtain a symmetrical stepwise change of the material properties, the middle layer was given a half stiffness of the inner layer. Consequently, a constitutive model describing the hyperplastic, isotropic behavior [25] of the ILT tissues was selected. In this case, Neo-Hook material model was used due to a transparency of its material parameters. Since the material was considered incompressible [3,25,26], the strain energy of the Neo-Hook model is given by equation 10.

$$W = \frac{G}{2} \left(\bar{I}_1 - 3 \right) \tag{10}$$

In equation 10, W is the strain energy function, G is the shear modulus and I_1 corresponds to the modified first invariant of the right Cauchy-Green tensor of deformation.

Similarly, the negligible-stiffness outer ILT layer was modeled using the Neo-Hook material assumption. Due to numerical reasons, the stiffness of the degraded tissue was set equal to 1 kPa, which corresponds to $G = 0.333$ kPa, since for incompressible material $G = E/3$. Comparison of the Neo-Hook and Ogden material models describing ILT properties of patients 3, 4 and 5 is shown in figure 39.
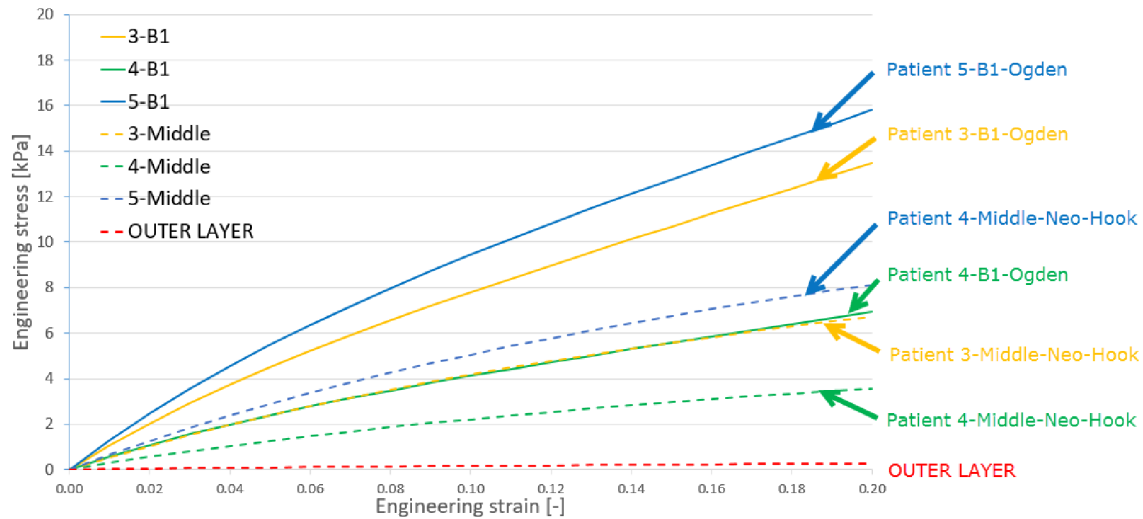
Figure 39 Comparison of the Neo-Hook and Ogden equibiaxial stress-strain response, representing the three ILT layers material behavior for patients 3, 4 and 5. Note the outer negligible-stiffness layers plotted in red.

After determination of the material properties, the thickness of each ILT material layer needed to by defined. Since, in cases of mean stiffness values, no thickness determination of the three layers (luminal, medial, abluminal) exists, the layers were evenly divided across the ILT thickness. In the case of patient-specific approach, the thickness of each layer derived from the positions of tested specimens and their thicknesses (table 2). Even though for patients 1 and 4 specimen B1 was not located at the lumen, the material parameters from the lumen to specimen B1 were assumed constant. Additionally, for patients 3, 4 and five, since the values of the additional layer were derived from calculations, instead of testing specimens with a location within the ILT, the remaining two layer were split evenly across the remaining tissue. Schematic summary of the ILT material topologies for all 5 patients is shown in figure 40 and an example of the geometry model with patient-specific and mean distribution of material layers is shown in figure 41.
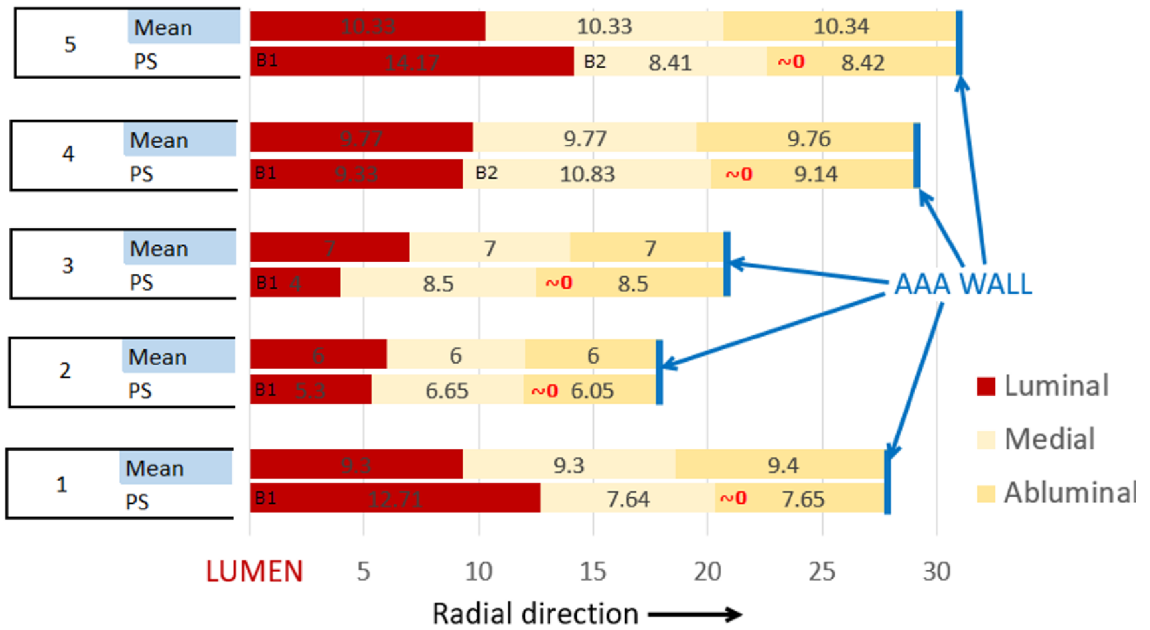
Figure 40 Comparison of material distribution [mm] for mean and patient-specific (PS) ILT models. Layers corresponding to the tested specimens and negligible-stiffness layers are labeled. Note that since some of the tested samples were not harvested from the maximum ILT region, distances of the specimen's position were proportionally recalculated.

Figure 41 Differences between the material distribution of the patient-specific (PS) and mean approach.

8 Results

FEM stress-strain analysis of 10 computational models based on 5 patient-specific geometry and two material models, was performed. The purpose of this chapter is the result overview. Since the motivation for the FEM stress-strain analysis was determination and comparison of stresses in the AAA wall, these stresses were the only subjects of focus.
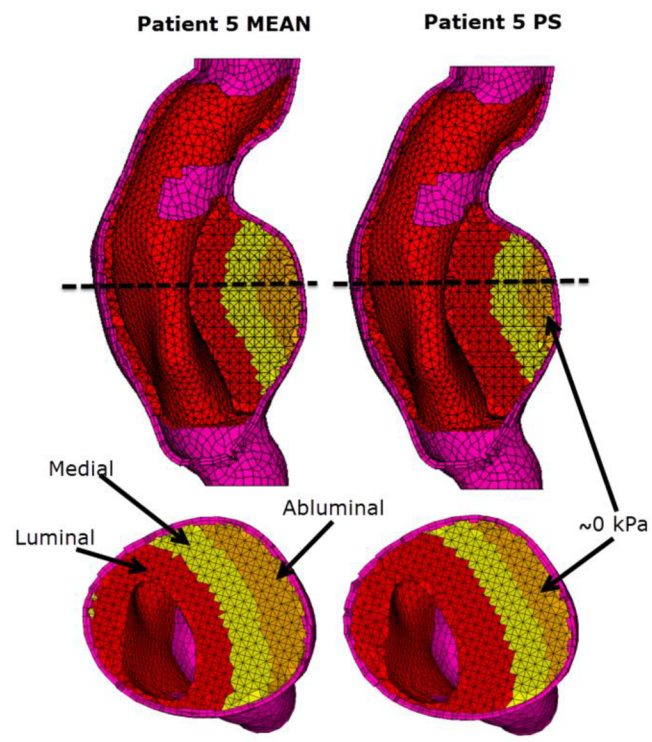
As it was mentioned in the section derived to the model of boundary conditions (7.3.3), during CT imaging, instant values of pressure are not recorded causing the obtained geometry to be in an unknown stress-strain state. Consequently, loading the structure be the systolic pressure is a certain simplification. However, this is often used in the literature [2,41,47,53,55,57,65,73,76] and it is also considered acceptable for the purposes of this thesis, which is a determination of uncertainties, caused by using mean values of ILT stiffness.

For evaluating maximum stresses in AAA, many studies use equivalent stress [2,53,54,60,63,65,66] which is generally used for metal materials analysis with excessive shear stresses [21]. However, it was suggested [43,61,64] that failure of AAA tissue is caused by maximal normal stresses with the main normal direction for AAAs being the circumferential direction [47]. Also, due to the unknown initial stress-strain state, comparison of the resulting stresses with limit values is not determinative. Thus, in this thesis, for evaluation of the stress states in AAA wall, the first principal stress was selected [45,47,55,62,64,73,75,76]. Additionally, even though the ILT played a main role in the computational model, stresses in the ILT model were not investigated since the stress in the aneurysmal wall is the principal feature determining possible AAA rupture.

First, before evaluation of magnitudes and distribution of stress in the 10 computational models, statistical comparison of the whole stress fields was conducted in order to determine their statistically significant difference. Consequently, two data sets were created, one containing stress values from all nodes of the PS computational model and one from the mean values computational model. Since these data were considered of unknown distribution, a non-parametric Mann-Whitney U test was performed. According to the Mann-Whitney test, in order to reject the null hypothesis, the minimum of the calculated U-values (U_1, U_2) needs to be equal or less than the critical U-value (U_{crit}). The data are summarized in table 7.

Null hypothesis (H_0): Stresses from PS and mean data computational models are the same. Alternative hypothesis: Stresses from PS and mean data computational models are the different.					
Patient #	p value	$U_1 [\times 10^6]$	$U_2 [\times 10^6]$	$U_{crit} [\times 10^6]$	
1	<0.01	194.0	97.5	144.0	H_0 rejected
2	<0.01	38.5	43.7	40.2	H_0 rejected
3	<0.01	56.8	71.6	62.9	H_0 rejected
4	<0.01	28.6	60.5	43.5	H_0 rejected
5	<0.01	43.4	45.5	43.5	H_0 rejected

Table 7 Summary of the Mann-Whitney U test calculations

As confirmed by the Mann-Whitney U test conducted at a significance level of *0.01*, the stress fields among the geometry couples report the statistically significant difference. Therefore, this states the difference in material models changes the wall stress distribution.

Next, the results are presented in form of stress fields, displayed by 3D contour plots of the first principal wall stress for each AAA structure (figures 42 and 43), and bar charts, representing the maximum stresses in the AAA walls of each computational model (figure 44), allowing the comparison of wall stresses within the same geometry model couples. Additionally, in order to evaluate the maximum deviation of the two approaches, nodes with the biggest differences of stresses were located and the values are summarized in figure 46.

Figure 42 The influence of using mean ILT stiffness values against patient-specific values. Stress fields (1. Principal stress [kPa]) for patient 1.

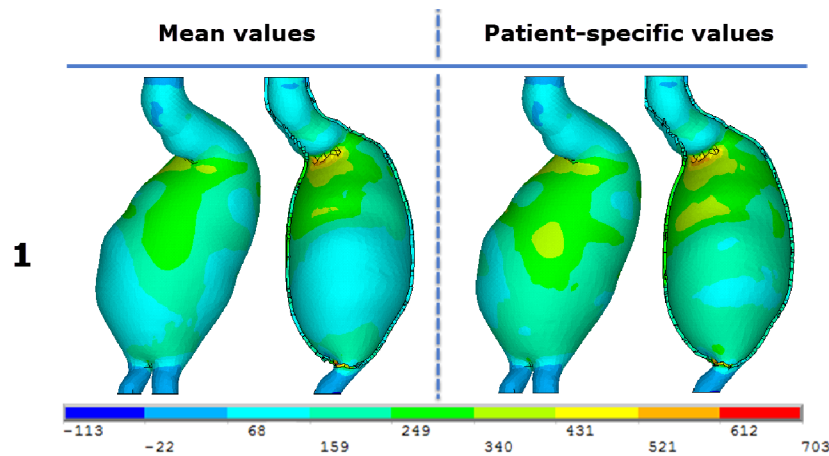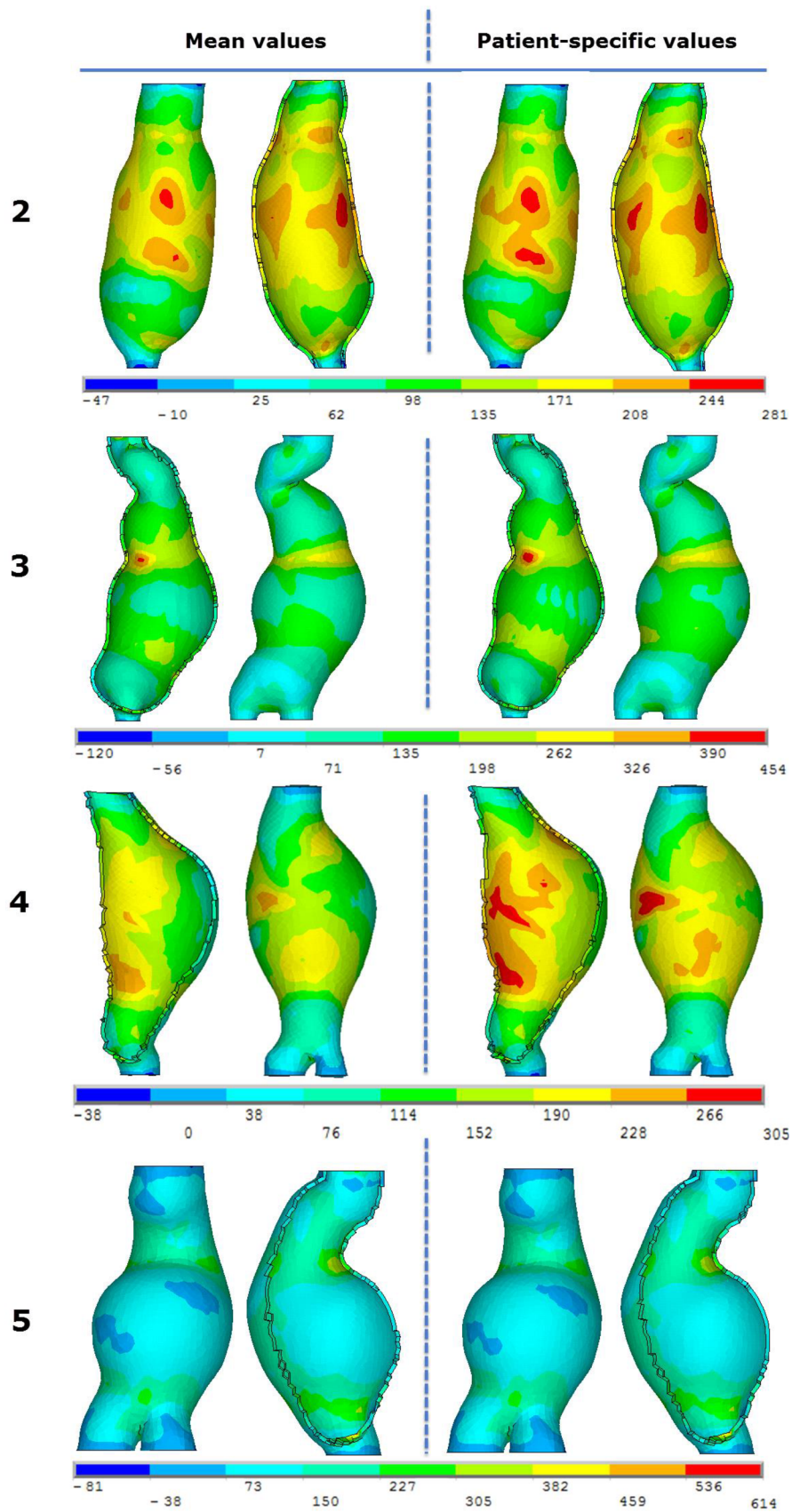*Figure 43 The influence of using mean ILT stiffness values against patient-specific values. Stress fields (1. Principal stress [kPa]) for patients 2, 3, 4 and 5.*

Figures 42 and 43 manifest that different material models of ILT result in variable differences in AAA wall stress fields since in the case of patient 4 significantly different stress fields can be observed while in other cases the changes are rather negligible. The percentual difference of the peak wall stresses for all five geometry couples has a mean value of 6% and ranges from 0.2% (patient 5) to 16.1% (patient 4). A detailed comparison of the peak wall stresses within the geometry couples together with the maximal ILT thickness for each patient is shown in figure 44.

	Patient 1	Patient 2	Patient 3	Patient 4	Patient 5
■ PS	703	281	454	305	613
■ MEAN	678	275	420	263	614
▦ Max. ILT [mm]	28	18	21	29.3	31
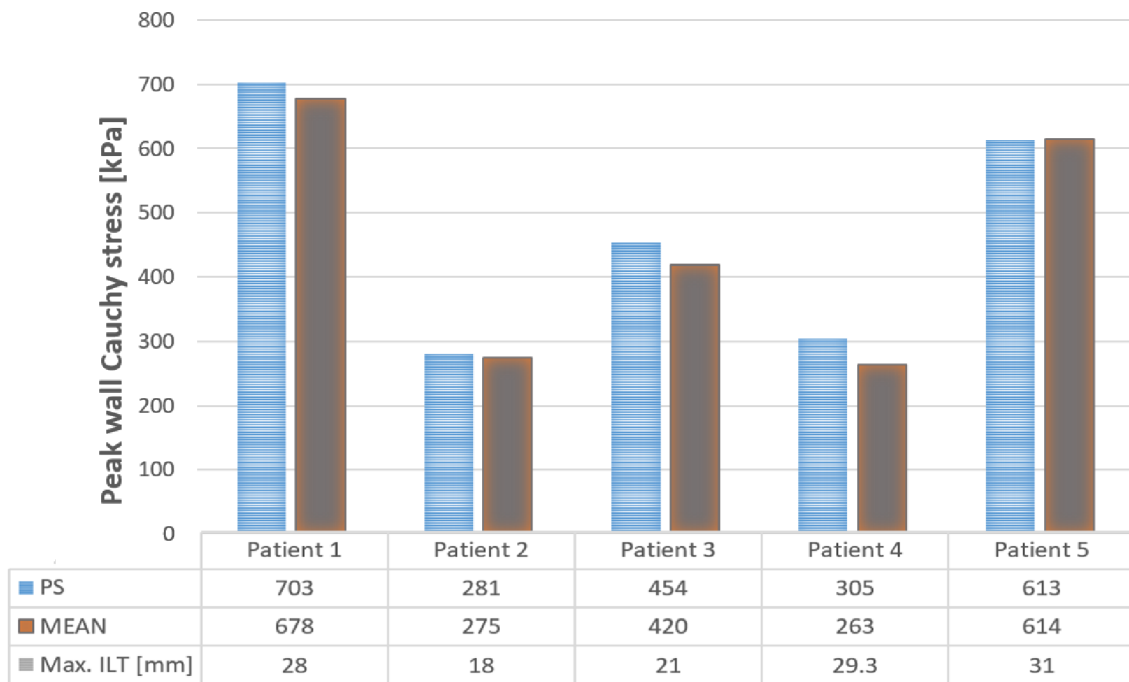
Figure 44. Peak wall Cauchy stresses compared to maximal ILT thickness for patients 1-5.

The resulting maximum stresses were statistically analyzed by using the non-parametric Man-Whitney U test for data with unknown distribution. The null hypothesis stating that the maximum stresses obtained from both approaches are the same has been rejected on the level of significance of *p=0.67*. Therefore, the differences in maximum stresses induced by the different ILT material models are not statistically significant and additional modeling would need to be performed in order to increase the size of the evaluated data and prove that the patient-specific approach alters the maximum AAA wall stresses on a statistically significant level.

However, a single stress value may not give a comprehensive comparison of the two different computational approaches, therefore a more advanced evaluation is provided. In order to further investigate the influence of different material models, whole stress fields were compared on a node-by-node basis and plotted in form of histograms. For all five geometry couples, at each node, stresses obtained from the analysis using patient-specific model and model with mean stiffness values, were compared. The stress differences at each node were divided into magnitude based groups. Followingly, a histogram was plotted revealing the group's appearance frequencies (figure 45).
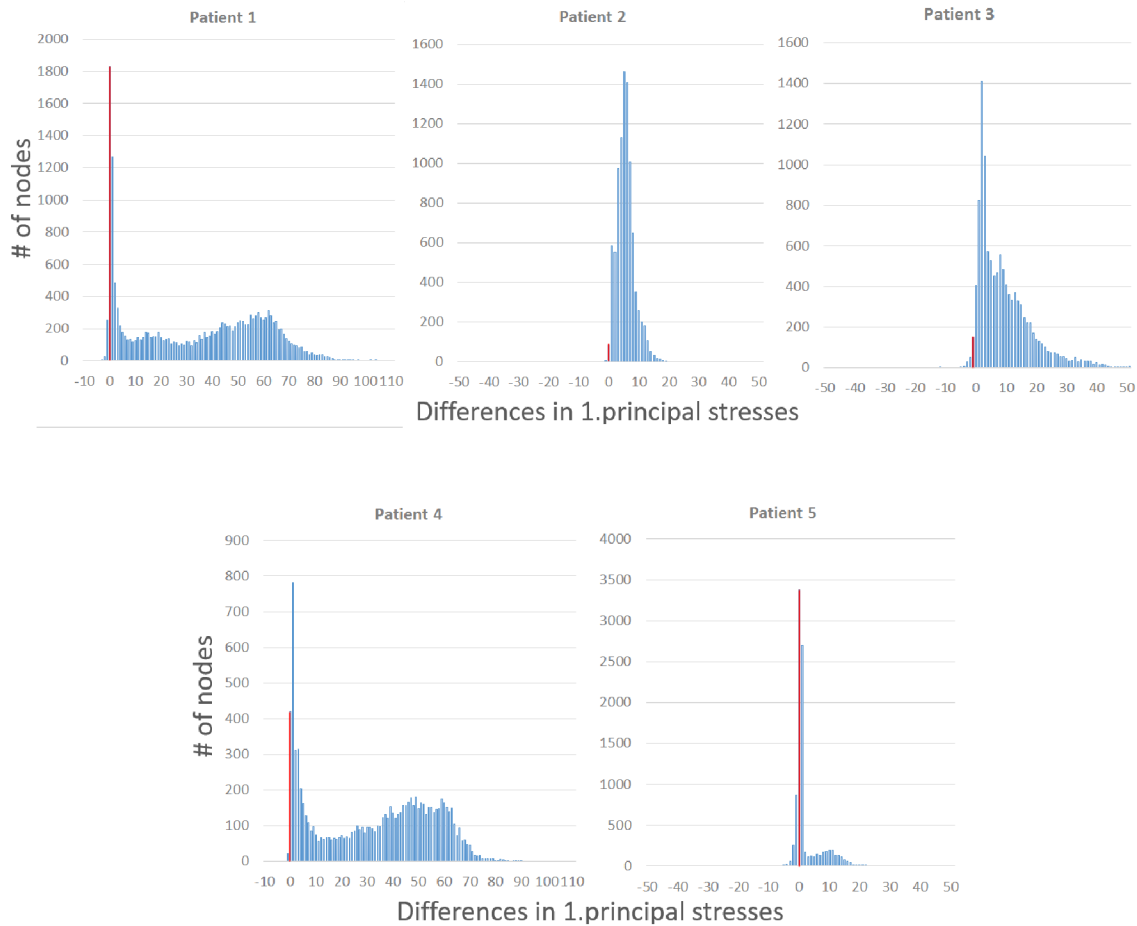
Figure 45 Node-by-node comparison of the result obtained from mean values of ILT properties and patient-specific values, plotted in form of histogram for all 5 patients. Red column indicates zero difference between stresses compared. Columns with positive values of differences represent nodes where the stresses computed with the mean values of stiffness were underestimated according to the patient-specific approach.

In figure 45, a sharp distribution around the 0 kPa differences indicates a certain level of coherency among models of the tested couples. On the other hand, in cases of patients 1 and 4, a wide and flat part of the distributions represent zones with low coherence zones on the two approaches. However, in all cases, the majority of values is located to the right from zero value (indicating the same stresses in corresponding nodes), which shows that in all cases using mean data for ILT description underestimates the resulting stresses in the AAA wall. According to the node-by-node comparison, the biggest difference among the stress fields can be observed in the case of patient 1 with the average nodal stress difference of 33 kPa.

Additionally, nodes with the biggest differences of stresses were located. These nodes represent the biggest deviation of the two approaches and are their quantitative comparison is provided in figure 46.

	Patient 1	Patient 2	Patient 3	Patient 4	Patient 5
PS	278	171	242	210	126
MEAN	174	153	190	120	105
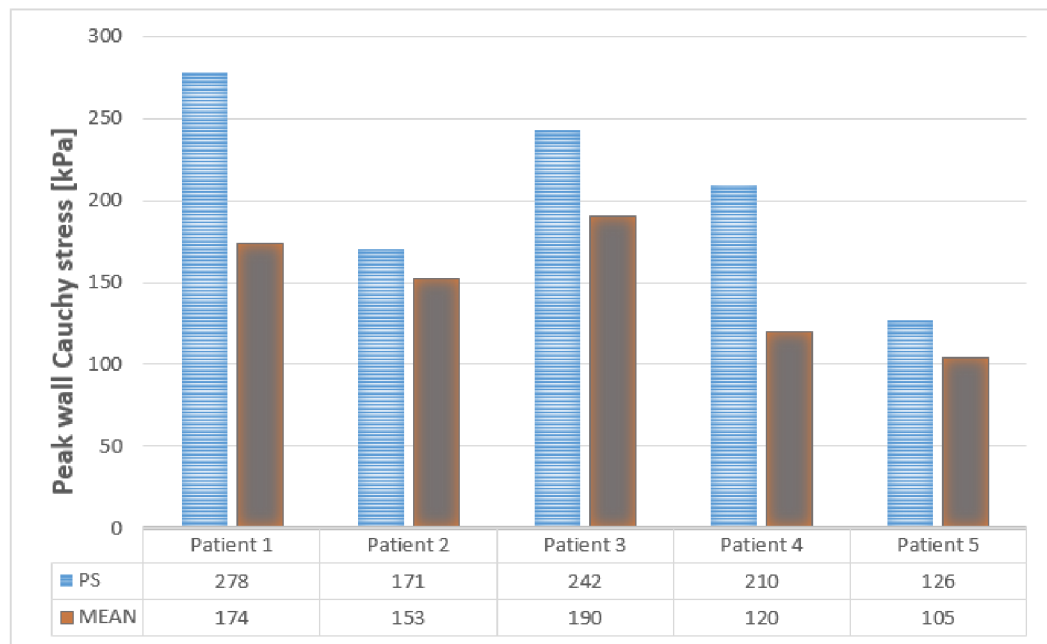
Figure 46. Peak wall Cauchy stresses differences for patients 1-5.

As it can be observed in figure 46, in all cases, at the locations where the both approaches differ the most, computing the AAA wall stress using the mean population ILT material model cause underestimation of the stresses from 18 kPa (patient 2) up to 104 kPa in the case of patient 1. This difference in local stress can play a significant role in AAA rupture risk evaluation since local peak wall stresses are compared with local wall strength [2]. Statistically, it was analyzed by Wilcoxon signed rank test to confirm whether median of observed stresses which differ most between PS and mean analyses are statistically different as well. The median of the PS stresses from Figure 46 is 210kPa, which was confirmed to be statistically greater than median of stress from mean analyses 153kPa. (p=0.03) Therefore, according to this fact, the findings that the PS ILT mechanical properties, including negligibility of the outer layer increase local stresses, can be considered as generally valid. On the other hand, by looking at the specific locations of the nodes with maximum stress differences, except the fact that in all cases the nodes were located in the regions influenced by the presence of the ILT tissue, no significant correlation can be observed as the nodes seem to be rather randomly distributed across the AAA bulk (figure 47).
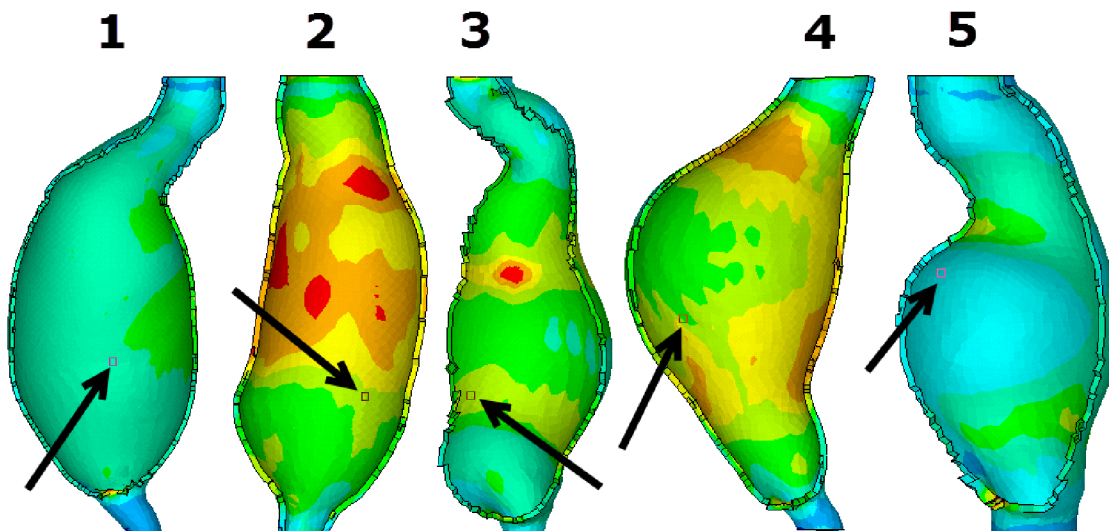
Figure 47 Locations of the node reporting the largest underestimations of stresses when calculating with mean ILT material properties. Scales describing the contour plots are identical to those in figures 40 and 41 respectively for each patient number, however for the purpose of this figure are not important.

For further statistical evaluation of the data obtained by comparing stresses in every node, basic statistical parameters for each of the 5 datasets were calculated and are listed in table 8.

Patient #	Mean [kPa]	Modus [kPa]	Median [kPa]	Standart deviation [kPa]
1	33	0	35	26
2	5	5	5	3
3	9	2	6	9
4	32	3	36	23
5	2	0	0	4

Table 8 Statistical parameters of stress differences data sets for patients 1-5.

9 Discussion

In this thesis, the influence of using patient-specified ILT mechanical properties in comparison with mean population mechanical properties was tested. To do so, ILT samples from 5 patients were obtained together with corresponding patient-specific geometries of the whole AAA structures. AAA wall geometry models were meshed with 3D hexahedral elements while tetrahedral elements were used to discretize the model of ILT, equipped either with the mean population material characteristics or characteristics obtained from mechanical testing of the 5 ILT samples. Therefore, in total 10 computational models based on 5 different geometries were created. Within the same geometry couples, each computational model was prescribed with one of the two material characteristics. Moreover, not only the patient-specific mechanical properties of the ILT tissue but also a distribution of the ILT material layers across the ILT thickness was optimized according to a biaxial mechanical testing performed in this thesis (figure 40). Even though, there are studies that use a single stress value based characteristics to compare the AAA wall stress-strain states [40, 47, 53, 54, 59], in this thesis, to extend the basic comparison of the maximal principal wall stresses among the same geometry couples, the whole stress fields were compared on node-to-node basis, representing a more complex comparison of the two approaches. Moreover, due to an existing stress gradient across the AAA wall thickness most probably caused by neglecting of residual forces, the importance of the node-by-node comparison raises [60]. In addition, the statistical significance of the obtained results was tested.

According to the result section (see chapter 8), using mean population values of the ILT properties when computing AAA wall stresses, globally alters the AAA wall stress fields on a statistically significant level. The computational model, prescribed with mean data ILT properties, underestimated the resulting maximum wall stresses in all cases, however, only in cases of patient 3 and 4 the percentual difference, was above the 5% value (8.1% and 16% respectively) which was previously considered as negligible. Moreover, nodes experiencing the biggest stress differences of the two approaches were analyzed. In these nodes, the stresses, that were computed under the assumptions of mean ILT values, were in average lower by 38.8% and ranging from 11.8% up to 75% for patients 2 and 4 respectively. A stress underestimation like this can play a significant role when calculating the AAA risk factors since local wall stress is compared with the AAA wall strength as used in some approaches for rupture risk assessment of AAA [41]. Additionally, the stress fields were globally compared on a node-by-node basis to demonstrate that the difference in stress derived from the different material definition was not a local phenomenon. In this case, the performed Wilcoxon non-parametric test confirmed a statistical significance between both approaches for the maximum stress differences. Therefore, it has been found that the ILT PS properties including the negligible outer ILT layer, alters the resulting AAA wall stress field on a statistically significant level affecting mainly the local stresses. Consequently, this analysis can be considered general as long as it includes all typical shapes of the AAA. Thus, it is suggested to extend this study to more cases anyway.

The findings of this thesis cannot be easily compared with the finding of other studies since to this date no studies have tested the influence of negligible stiffness of the ILT outer layer even though, a high level of degradation, making the mechanical testing of the outer layer impossible, has been suggested by Wang et al. [22] and Vande Geest et al. [27]. Also, it is necessary to mention that the biaxial mechanical testing of the ILT

tissue (chapter 6) provided data similar to those presented by Gasser et al. [3] or Vande Geest et al. [30] as compared in figure 28. Therefore, it can be concluded that performed mechanical testing most likely did not include any systemic error and provided results are realistic. Consequently, the majority of the stress differences described in the result section (chapter 8) can by assigned to the influence of ILT's outer layer negligible stiffness.

9.1 Limitations

It is necessary to mention that there are several limitations and potential inaccuracies under which the results have been obtained.

9.1.1 AAA geometry

First, when reconstructing patient-specific geometries, every part of this difficult multi-step process induces some level of geometrical inaccuracies in the model, since the imagining methods scanning properties are limited by the size of voxel and quality of segmentation is highly dependent on the operator experience. Above that, calcifications that may be present in AAA walls were not considered. It was suggested, that the calcifications cause stress peak zones by increasing the stress by 22% [73]. This phenomenon can be included in the geometry models during segmentation since it is visible on CT scans, however, calcifications are, by most researchers, not included in their analysis due to its strong dependence on constitutive information, which determines the reliability of modeling [41]. In this thesis, ILTs were assumed to be crack-free, however, it has been previously suggested by Polzer et al. [2] that ILT fissures can elevate the resulting stresses in the AAA wall by 30%. Also, even though the thickness of the AAA wall changes as the aneurysm grows, due to an advanced complexity, in this thesis, the wall was modeled as of uniform thickness, noting the fact that the wall stress increases as the wall thickness decreases.

9.1.2 Boundary conditions

The surroundings of abdominal aorta consist of the vertebral column, running along the aortic posterior side, and soft tissue components of the abdominal cavity. Therefore, in terms of stiffness, the surroundings of AAA are strongly non-homogenous. In reality, it is likely to happen that the AAA expansion is limited by a component of the abdominal cavity introducing external loads to the AAA wall. Despite the fact that, modeling of this aspect would be possible by restricting deformation at a certain region, due to lack of information, this external boundary conditions were neglected similarly as in the most available studies [2, 40, 41, 47, 53, 54, 55, 57, 59, 60, 62, 63, 64, 65, 68, 73, 74, 75,77].

9.1.3 Structural properties

In terms of experimental testing conducted in this thesis, a greater number of biaxial specimens for each ILT would allow to better describe the ILTs properties across its thickness, since in 3 cases only one biaxial specimen was obtained due to the sample's unsuitable geometry or poor structure. Also, a lack of equipment, that would allow precise slicing of the ILT sample into layers with uniform thickness, which is difficult due to the non-homogenous composition of the tissue, induced uncertainties in engineering stress calculations, derived from the specimen's cross-section. Additionally, the data obtained

from mechanical testing were fitted with constitutive material models with a limited precision. Moreover, as mentioned earlier, ILT tissue is rather porous structure. Therefore, implementing the poroelastic material model in FEM analysis would better simulate physiological conditions. However, according to Polzer et al. [8], who used the poroelastic material model of ILT for FE analysis of AAA, the decrease of pressure caused by the shielding properties of the ILT is small and suggested that in term of AAA wall stress distribution, the poroelastic nature of the ILT can be neglected. Therefore, in this thesis, the non-shielding properties of the ILT has been accounted for by applying the loading pressure directly to the AAA inner wall but homogenous single-phase material for modeling ILT tissue has been used. Also, the material was considered hyperelastic since, in most of physiologic and pathophysiologic states, the assumption of hyperelasticity is relevant [20]. Additionally, according to [24], anisotropic properties of the normal aorta that are caused by the orientation of collagen fibers, disappear with the aneurysmal disease. This assumption has been accepted for the whole AAA wall, despite the non-aneurysmal end parts of the AAA geometry models.

Mechanical properties of human arteries are temperature dependent. With increased temperature, the aortic tissue seems to become more compliant [70]. This was respected only by performing the biaxial testing in the temperature controlled bath. Again, this approach is consistent with available literature [2, 40, 41, 47, 53, 54, 55, 57, 59, 60, 62, 63, 64, 65, 68, 73, 74, 75,77].

9.1.4 Residual stresses, pre-stressing, and pulsatile pressure

Moreover, as being mentioned above, neglecting the residual stresses in AAA wall is most likely responsible for non-realistic stress gradient across the AAA wall, however, determination of residual stresses for a complex geometry structure such as AAA, is a difficult task, therefore in most studies, residual stresses remain unknown and are generally neglected [2,40,59,60,62,68]. Similarly, since the arterial pre-strain decreases with age [69], for the population in danger of AAA development this value is insignificant and has been neglected in this thesis. Additionally, as discussed in 7.1, geometry obtained from CT scans were treated as unloaded, accepting the consequences of globally increased stresses. Ideally, a computational model of AAA would induce a fluid-structure interaction, would be loaded by a dynamic load corresponding to the pulsatile nature of blood pressure, and would incorporate the viscoelastic properties (creep, stress relaxation and hysteresis) of the ILT and AAA wall. Above that, according to Scotti et al. [58], performing a fluid-structure analysis instead of loading the AAA wall with static pressure increases maximum wall stress by 20%. On the other hand, others suggest that the influence of blood flow on in terms of loading the AAA structure is negligible and steady activation is fully acceptable [40,81]. Therefore, this contradiction is a possible subject of further investigation.

9.1.5 Dynamics

Even though the load was applied under static conditions, worst possible scenario was simulated by loading the structure by systolic pressure. When including fatigue in rupture risk calculations, it has been suggested to lower the static ILT and AAA wall strengths to 40% and 50%, respectively [3,41].

Despite the assumptions and simplification that has been made, it is unlikely to assume that more complex modeling of the AAA structure would have resulted in

different findings since the conclusions of this thesis are based on computational models comparisons which were all calculated under the same assumptions. Above that, it has been suggested by Gasser et al. [41] and Polzer et al. [2] that including a patient-specific model of geometry, that has been used in this thesis, is the most crucial part of the structural analysis.

10 Conclusion

In this thesis, the uncertainties of finite element stress-train analysis of the abdominal aortic aneurysm, caused by neglecting patient-specific material properties of the ILT tissue, were analyzed. To do so, **two types** of geometry models were created. First, an idealized geometry model was developed to conduct a finite element mesh convergence study. Also, there is a gradient of material properties across the ILT stiffness which is modeled by materially different layers to create an onion-like structure. Therefore, in this thesis, a study determining the AAA wall stress dependence on the number of ILT materially different layers was conducted on the idealized geometry using a macro which prescribed each element of the ILT FE mesh with material properties based on the element's distance from the lumen.

Following, 5 **patient-specific geometries** reconstructed from CT scans prior the AAA elective repairs were used. The geometries of AAA walls were meshed with **hexagonal elements** using the ICEM CFD software. Then, in order to determine the **patient-specific material properties** of the ILT structure, **biaxial experimental testing** was conducted, examining ILT samples harvested from the five elective repairs to match the patient-specific mechanical properties with the corresponding geometries. The experimental testing gave **comparable results** to those presented by Gasser et al. [3] and Vande Geest et al. [30] which are the most frequently cited studies on this topic. Importantly, the experimental testing confirmed the **stiffness negligibility of the intraluminal thrombus's outer layer**, which is mentioned is several studies [22,27], however, the influence of this layer on resulting aneurysmal wall stress has been to this date not tested.

Therefore, in this thesis, the close to **zero stiffness** of the ILT outer layer **was included** in the material modeling. In terms of material modeling, both, the ILT and AAA wall were modeled with **hyperelastic** constitutive material models. The results have been presented in form contour plots, peak stresses comparisons and histograms, comparing the stress fields on a node-by-node basis and allowing to determine the probability density function for each geometry couple that has been compared.

The result has been statistically analyzed by using the non-parametric tests which confirmed that the **ILT patient specific material properties** with considering the outer layer as of zero-like stiffness **alter the resulting AAA wall stress fields on a statistically significant level**.

In conclusion, this study highlighted the importance of using mechanically negligible ILT outer layer in order to obtain more realistic wall stresses.

11 List of used abbreviations and symbols

AAA	[-]	aortic abdominal aneurysm
C_{ij}	[-]	Cauchy-Green deformation tensor
$c_{10}, c_{20}, \mu_p, \alpha_p$		material parameters
CCD	[-]	charged-coupled device
CT	[-]	computer topography
E_{ij}^L	[-]	Green-Lagrange strain tensor
FE	[-]	finite element
FEM	[-]	finite element method
G	[Pa]	shear modulus
ILT	[-]	intraluminal thrombus
I_1, I_2, I_3		Cauchy-Green deformation tensor invariants
MLU	[-]	medial lamellar unit
PS	[-]	patient-specific
RBC	[-]	red blood cell
S_i	[Pa]	engineering stress
S_{ij}	[-]	second Piola-Kirchhoff stress tensor
SMC	[-]	smooth muscle cell
u_i	[m]	displacement
W	[-]	strain energy
X_i	[m]	coordinates in initial undeformed state
x_i	[m]	coordinates in final deformed state
$\lambda x, \lambda y, \lambda z$	[-]	stretch ratios

12 References

[1] RUIZ DE GALARRETA, Sergio, Raúl ANTÓN, Aitor CAZON, Gorka S. LARRAONA a Ender A. FINOL. Anisotropic abdominal aortic aneurysm replicas with biaxial material characterization. *Medical Engineering & Physics* [online]. 2016, **38**(12), 1505-1512 [cit. 2017-02-23]. DOI: 10.1016/j.medengphy.2016.09.010. ISSN 13504533. Available from: http://linkinghub.elsevier.com/retrieve/pii/S1350453316302107

[2] POLZER, S., T.C. GASSER, J. SWEDENBORG a J. BURSA. The Impact of Intraluminal Thrombus Failure on the Mechanical Stress in the Wall of Abdominal Aortic Aneurysms. *European Journal of Vascular and Endovascular Surgery* [online]. 2011, **41**(4), 467-473 [cit. 2017-02-23]. DOI: 10.1016/j.ejvs.2010.12.010. ISSN 10785884. Available from: http://linkinghub.elsevier.com/retrieve/pii/S1078588410007823

[3] GASSER, T. Christian, Göray GÖRGÜLÜ, Maggie FOLKESSON a Jesper SWEDENBORG. Failure properties of intraluminal thrombus in abdominal aortic aneurysm under static and pulsating mechanical loads. *Journal of Vascular Surgery* [online]. 2008, **48**(1), 179-188 [cit. 2017-02-23]. DOI: 10.1016/j.jvs.2008.01.036. ISSN 07415214. Available from: http://linkinghub.elsevier.com/retrieve/pii/S0741521408001262

[4] GANONG, William F. *Přehled lékařské fyziologie*. 20. vyd. Praha: Galén, c2005. ISBN 9788072623112.

[5] THIRIET, Marc. *Biology and mechanics of blood flows*. Online-Ausg. New York, NY: Springer, 2008. ISBN 9780387748498.

[6] Blood Rheology and Hemodynamics. *Seminars in Thrombosis and Hemostasis* [online]. 2003, **29**(5), 435-450 [cit. 2017-04-04]. DOI: 10.1055/s-2003-44551. ISSN 00946176. Available from: http://www.thieme-connect.de/DOI/DOI?10.1055/s-2003-44551

[7] SUN, Chenghai a Lance L. MUNN. Particulate Nature of Blood Determines Macroscopic Rheology: A 2-D Lattice Boltzmann Analysis. *Biophysical Journal* [online]. 2005, **88**(3), 1635-1645 [cit. 2017-04-05]. DOI: 10.1529/biophysj.104.051151. ISSN 00063495. Available from: http://linkinghub.elsevier.com/retrieve/pii/S0006349505732306

[8] POLZER, S. a J. BURSA. *Poroelastic Model of Intraluminal Thrombus in FEA of Aortic Aneurysm* [online]. s. 763 [cit. 2017-05-12]. DOI: 10.1007/978-3-642-14515-5_194. Available from: http://link.springer.com/10.1007/978-3-642-14515-5_194

[9] BIASETTI, Jacopo. *Physics of blood flow in arteries and its relation to intraluminal thrombus and atherosclerosis*. Stockholm, 2013. Doctoral thesis. KTH School of Engineering Sciences.

[10] PÁČ, Libor. *Anatomie člověka II: splanchnologie, kardiovaskulární systém, žlázy s vnitřní sekrecí*. Brno: Masarykova univerzita, 2007. ISBN 9788021042919.

[11] O'ROURKE, Michael F. a Audrey ADJI. Basis for use of central blood pressure measurement in office clinical practice. *Journal of the American Society of Hypertension* [online]. 2008, **2**(1), 28-38 [cit. 2017-05-12]. DOI: 10.1016/j.jash.2007.08.006. ISSN 19331711. Available from: http://linkinghub.elsevier.com/retrieve/pii/S1933171107001726

[12] KU, David N. BLOOD FLOW IN ARTERIES. *Annual Review of Fluid Mechanics* [online]. 1997, **29**(1), 399-434 [cit. 2017-04-07]. DOI: 10.1146/annurev.fluid.29.1.399. ISSN 00664189. Available from: http://www.annualreviews.org/doi/10.1146/annurev.fluid.29.1.399

[13] TEZDUYAR, Tayfun E. Arterial fluid mechanics modeling with the stabilized space–timefluid–structure interaction technique. *INTERNATIONAL JOURNAL FOR NUMERICAL METHODS IN FLUIDS* [online]. 2007, **2008**(57), 601–629 [cit. 2017-04-07]. Available from: http://onlinelibrary.wiley.com/doi/10.1002/fld.1633/epdf

[14] ROGERS, Walter J, Yong-Lin HU, Douglas COAST, Diane A VIDO, Christopher M KRAMER, Reed E PYERITZ a Nathaniel REICHEK. Age-associated changes in regional aortic pulse wave velocity. *Journal of the American College of Cardiology* [online]. 2001, **38**(4), 1123-1129 [cit. 2017-04-07]. DOI: 10.1016/S0735-1097(01)01504-2. ISSN 07351097. Available from: http://linkinghub.elsevier.com/retrieve/pii/S0735109701015042

[15] LATHAM, R. D., N. WESTERHOF, P. SIPKEMA, B. J. RUBAL, P. REUDERINK a J. P. MURGO. Regional wave travel and reflections along the human aorta: a study with six simultaneous micromanometric pressures. *Circulation* [online]. 1985, **72**(6), 1257-1269 [cit. 2017-04-07]. DOI: 10.1161/01.CIR.72.6.1257. ISSN 00097322. Available from: http://circ.ahajournals.org/cgi/doi/10.1161/01.CIR.72.6.1257

[16] CHO, Sung Woo, Byung Kyu KIM, Jeong Hoon KIM, et al. Non-invasively measured aortic wave reflection and pulse pressure amplification are related to the severity of coronary artery disease. *Journal of Cardiology* [online]. 2013, **62**(2), 131-137 [cit. 2017-04-08]. DOI: 10.1016/j.jjcc.2013.03.014. ISSN 09145087. Available from: http://linkinghub.elsevier.com/retrieve/pii/S091450871300124X

[17] VAN VARIK, Bernard J., Roger J. M. W. RENNENBERG, Chris P. REUTELINGSPERGER, Abraham A. KROON, Peter W. DE LEEUW a Leon J. SCHURGERS. Mechanisms of arterial remodeling: lessons from genetic diseases. *Frontiers in Genetics* [online]. 2012, **3**(290), - [cit. 2017-04-08]. DOI: 10.3389/fgene.2012.00290. ISSN 16648021. Available from: http://journal.frontiersin.org/article/10.3389/fgene.2012.00290/abstract

[18] SEGERS, Patrick, Jan KIPS, Bram TRACHET, et al. Limitations and pitfalls of non-invasive measurement of arterial pressure wave reflections and pulse wave velocity. *Artery Research* [online]. 2009, **3**(2), 79-88 [cit. 2017-04-08]. DOI: 10.1016/j.artres.2009.02.006. ISSN 18729312. Available from: http://linkinghub.elsevier.com/retrieve/pii/S1872931209000118

[19] ČIHÁK, Radomír, DRUGA, Rastislav a Miloš GRIM, ed. *Anatomie III*. 2., upr. a dopl. vyd. Praha: Grada, 2004. ISBN 802471132x.

[20] TAYLOR, C.A. a J.D. HUMPHREY. Open problems in computational vascular biomechanics: Hemodynamics and arterial wall mechanics. *Computer Methods in Applied Mechanics and Engineering* [online]. 2009, **198**(45-46), 3514-3523 [cit. 2017-04-10]. DOI: 10.1016/j.cma.2009.02.004. ISSN 00457825. Available from: http://linkinghub.elsevier.com/retrieve/pii/S0045782509000899

[21] HUMPHREY, J.D. a G.A. HOLZAPFEL. Mechanics, mechanobiology, and modeling of human abdominal aorta and aneurysms. *Journal of Biomechanics* [online]. 2012, **45**(5), 805-814 [cit. 2017-04-11]. DOI: 10.1016/j.jbiomech.2011.11.021. ISSN 00219290. Available from: http://linkinghub.elsevier.com/retrieve/pii/S0021929011007032

[22] MAKAROUN, Michel. Mechanical Properties and Microstructure of Intraluminal Thrombus From Abdominal Aortic Aneurysm. *Journal of Biomechanical Engineering* [online]. 2001, **123**(6), 536- [cit. 2017-04-11]. DOI: 10.1115/1.1411971. ISSN 01480731. Available from: http://biomechanical.asmedigitalcollection.asme.org/article.aspx?doi=10.1115/1.1411971

[23] BIASETTI, Jacopo, T. Christian GASSER, Martin AUER, Ulf HEDIN a Fausto LABRUTO. Hemodynamics of the Normal Aorta Compared to Fusiform and Saccular Abdominal Aortic Aneurysms with Emphasis on a Potential Thrombus Formation Mechanism. *Annals of Biomedical Engineering* [online]. 2010, **38**(2), 380-390 [cit. 2017-04-11]. DOI: 10.1007/s10439-009-9843-6. ISSN 00906964. Available from: http://link.springer.com/10.1007/s10439-009-9843-6

[24] BACK, M., T. C. GASSER, J.-B. MICHEL a G. CALIGIURI. Biomechanical factors in the biology of aortic wall and aortic valve diseases. *Cardiovascular Research* [online]. 2013, **99**(2), 232-241 [cit. 2017-04-15]. DOI: 10.1093/cvr/cvt040. ISSN 00086363. Available from: https://academic.oup.com/cardiovascres/article-lookup/doi/10.1093/cvr/cvt040

[25] WILSON, J. S., L. VIRAG, P. DI ACHILLE, I. KARŠAJ a J. D. HUMPHREY. Biochemomechanics of Intraluminal Thrombus in Abdominal Aortic Aneurysms. *Journal of Biomechanical Engineering* [online]. 2013, **135**(2), 021011- [cit. 2017-04-15]. DOI: 10.1115/1.4023437. ISSN 01480731. Available from: http://biomechanical.asmedigitalcollection.asme.org/article.aspx?doi=10.1115/1.4023437

[26] VORP, D. Potential influence of intraluminal thrombus on abdominal aortic aneurysm as assessed by a new non-invasive method. *Cardiovascular Surgery* [online]. 1996, **4**(6), 732-739 [cit. 2017-04-18]. DOI: 10.1016/S0967-2109(96)00008-7. ISSN 09672109. Available from: http://linkinghub.elsevier.com/retrieve/pii/S0967210996000087

[27]   VANDE GEEST, Jonathan P., Michael S. SACKS a David A. VORP. A planar biaxial constitutive relation for the luminal layer of intra-luminal thrombus in abdominal aortic aneurysms. *Journal of Biomechanics* [online]. 2006, **39**(13), 2347-2354 [cit. 2017-04-18]. DOI: 10.1016/j.jbiomech.2006.05.011. ISSN 00219290. Available from: http://linkinghub.elsevier.com/retrieve/pii/S0021929006001655

[28]   Abdominal aortic aneurysm (AAA). In: *Hunter Vascular* [online]. Gateshead: huntervascular, 2013 [cit. 2017-04-19]. Available from: http://www.huntervascular.com/aaa/

[29]   SACKS, Michael S. Biaxial Mechanical Evaluation of Planar Biological Materials. *Journal of Elasticity* [online]. 2000, **61**(1/3), 199-246 [cit. 2017-04-20]. DOI: 10.1023/A:1010917028671. ISSN 03743535. Available from: http://link.springer.com/10.1023/A:1010917028671

[30]   VANDE GEEST, Jonathan P., Michael S. SACKS a David A. VORP. The effects of aneurysm on the biaxial mechanical behavior of human abdominal aorta. *Journal of Biomechanics* [online]. 2006, **39**(7), 1324-1334 [cit. 2017-04-21]. DOI: 10.1016/j.jbiomech.2005.03.003. ISSN 00219290. Available from: http://linkinghub.elsevier.com/retrieve/pii/S0021929005001326

[31]   FUNG, Yuan-Cheng. *Biomechanics Mechanical Properties of Living Tissues*. Second edition. New York, NY: Springer New York, 1993. ISBN 9781475722574.

[32]   FERRARA, Anna, Simone MORGANTI, Pasquale TOTARO, Alessandro MAZZOLA a Ferdinando AURICCHIO. Human dilated ascending aorta: Mechanical characterization via uniaxial tensile tests. *Journal of the Mechanical Behavior of Biomedical Materials* [online]. 2016, **53**(1), 257-271 [cit. 2017-04-21]. DOI: 10.1016/j.jmbbm.2015.08.021. ISSN 17516161. Available from: http://linkinghub.elsevier.com/retrieve/pii/S1751616115002921

[33]   ALEXANDER, J.Jeffrey. The pathobiology of aortic aneurysms. *Journal of Surgical Research* [online]. 2004, **117**(1), 163-175 [cit. 2017-04-22]. DOI: 10.1016/j.jss.2003.11.011. ISSN 00224804. Available from: http://linkinghub.elsevier.com/retrieve/pii/S0022480403007479

[34]   J. THUBRIKAR, M. LABROSSE, F. ROBIC, M. Mechanical properties of abdominal aortic aneurysm wall. *Journal of Medical Engineering & Technology* [online]. 2009, **25**(4), 133-142 [cit. 2017-04-22]. DOI: 10.1080/03091900110057806. ISSN 03091902. Available from: https://www.ncbi.nlm.nih.gov/pubmed/11601439

[35]   KENT, K. Craig, Robert M. ZWOLAK, Natalia N. EGOROVA, Thomas S. RILES, Andrew MANGANARO, Alan J. MOSKOWITZ, Annetine C. GELIJNS a Giampaolo GRECO. Analysis of risk factors for abdominal aortic aneurysm in a cohort of more than 3 million individuals. *Journal of Vascular Surgery* [online]. 2010, **52**(3), 539-548 [cit. 2017-04-22]. DOI: 10.1016/j.jvs.2010.05.090. ISSN

07415214. Available from: http://linkinghub.elsevier.com/retrieve/pii/S0741521410013029

[36] VORP, David A., Paul C. LEE, David H.J. WANG, Michel S. MAKAROUN, Edwin M. NEMOTO, Satoshi OGAWA a Marshall W. WEBSTER. Association of intraluminal thrombus in abdominal aortic aneurysm with local hypoxia and wall weakening. *Journal of Vascular Surgery* [online]. 2001, **34**(2), 291-299 [cit. 2017-04-22]. DOI: 10.1067/mva.2001.114813. ISSN 07415214. Available from: http://linkinghub.elsevier.com/retrieve/pii/S0741521401594288

[37] SCHURINK, G.W.H., J.M. VAN BAALEN, M.J.T. VISSER a J.H. VAN BOCKEL. Thrombus within an aortic aneurysm does not reduce pressure on the aneurysmal wall. *Journal of Vascular Surgery* [online]. 2000, **31**(3), 501-506 [cit. 2017-04-22]. DOI: 10.1067/mva.2000.103693. ISSN 07415214. Available from: http://linkinghub.elsevier.com/retrieve/pii/S0741521400903112

[38] VAN DAM, Evelyne A., Susanne D. DAMS, Gerrit W. M. PETERS, Marcel C. M. RUTTEN, Geert Willem H. SCHURINK, Jaap BUTH a Frans N. VAN DE VOSSE. Non-linear viscoelastic behavior of abdominal aortic aneurysm thrombus. *Biomechanics and Modeling in Mechanobiology* [online]. 2008, **7**(2), 127-137 [cit. 2017-04-22]. DOI: 10.1007/s10237-007-0080-3. ISSN 16177959. Available from: http://link.springer.com/10.1007/s10237-007-0080-3

[39] DOTTER, Charles T., Douglas J. ROBERTS a Israel STEINBERG. Aortic Length: Angiocardiographic Measurements. *Circulation* [online]. 1950, **2**(6), 915-920 [cit. 2017-05-12]. Available from: http://circ.ahajournals.org/content/2/6/915

[40] WANG, David H.J., Michel S. MAKAROUN, Marshall W. WEBSTER a David A. VORP. Effect of intraluminal thrombus on wall stress in patient-specific models of abdominal aortic aneurysm. *Journal of Vascular Surgery* [online]. 2002, **36**(3), 598-604 [cit. 2017-04-23]. DOI: 10.1067/mva.2002.126087. ISSN 07415214. Available from: http://linkinghub.elsevier.com/retrieve/pii/S074152140200099X

[41] GASSER, T.C., M. AUER, F. LABRUTO, J. SWEDENBORG a J. ROY. Biomechanical Rupture Risk Assessment of Abdominal Aortic Aneurysms: Model Complexity versus Predictability of Finite Element Simulations. *European Journal of Vascular and Endovascular Surgery* [online]. 2010, **40**(2), 176-185 [cit. 2017-05-21]. DOI: 10.1016/j.ejvs.2010.04.003. ISSN 10785884. Available from: http://linkinghub.elsevier.com/retrieve/pii/S1078588410002364

[42] TONG, J., T. COHNERT, P. REGITNIG a G.A. HOLZAPFEL. Effects of Age on the Elastic Properties of the Intraluminal Thrombus and the Thrombus-covered Wall in Abdominal Aortic Aneurysms: Biaxial Extension Behaviour and Material Modelling. *European Journal of Vascular and Endovascular Surgery* [online]. 2011, **42**(2), 207-219 [cit. 2017-04-23]. DOI: 10.1016/j.ejvs.2011.02.017. ISSN 10785884. Available from: http://linkinghub.elsevier.com/retrieve/pii/S107858841100089X

[43] RAGHAVAN, Madhavan L., Jarin KRATZBERG, Erasmo Magalhães CASTRO DE TOLOSA, Mauro M. HANAOKA, Patricia WALKER a Erasmo Simão DA SILVA. Regional distribution of wall thickness and failure properties of human

abdominal aortic aneurysm. *Journal of Biomechanics* [online]. 2006, **39**(16), 3010-3016 [cit. 2017-05-18]. DOI: 10.1016/j.jbiomech.2005.10.021. ISSN 00219290. Available from: http://linkinghub.elsevier.com/retrieve/pii/S0021929005004781

[44] ROY, Joy, Fausto LABRUTO, Mats O. BECKMAN, Jesper DANIELSON, Gunnar JOHANSSON a Jesper SWEDENBORG. Bleeding into the intraluminal thrombus in abdominal aortic aneurysms is associated with rupture. *Journal of Vascular Surgery* [online]. 2008, **48**(5), 1108-1113 [cit. 2017-04-23]. DOI: 10.1016/j.jvs.2008.06.063. ISSN 07415214. Available from: http://linkinghub.elsevier.com/retrieve/pii/S0741521408011038

[45] DI MARTINO, E., S. MANTERO, F. INZOLI, G. MELISSANO, D. ASTORE, R. CHIESA a R. FUMERO. Biomechanics of abdominal aortic aneurysm in the presence of endoluminal thrombus: Experimental characterisation and structural static computational analysis. *European Journal of Vascular and Endovascular Surgery* [online]. 1998, **15**(4), 290-299 [cit. 2017-04-23]. DOI: 10.1016/S1078-5884(98)80031-2. ISSN 10785884. Available from: http://linkinghub.elsevier.com/retrieve/pii/S1078588498800312

[46] WOLF, Yehuda G., Winston S. THOMAS, Frank J. BRENNAN, Walter G. GOFF, Michael J. SISE a Eugene F. BERNSTEIN. Computed tomography scanning findings associated with rapid expansion of abdominal aortic aneurysms. *Journal of Vascular Surgery* [online]. 1994, **20**(4), 529-538 [cit. 2017-05-09]. DOI: 10.1016/0741-5214(94)90277-1. ISSN 07415214. Available from: http://linkinghub.elsevier.com/retrieve/pii/0741521494902771

[47] SPEELMAN, L., E.M.H. BOSBOOM, G.W.H. SCHURINK, F.A.M.V.I. HELLENTHAL, J. BUTH, M. BREEUWER, M.J. JACOBS a F.N. VAN DE VOSSE. Patient-Specific AAA Wall Stress Analysis: 99-Percentile Versus Peak Stress. *European Journal of Vascular and Endovascular Surgery* [online]. 2008, **36**(6), 668-676 [cit. 2017-05-09]. DOI: 10.1016/j.ejvs.2008.09.007. ISSN 10785884. Available from: http://linkinghub.elsevier.com/retrieve/pii/S1078588408004887

[48] DE PUTTER, Sander, Marcel BREEUWER, Ursula KOSE, et al. Automatic determination of the dynamic geometry of abdominal aortic aneurysm from MR with application to wall stress simulations. *International Congress Series* [online]. 2005, **1281**, 339-344 [cit. 2017-05-09]. DOI: 10.1016/j.ics.2005.03.256. ISSN 05315131. Available from: http://linkinghub.elsevier.com/retrieve/pii/S0531513105005145

[49] STRBAC, V., D.M. PIERCE, B. RODRIGUEZ-VILA, J. VANDER SLOTEN a N. FAMAEY. Rupture risk in abdominal aortic aneurysms: A realistic assessment of the explicit GPU approach. *Journal of Biomechanics* [online]. 2017, **56**(1), 1-9 [cit. 2017-05-09]. DOI: 10.1016/j.jbiomech.2017.02.019. ISSN 00219290. Available from: http://linkinghub.elsevier.com/retrieve/pii/S0021929017301197

[50] ENE, Florentina, Carine GACHON, Patrick DELASSUS, Ronan CARROLL, Florian STEFANOV, Padraig O'FLYNN a Liam MORRIS. In vitro evaluation of

the effects of intraluminal thrombus on abdominal aortic aneurysm wall dynamics. *Medical Engineering & Physics* [online]. 2011, **33**(8), 957-966 [cit. 2017-05-09]. DOI: 10.1016/j.medengphy.2011.03.005. ISSN 13504533. Available from: http://linkinghub.elsevier.com/retrieve/pii/S1350453311000646

[51]   KAZI, Monsur, Johan THYBERG, Piotr RELIGA, Joy ROY, Per ERIKSSON, Ulf HEDIN a Jesper SWEDENBORG. Influence of intraluminal thrombus on structural and cellular composition of abdominal aortic aneurysm wall. *Journal of Vascular Surgery* [online]. 2003, **38**(6), 1283-1292 [cit. 2017-05-09]. DOI: 10.1016/S0741-5214(03)00791-2.   ISSN   07415214.   Available   from: http://linkinghub.elsevier.com/retrieve/pii/S0741521403007912

[52]   HOLZAPFEL, Gerhard A. *Nonlinear solid mechanics: a continuum approach for engineering*. New York: Wiley, c2000. ISBN 9780471823193.

[53]   VENKATASUBRAMANIAM, A.K, M.J FAGAN, T MEHTA, K.J MYLANKAL, B RAY, G KUHAN, I.C CHETTER a P.T MCCOLLUM. A Comparative Study of Aortic Wall Stress Using Finite Element Analysis for Ruptured and Non-ruptured Abdominal Aortic Aneurysms. *European Journal of Vascular and Endovascular Surgery* [online].   2004, **28**(2),   168-176   [cit.   2017-05-10].   DOI: 10.1016/j.ejvs.2004.03.029.   ISSN   10785884.   Available   from: http://linkinghub.elsevier.com/retrieve/pii/S1078588404001789

[54]   VORP, David A. Biomechanics of abdominal aortic aneurysm. *Journal of Biomechanics* [online].   2007, **40**(9),   1887-1902   [cit.   2017-05-10].   DOI: 10.1016/j.jbiomech.2006.09.003.   ISSN   00219290.   Available   from: http://linkinghub.elsevier.com/retrieve/pii/S002192900600323X

[55]   SPEELMAN, Lambert, Geert Willem H. SCHURINK, E. Marielle H. BOSBOOM, Jaap BUTH, Marcel BREEUWER, Frans N. VAN DE VOSSE a Michael H. JACOBS. The mechanical role of thrombus on the growth rate of an abdominal aortic aneurysm. *Journal of Vascular Surgery* [online]. 2010, **51**(1), 19-26 [cit. 2017-05-10]. DOI: 10.1016/j.jvs.2009.08.075. ISSN 07415214. Available from: http://linkinghub.elsevier.com/retrieve/pii/S0741521409017959

[56]   RAGHAVAN, M. L., Baoshun MA a Mark. F. FILLINGER. Non-Invasive Determination of Zero-Pressure Geometry of Arterial Aneurysms. *Annals of Biomedical Engineering* [online]. 2006, **34**(9), 1414-1419 [cit. 2017-05-10]. DOI: 10.1007/s10439-006-9115-7.   ISSN   00906964.   Available   from: http://link.springer.com/10.1007/s10439-006-9115-7

[57]   LU, Jia, Xianlian ZHOU a Madhavan L. RAGHAVAN. Inverse elastostatic stress analysis in pre-deformed biological structures: Demonstration using abdominal aortic aneurysms. *Journal of Biomechanics* [online]. 2007, **40**(3), 693-696 [cit. 2017-05-21]. DOI: 10.1016/j.jbiomech.2006.01.015. ISSN 00219290. Available from: http://linkinghub.elsevier.com/retrieve/pii/S0021929006000406

[58]   SCOTTI, Christine M., Jorge JIMENEZ, Satish C. MULUK a Ender A. FINOL. Wall stress and flow dynamics in abdominal aortic aneurysms: finite element analysis vs. fluid–structure interaction. *Computer Methods in Biomechanics and Biomedical Engineering* [online]. 2008, **11**(3), 301-322 [cit. 2017-05-11]. DOI:

10.1080/10255840701827412. ISSN 10255842. Available from: http://www.tandfonline.com/doi/abs/10.1080/10255840701827412

[59]   RAGHAVAN, M.L. a David A. VORP. Toward a biomechanical tool to evaluate rupture potential of abdominal aortic aneurysm: identification of a finite strain constitutive model and evaluation of its applicability. *Journal of Biomechanics* [online]. 2000, **33**(4), 475-482 [cit. 2017-05-11]. DOI: 10.1016/S0021-9290(99)00201-8. ISSN 00219290. Available from: http://linkinghub.elsevier.com/retrieve/pii/S0021929099002018

[60]   POLZER, Stanislav, T. CHRISTIAN GASSER, Jiri BURSA, Robert STAFFA, Robert VLACHOVSKY, Vojtech MAN a Pavel SKACEL. Importance of material model in wall stress prediction in abdominal aortic aneurysms. *Medical Engineering & Physics* [online]. 2013, **35**(9), 1282-1289 [cit. 2017-05-14]. DOI: 10.1016/j.medengphy.2013.01.008. ISSN 13504533. Available from: http://linkinghub.elsevier.com/retrieve/pii/S1350453313000246

[61]   RAGHAVAN, Madhavan L., Mauro M. HANAOKA, Jarin A. KRATZBERG, Maria de Lourdes HIGUCHI a Erasmo Simao DA SILVA. Biomechanical failure properties and microstructural content of ruptured and unruptured abdominal aortic aneurysms. *Journal of Biomechanics* [online]. 2011, **44**(13), 2501-2507 [cit. 2017-05-18]. DOI: 10.1016/j.jbiomech.2011.06.004. ISSN 00219290. Available from: http://linkinghub.elsevier.com/retrieve/pii/S0021929011004398

[62]   POLZER, Stanislav, T GASSER, Bernd MARKERT, Jiri BURSA a Pavel SKACEL. Impact of poroelasticity of intraluminal thrombus on wall stress of abdominal aortic aneurysms. *BioMedical Engineering OnLine* [online]. 2012, **11**(1), 62- [cit. 2017-05-18]. DOI: 10.1186/1475-925X-11-62. ISSN 1475925x. Available from: http://biomedical-engineering-online.biomedcentral.com/articles/10.1186/1475-925X-11-62

[63]   POLZER, Stanislav, Jiri BURSA, T. Christian GASSER, Robert STAFFA a Robert VLACHOVSKY. A Numerical Implementation to Predict Residual Strains from the Homogeneous Stress Hypothesis with Application to Abdominal Aortic Aneurysms. *Annals of Biomedical Engineering* [online]. 2013, **41**(7), 1516-1527 [cit. 2017-05-18]. DOI: 10.1007/s10439-013-0749-y. ISSN 00906964. Available from: http://link.springer.com/10.1007/s10439-013-0749-y

[64]   FILLINGER, Mark F., M.L. RAGHAVAN, Steven P. MARRA, Jack L. CRONENWETT a Francis E. KENNEDY. In vivo analysis of mechanical wall stress and abdominal aortic aneurysm rupture risk. *Journal of Vascular Surgery* [online]. 2002, **36**(3), 589-597 [cit. 2017-05-18]. DOI: 10.1067/mva.2002.125478. ISSN 07415214. Available from: http://linkinghub.elsevier.com/retrieve/pii/S0741521402000988

[65]   DORFMANN, A., C. WILSON, E. S. EDGAR a R. A. PEATTIE. Evaluating patient-specific abdominal aortic aneurysm wall stress based on flow-induced loading. *Biomechanics and Modeling in Mechanobiology* [online]. 2010, **9**(2),

127-139 [cit. 2017-05-22]. DOI: 10.1007/s10237-009-0163-4. ISSN 16177959. Available from: http://link.springer.com/10.1007/s10237-009-0163-4

[66] FILLINGER, Mark F., Steven P. MARRA, M.L. RAGHAVAN a Francis E. KENNEDY. Prediction of rupture risk in abdominal aortic aneurysm during observation: Wall stress versus diameter. *Journal of Vascular Surgery* [online]. 2003, **37**(4), 724–732 [cit. 2017-05-19]. Available from: http://www.sciencedirect.com/science/article/pii/S0741521402753482

[67] POLZER, S. a J. BURSA. *Simulation of Residual Stresses (Strains) in Arteries* [online]. s. 454 [cit. 2017-05-19]. DOI: 10.1007/978-3-642-23508-5_118. Available from: http://link.springer.com/10.1007/978-3-642-23508-5_118

[68] SPEELMAN, L., E.M.H. BOSBOOM, G.W.H. SCHURINK, J. BUTH, M. BREEUWER, M.J. JACOBS a F.N. VAN DE VOSSE. Initial stress and nonlinear material behavior in patient-specific AAA wall stress analysis. *Journal of Biomechanics* [online]. 2009, **42**(11), 1713-1719 [cit. 2017-05-19]. DOI: 10.1016/j.jbiomech.2009.04.020. ISSN 00219290. Available from: http://linkinghub.elsevier.com/retrieve/pii/S0021929009002206

[69] HORNY, Lukas, Tomas ADAMEK, Jan VESELY, Hynek CHLUP, Rudolf ZITNY a Svatava KONVICKOVA. Age-related distribution of longitudinal pre-strain in abdominal aorta with emphasis on forensic application. *Forensic Science International* [online]. 2012, **214**(1-3), 18-22 [cit. 2017-05-21]. DOI: 10.1016/j.forsciint.2011.07.007. ISSN 03790738. Available from: http://linkinghub.elsevier.com/retrieve/pii/S0379073811003227

[70] ATIENZA, José M., Gustavo V. GUINEA, Francisco J. ROJO, Raúl J. BURGOS, Carlos GARCÍA-MONTERO, Francisco J. GOICOLEA, Paloma ARAGONCILLO a Manuel ELICESA. The Influence of Pressure and Temperature on the Behavior of the Human Aorta and Carotid Arteries. *Revista Española de Cardiología (English Edition)* [online]. 2007, **60**(3), 259-267 [cit. 2017-05-21]. DOI: 10.1016/S1885-5857(07)60150-9. ISSN 18855857. Available from: http://linkinghub.elsevier.com/retrieve/pii/S1885585707601509

[71] BÄCK, Magnus, T. Christian GASSER, Jean-Baptiste MICHEL a Giuseppina CALIGIURI. Biomechanical factors in the biology of aortic wall and aortic valve diseases. *Cardiovascular Research* [online]. 2013-7-15, **99**(2), 232-241 [cit. 2017-05-21]. DOI: 10.1093/cvr/cvt040. ISSN 17553245. Available from: https://academic.oup.com/cardiovascres/article-lookup/doi/10.1093/cvr/cvt040

[72] INZOLI, Fabio, Federica BOSCHETTI, Mario ZAPPA, Tito LONGO a Roberto FUMERO. Biomechanical factors in abdominal aortic aneurysm rupture. *European Journal of Vascular Surgery* [online]. 1993, **7**(6), 667-674 [cit. 2017-04-23]. DOI: 10.1016/S0950-821X(05)80714-5. ISSN 0950821x. Available from: http://linkinghub.elsevier.com/retrieve/pii/S0950821X05807145

[73] SPEELMAN, Lambert, Ajay BOHRA, E. Marielle H. BOSBOOM, Geert Willem H. SCHURINK, Frans N. VAN DE VOSSE, Michel S. MAKAROUN a David A. VORP. Effects of Wall Calcifications in Patient-Specific Wall Stress Analyses of

Abdominal Aortic Aneurysms. *Journal of Biomechanical Engineering* [online]. 2007, **129**(1), 105- [cit. 2017-05-21]. DOI: 10.1115/1.2401189. ISSN 01480731. Available from: http://Biomechanical.asmedigitalcollection.asme.org/article.aspx?articleid=1417824

[74]   RAGHAVAN, M.L., David A. VORP, Michael P. FEDERLE, Michel S. MAKAROUN a Marshall W. WEBSTER. Wall stress distribution on three-dimensionally reconstructed models of human abdominal aortic aneurysm. *Journal of Vascular Surgery* [online]. 2000, **31**(4), 760-769 [cit. 2017-05-21]. DOI: 10.1067/mva.2000.103971. ISSN 07415214. Available from: http://linkinghub.elsevier.com/retrieve/pii/S074152140064421X

[75]   WOLTERS, B.J.B.M., M.C.M. RUTTEN, G.W.H. SCHURINK, U. KOSE, J. DE HART a F.N. VAN DE VOSSE. A patient-specific computational model of fluid–structure interaction in abdominal aortic aneurysms. *Medical Engineering & Physics* [online]. 2005, **27**(10), 871-883 [cit. 2017-05-21]. DOI: 10.1016/j.medengphy.2005.06.008. ISSN 13504533. Available from: http://linkinghub.elsevier.com/retrieve/pii/S1350453305001396

[76]   RODRÍGUEZ, J.F., C. RUIZ, G. HOLZAPFEL a M. DOBLARÉ. Mechanical stress in abdominal aneurysm: influence of GEOMETRY and material anisotropy. *Journal of Biomechanics* [online]. 2008, **39**(1), S272-S273 [cit. 2017-05-22]. DOI: 10.1016/S0021-9290(06)84049-2. ISSN 00219290. Available from: http://linkinghub.elsevier.com/retrieve/pii/S0021929006840492

[77]   RISSLAND, Peter, Yared ALEMU, Shmuel EINAV, John RICOTTA a Danny BLUESTEIN. Abdominal Aortic Aneurysm Risk of Rupture: Patient-Specific FSI Simulations Using Anisotropic Model. *Journal of Biomechanical Engineering* [online]. 2009, **131**(3), 031001- [cit. 2017-05-22]. DOI: 10.1115/1.3005200. ISSN 01480731. Available from: http://Biomechanical.asmedigitalcollection.asme.org/article.aspx?articleid=1475645

[78]   HOLZAPFEL, Gerhard A., Thomas C. GASSER a Ray W. OGDEN. A New Constitutive Framework for Arterial Wall Mechanics and a Comparative Study of Material Models. *Journal of Elasticity* [online]. 2000, **61**(1/3), 1-48 [cit. 2017-05-22]. DOI: 10.1023/A:1010835316564. ISSN 03743535. Available from: http://link.springer.com/10.1023/A:1010835316564

[79]   DEMIRAY, Hilmi. A note on the elasticity of soft biological tissues. *Journal of Biomechanics* [online]. 1972, **5**(3), 309-311 [cit. 2017-05-22]. DOI: 10.1016/0021-9290(72)90047-4. ISSN 00219290. Available from: http://linkinghub.elsevier.com/retrieve/pii/0021929072900474

[80]   Operation showing a large aneurysm of the abdominal aorta. In: *Northern Sydney Vascular* [online]. Sydney: Northern Sydney Vascular [cit. 2017-05-22]. Available from: http://www.northernsydneyvascular.com.au/AorticAneurysms.html

[81]   BUDWIG, R., D. ELGER, H. HOOPER a J. SLIPPY. Steady Flow in Abdominal Aortic Aneurysm Models. *Journal of Biomechanical Engineering* [online]. 1993, **115**(4A), 418- [cit. 2017-05-24]. DOI: 10.1115/1.2895506. ISSN 01480731. Available from: http://Biomechanical.asmedigitalcollection.asme.org/article.aspx?articleid=1399546

[82]   PETRUŠKA, Jindřich a Jiři BURŠA. Studijni opory UMTMB: Nelinearni ulohy mechaniky v MKP. Dostupne z: http://www.umtold.fme.vutbr.cz/index.php?option=com_content&task=view&id=46&Itemid=37

[83]   MICHEL, J.-B., J.-L. MARTIN-VENTURA, J. EGIDO, et al. Novel aspects of the pathogenesis of aneurysms of the abdominal aorta in humans. *Cardiovascular Research* [online]. 2011, **90**(1), 18-27 [cit. 2017-05-25]. DOI: 10.1093/cvr/cvq337. ISSN 00086363. Available from: https://academic.oup.com/cardiovascres/article-lookup/doi/10.1093/cvr/cvq337